Spring 1-1-2012

Structural and Functional Studies of the Bacterial Chemoreceptor, EBV's LMP-1, and S. cerevisiae's Kar3Cik1

Miguel Angel Gonzalez Jr.
University of Colorado at Boulder, miguel.gonzalez@colorado.edu

Structural and Functional Studies of the Bacterial Chemoreceptor, EBV's LMP-1, and S. cerevisiae's Kar3Cik1

by

MIGUEL ANGEL GONZALEZ JR

B.S., California State University, Los Angeles, 2005

A thesis submitted to the

Faculty of the Graduate School of the

University of Colorado in partial fulfillment

of the requirement for the degree of

Doctor of Philosophy

Department of Molecular, Cellular, and Developmental Biology

2012

This thesis entitled:

Structural and Functional Studies of the Bacterial Chemoreceptor, EBV's LMP-1, and S. cerevisiae's Kar3Cik1

written by Miguel Angel Gonzalez Jr

has been approved for the Department of

Molecular, Cellular, and Developmental Biology

_____

Dr. Mark Winey, Ph.D., Chair of Committee

_____

Dr. Andreas Hoenger, Ph.D., Thesis Advisor

Date_____

The final copy of this thesis has been examined by the signatories, and we

Find that both the content and the form meet acceptable presentation standards

Of scholarly work in the above mentioned discipline.

Gonzalez Jr, Miguel Angel (Ph.D., Molecular, Cellular, and Developmental Biology)

Structural and Functional Studies of the Bacterial Chemoreceptor, EBV's LMP-1, and S. cerevisiae's Kar3Cik1.

Thesis directed by Associate Professor Andreas Hoenger, Ph.D.

Structural biology is a discipline in biology that focuses on the relationship between structure and function in macromolecules, nucleic acids and lipids. In the studies presented in this thesis, the structure and function of three different proteins were investigated by using techniques from molecular biology, biochemistry, and biophysics: bacterial aspartate chemoreceptor (Tar), EBV's latent membrane protein-1 (LMP-1), and the kinesin-14 Kar3Cik1.

In the first part I was using molecular modeling to identify residues that are involved in coiled-coil interactions of the 4-helix bundle of the Tar chemoreceptor in *S. typhimurium*. The receptor was mutated at distinct residues that perturb the helix-helix interactions and analyzed for function. My studies found that by weakening the helical interactions in the so-called protein interaction region of the receptor, the receptor remained mostly in its on-state. Whereas weakening helical interactions in the so-called adaptation region of the chemoreceptor favored the receptor's off-state. These results may be evidence for a Ying-Yang relationship between the chemoreceptor's adaptation and protein interaction region. Signal transduction through the chemoreceptor may be a result of changes in the helical interactions caused by the binding of ligand.

The second part of my thesis dealt with the oncogenic Barr-Epstein virus membrane protein LMP-1 that affects B-cells in humans and is associated with several

malignancies. LMP-1's main role is to mimic the signal produced by CD40, but LMP-1 is also involved in several other signaling pathways. It is unknown whether LMP-1 functions in a signaling complex with multiple outputs or in multiple complexes with unique signaling outputs. To probe this question, size exclusion chromatography was used to fractionate cellular lysates of EBV positive cells and they were co-immunoprecipitated for LMP-1. The Co-IP samples were sent for Multidimensional Protein Identification Technology (MudPIT) analysis to identify LMP-1 associated signaling partners.

Kinesin motors are involved in many cellular functions in eukaryotes. In a simple eukaryote like budding yeast, kinesins are involved in 3 main functions: nuclear migration, chromosomal segregation, and karyogamy. Here we investigated Kar3Cik1, a heterodimeric member of the kinesin-14 family. Kar3Cik1 is involved in mating and mitotic cells, but is not essential for mitosis. Using cryo-EM and helical 3-D image reconstruction techniques I was able to determine Kar3Cik1's binding configurations in complex with microtubules in the ADP, nucleotide-free, and ATP states. This provides information as to Kar3Cik1's mechanism of movement along microtubules.

Dedication

I would like to dedicate this thesis to my wife Norma and father Miguel. Without their constant support I would not have been able to achieve this goal.

Acknowledgements

I would like to thank all of the friends that I have made as a graduate student, they have made this long journey a more pleasant one.

I would like to thank Andy Hoenger for giving me the opportunity to work in his lab on the Kar3Cik1 project. I am grateful for all of the help and guidance that he provided me with. I would like to thank everyone in the Hoenger lab for making me feel welcome and helping me learn new techniques. I would like to acknowledge Cedric, Julia, Joey, Kristin, Maria, and Robert who shared office space with me and made things entertaining and a bit loud at times. I would especially like to thank Julia Cope and Robert Kirmse. Julia made the suggestion that I work on Kar3Cik1, taught me all of the necessary techniques and was always willing to answer my questions. Robert read all of my thesis chapters and provided helpful feedback on each chapter.

I would like to thank Jennifer Martin for giving me the opportunity to work on a project that was not typical in her lab. Jennifer was very supportive in making sure I received the guidance necessary that was required by my project. I enjoyed working in her lab and I consider everyone who worked in the lab with me a good friend.

I would also like to thank Joe Falke for all of his guidance and support while I worked in his lab. I would like to acknowledge Kalin Swain for finishing the socket project that I started.

Finally, I would like to thank Andy Hoenger, Jennifer Martin, Michael Stowell, Mark Winey, and Dylan Taatjes for being members of my thesis committee. I appreciate all of their guidance, support, and patience. I would especially like to thank Mark and Dylan for being late additions to my committee.

Table of Content

Introduction

Structural biology is the over-arching term that describes the science and methods investigating the structure–function relationships within and between proteins, lipids and nucleic acids. They may be operating as individual particles or combined within large functional macromolecular assemblies, but almost always interact with ligands, nucleotides, and other cellular structures. Of the vast amounts of macromolecules and complexes that exist within cells, three systems will be discussed here within this thesis: bacterial chemoreceptors, oncogenic viral membrane proteins, and molecular motors interacting with microtubules. By using techniques from molecular biology, biochemistry, and biophysics I was able to investigate the structural and functional features of each macromolecule listed above.

Bacterial chemoreceptors: In bacteria, chemoreceptors are vital to the cell to detect the presence of attractants and repellents. In the presence of an attractant, bacterial cells will produce an internal signal that causes the flagella to rotate counter-clockwise, thereby propelling the cell forward. In the lack of an attractant, the bacteria would produce a signal that causes the flagella to rotate in a clockwise fashion that causes the cell to tumble (Falke & Hazelbauer, 2001). These reactions are mediated by chemoreceptors. In enteric bacteria such as E. coli, chemoreceptors are found in the inner membrane of the cell, linking the periplasm with the cytosol. Chemoreceptors have three regions: the periplasmic region that binds ligand, the transmembrane region, and the cytoplasmic region transmitting the signal to an internal message system (Figure 1). Multiple studies have been done to look at these specific regions to

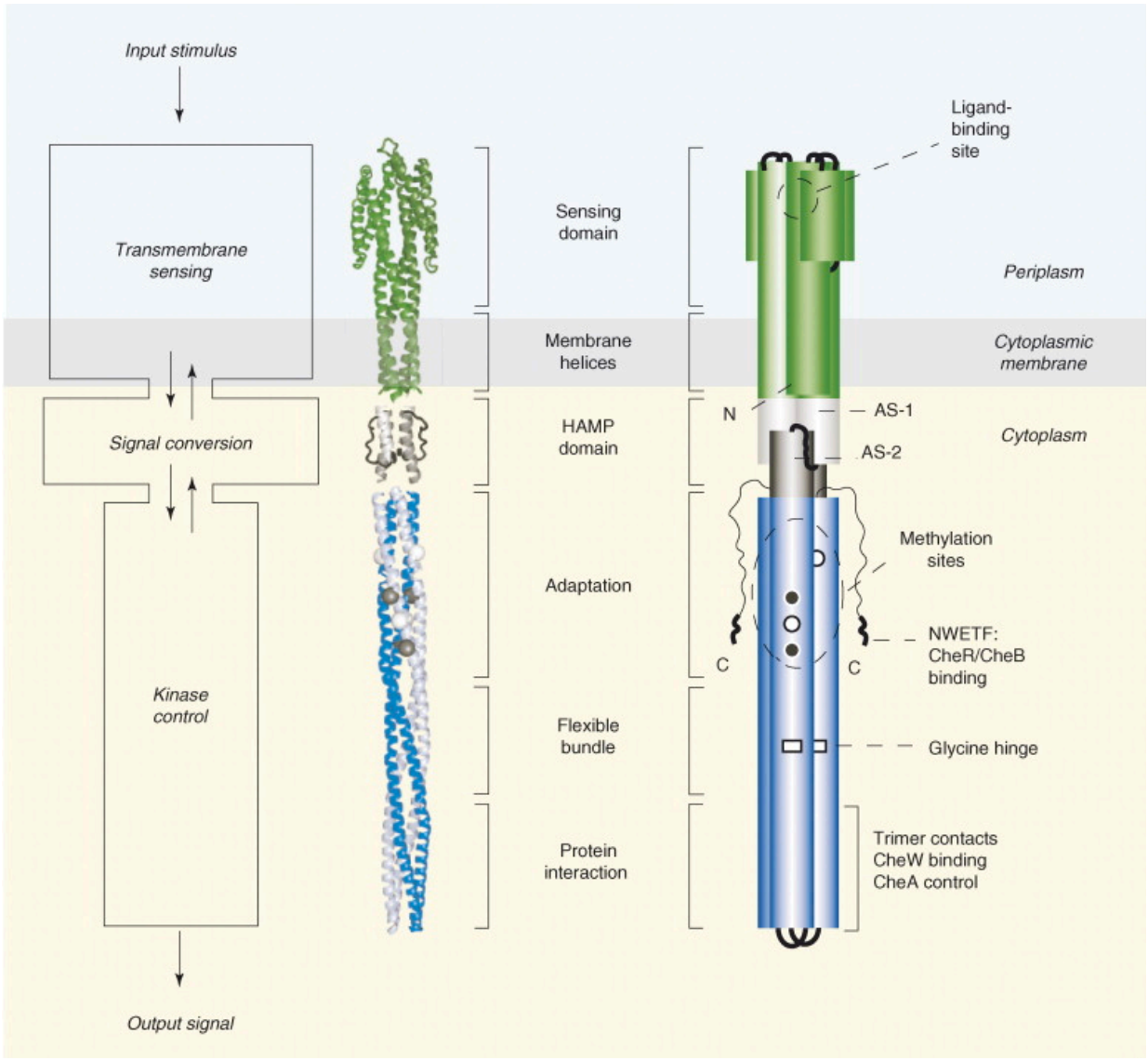

Hazelbauer et al. Trends Biochem Sci. 2008

Figure 1. Structure and Function of a Chemoreceptor Dimer.
The chemoreceptor is comprised of a homodimer. Ligand binds in the periplasmic region which produces a signal that moves down to the HAMP domain. The HAMP domain converts the signal, which is then transmitted through the kinase control module, and the signal can be output to CheA kinase. (Hazelbauer et al. 2008)

understand how sensing attractants/repellents transmits a signal down the length of the receptor and switches the CheA kinase on/off (Chervitz & Falke, 1996; Falke et al., 1997; Starrett & Falke, 2005; Swain & Falke, 2007). CheA in turn phosphorylates CheY, which in turn regulates flagellar rotation and will determine if the cell will swim or tumble by interacting with the flagellar motor which will cause the cell to swim (counter-clockwise rotation causes the all the flagella to come together and function as a unit) or tumble (clockwise rotation causes the each flagella to work independently and moves the cell without directionality).

Using structural biology methods such as computer modeling of chemoreceptor structures to identify conserved helical interaction I investigated a specific helix-helix interaction that drives the aspartate chemoreceptor. The receptor exhibits a characteristic antiparallel trans-membrane 4-helix bundle, which led us to devise the so-called Yin-Yang hypothesis. This hypothesis predicts that stabilization of the 4-helix bundle in the chemoreceptor within the protein interaction region will cause a destabilization in the adaptation region and vice versa. Stabilization of the protein interaction region will cause the receptor to be in the off-state, whereas stabilization of the adaptation region will cause the receptor to be in the on-state (actively phosphorylating CheA) (Figure 2).

Oncogenic viral membrane proteins: The Epstein-Barr virus (also called human herpesvirus 4: HHV-4), is a virus of the herpes family and is one of the most common viruses in humans. Latent membrane protein-1 (LMP-1) is an oncogenic viral protein in Epstein-Barr virus (e.g. associated with Hodgkin's lymphoma, Burkitt's lymphoma, nasopharyngeal carcinoma). LMP-1 is believed to have six transmembrane

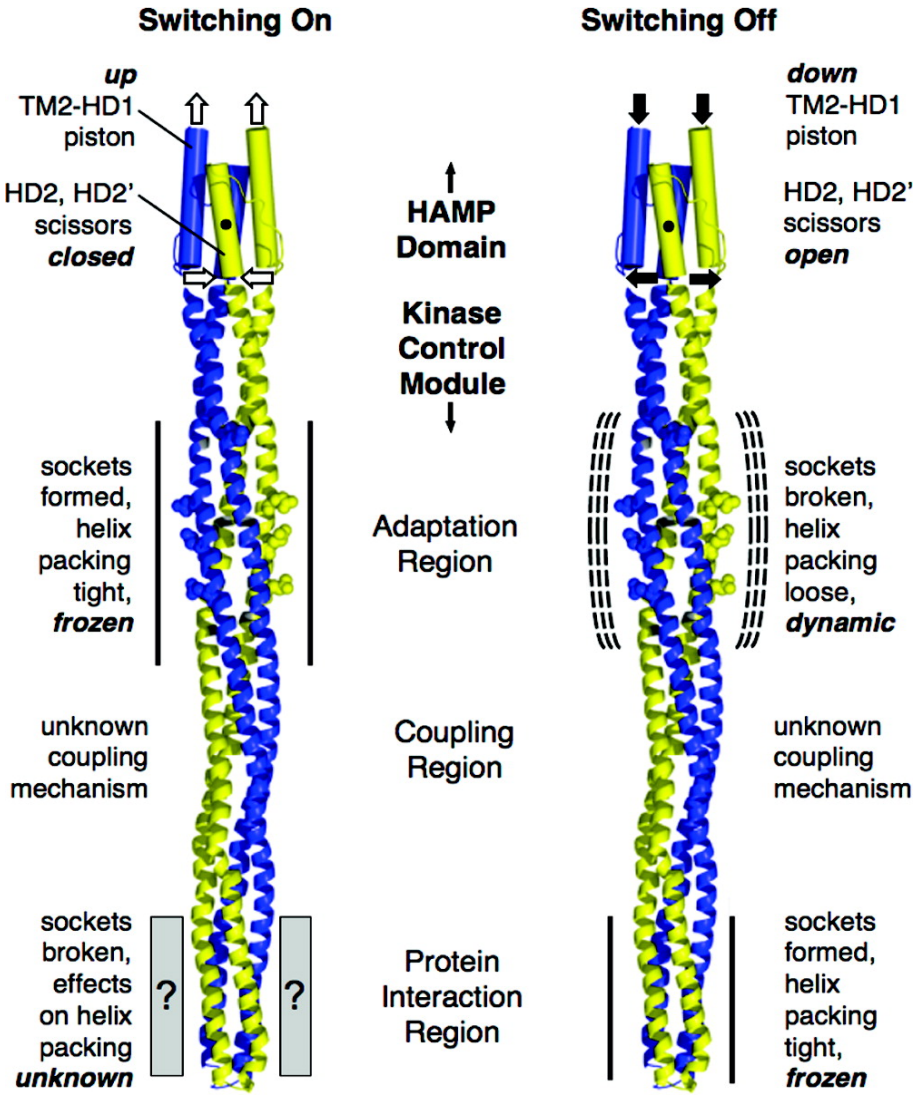

Figure 2. Conceptual Basis of the Yin−Yang Hypothesis.
In the on-state of the chemoreceptor, the sockets in the adaptation region are hypothesized to be formed with tight helical packing interactions while the protein interaction region has broken sockets and weak helical packing. In the off-state, the sockets in the adaptation region are hypothesized to be broken with weak helical packing while the protein interaction region has formed sockets with tight helical packing. (Swain et al. 2009)

helices and a charged cytoplasmic region of unknown structure (Fennewald et al. 1984). The lack of structural information along with a lack of significant sequence homology with other proteins presents a challenge to structural and functional studies of LMP-1. LMP-1 is involved in infected B cell immortalization, which is achieved by LMP-1's ability to mimic the CD40 signal (Kilger et al. 1998). The question asked here is how can LMP-1 associate with other signaling proteins to produce a deregulated signal? To probe this question methods such as protein purification and proteomics were used to determine if LMP-1 functions as a large signaling complex with multiple outputs or several signaling complexes with unique signaling outputs (Figure 3). Traditional 3-D crystallographic techniques, typically employed for X-ray crystallographic structural analysis are very unlikely to work on LMP-1 because of its large hydrophobic transmembrane region as well as a highly charged and presumably flexible cytoplasmic region. Although tricky and tedious, membrane proteins typically have a high tendency to insert in a lipid layer, and eventually forming 2-D crystalline arrays. Therefore, tilt-series recording and 2-D electron crystallography appears to be the more promising technique for obtaining structural information on LMP-1.

Kinesin – microtubule interactions: Motor proteins of the kinesin family interact with, and move along microtubules and are involved in several essential functions in a cell (Figure 4). In this thesis the *Saccharomyces cerevisiae* kinesin-14 member Kar3Cik1 is discussed. Kar3Cik1, like all kinesin-14s contains a C-terminal motor domain and a C-terminal cargo-binding region that are connected by a large coiled coil region. Kinesin-14s, including Kar3Vik1 are retrograde kinesin motors, but do

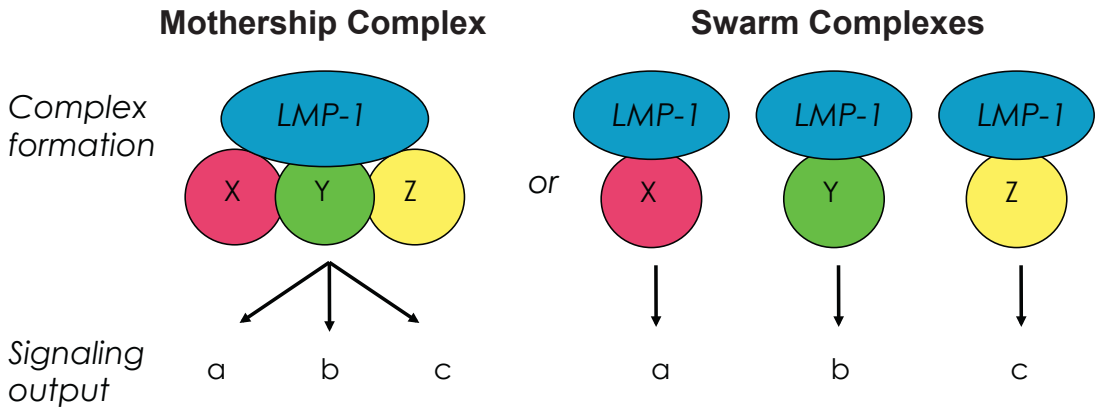

Figure 3. LMP-1 Signaling Complex or Signaling Complexes
The Mothership Complex model predicts that LMP-1 may function as a complex with multiple signaling outputs. The Swarm Complexes model predicts LMP-1 is involved in unique signaling complexes where each has their own signaling output.

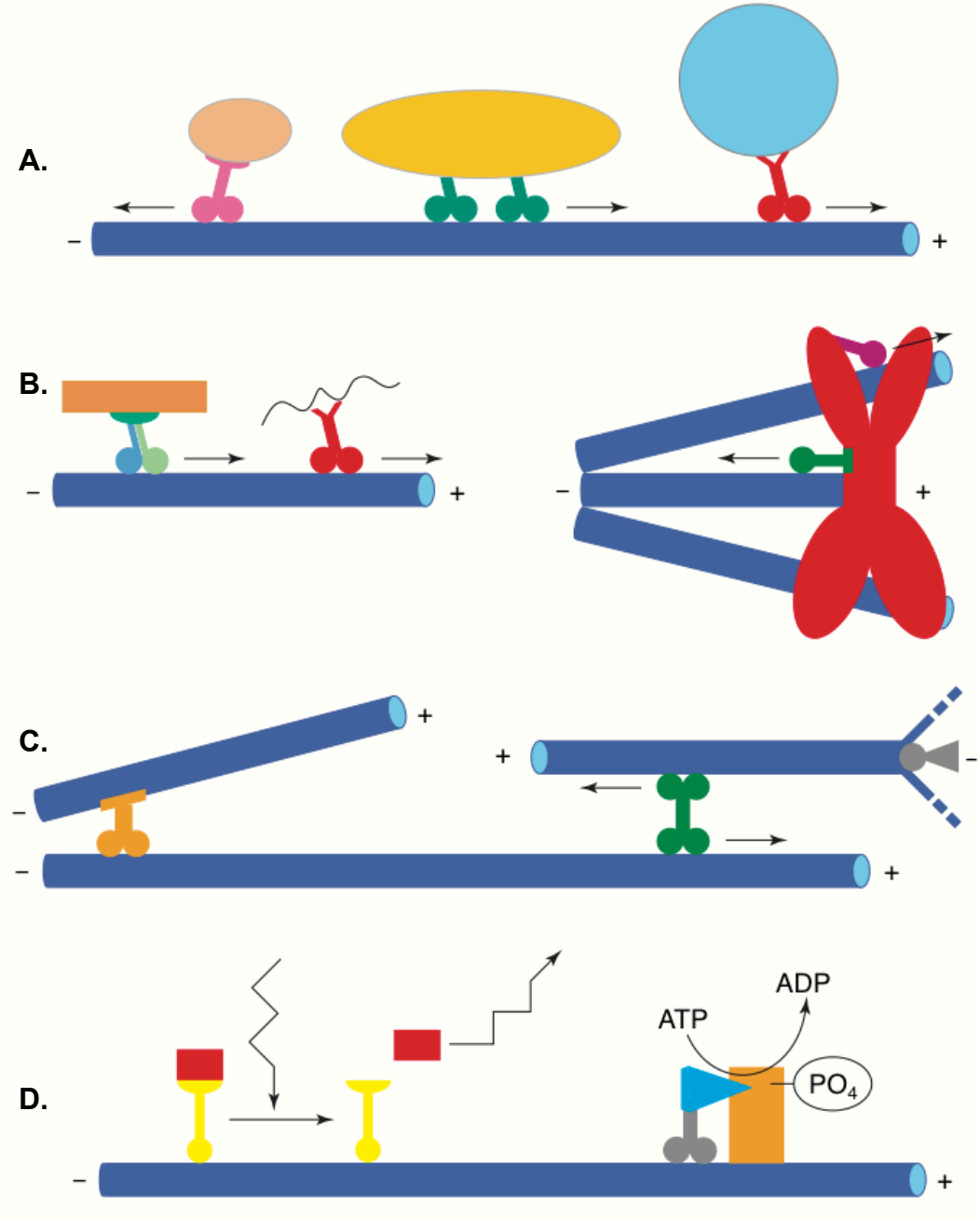

Manning & Synder. Trends Cell Bio. 2000

Figure 4. Various Functions of Kinesin Related Proteins.
A) Molecular motors are involved in transporting cargo such as organelles and vesicles along microtubules. **B)** They are also involved in transporting proteins and nucleic acids. **C)** They play a role in moving, organizing, and stabilizing microtubules. **D)** They may also be involved in signal transduction. (Manning & Synder, 2000)

not show strong processivity. In budding yeast Kar3Cik1 is involved in karyogamy and in vegetative cell division. In karyogamy, it is located to spindle pole bodies and cytoplasmic microtubules where it is involved in spindle formation (Page et al., 1994). In vegetative cells, Kar3Cik1 is localized to the mitotic spindle where it may be involved in chromosome segregation and spindle assembly (Meluh & Rose, 1990; Page et al., 1994). Using cryo-electron microscopy and helical 3-D image reconstruction, the structure of Kar3Cik1 in complex with microtubules can be investigated and its conformational states with respect to ATP hydrolysis may be analyzed to near-atomic detail (e.g. by docking X-ray data into the 3-D EM scaffolds). By carefully analyzing the conformations of the Kar3Cik1 motor, and motor-homology domain at different nucleotide states it may be possible to understand the mechanism of KarCik1's movement along a microtubule, thereby producing a retrograde powerstroke to the cargo.

Chapter 1. Testing the Ying-Yang Model of Signaling in the Bacterial Chemoreceptor Cytoplasmic Domain.

The work in this chapter has been published in Swain KE, **Gonzalez MA**, and Falke JJ. 2009. Engineered socket study of signaling through a four-helix bundle: evidence for a yin-yang mechanism in the kinase control module of the aspartate receptor. *Biochemistry* 48(39):9266-77.

Introduction

Bacterial chemotaxis has been extensively studied in *E. coli* and *S. typhimurium* focusing on the serine (Tsr) and aspartate (Tar) transmembrane receptor signaling systems (Falke et al., 1997). The general signaling pathway in which ligand binds to chemoreceptors causing a change in flagellar motor rotation is shown in Figure 1. In *S. typhimurium,* the receptor's apo state of the histidine kinase CheA is in its on state, characterized by autophosphorylation at His48. Phospho-CheA then transfers its phosphate to aspartate kinase CheY at Asp57. Phospho-CheY diffuses to the flagellar motors where it binds FliM protein, a switch protein in the c-ring of flagellar motors that causes clockwise flagella rotation, producing a tumbling bacterial movement. CheZ uses its phosphatase activity to hydrolyze phospho-CheY and thus inactivate the tumble signal. When attractant binds to a chemoreceptor a signal is sent to CheA that shuts off its autophosphorylation, this prevents CheY phosphorylation and CheY binding to FliM at the flagellar motor. CheY's inability to regulate flagellar motor rotation causes the flagella to rotate counter clockwise producing a smooth swimming phenotype (Falke & Hazelbauer, 2001). Although the signaling pathway of bacterial chemotaxis is well understood, the signal transduction mechanism through which ligand binding regulates CheA is not.

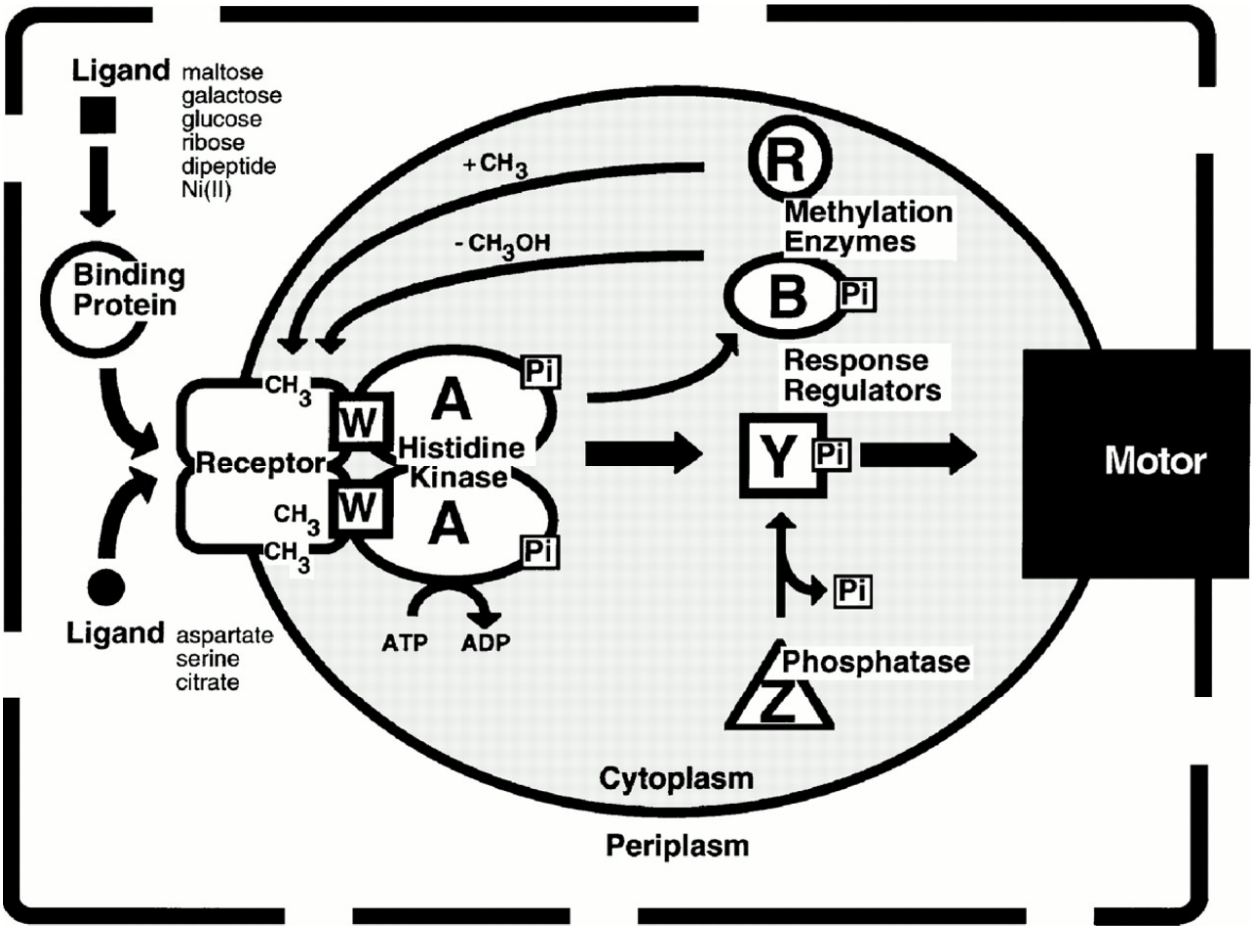

Falke et al. Annu Rev Cell Dev Biol. 1997

Figure 1. The bacterial chemotaxis signaling pathway for *E. coli* and *S. typhimurium*.
Attractants bind to the periplasmic region of the receptor and causes a change in receptor state that regulates CheA activity. CheA regulation directly affects CheY activity, which regulates flagellar motor activity. The methylation and demethylation enzymes CheR and CheB control receptor sensitivity and memory. CheZ inactivates the tumble signal by increasing the rate of phospho-CheY hydrolysis. (Falke et al., 1997)

Bacterial chemoreceptors are homo dimers consisting of α-helical transmembrane proteins, which form an antiparallel four-helix bundle structure via a U-turn at the signaling tip (Figure 2) (Kim et al., 1999). In *E. coli* and *S. typhimurium* the chemoreceptor spans from the periplasmic space to the cytoplasm with a total length of ~ 380 Å. Ligand binds to the periplasmic region where the binding signal is transmitted through the membrane into the cytoplasmic region of the chemoreceptor. A piston displacement model has been proposed that describes how the signal travels into the transmembrane region, however, the exact signaling process/mechanism through the cytoplasmic domain remains unknown (Figure 3) (Chervitz & Falke, 1996). The cytoplasmic domain retains the antiparallel four-helix bundle, where two sets of antiparallel coiled coils are supercoiled with each other. Coiled coils are made up of specific heptad motifs comprised of hydrophobic (H) and polar (P) residues HPPHPPP in positions “abcdefg”. Figure 4A, shows a general model of various interactions that stabilize the four-helix bundle structure. The center of the bundle is comprised of ‘a’ and ‘d’ residues which are hydrophobic and produce the core of the bundle, whereas residues ‘g’-‘c’ and ‘b’-‘e’ are polar and form a barrier that protects the hydrophobic core (Oakley & Hollenbeck, 2001). Coiled coils can be broken down into simple units called sockets. A socket is an arrangement of residues that follow knobs-into-holes packing where a knob consisting of single residue from one helix will interact with a hole comprised of four residues of a different helix (Walshaw & Woolfson, 2001). Figure 4B shows the structure of a socket (Alexander & Zhulin, 2007). Since the structure of the cytoplasmic domain of the receptor is a four-helix bundle, the entire region spanning

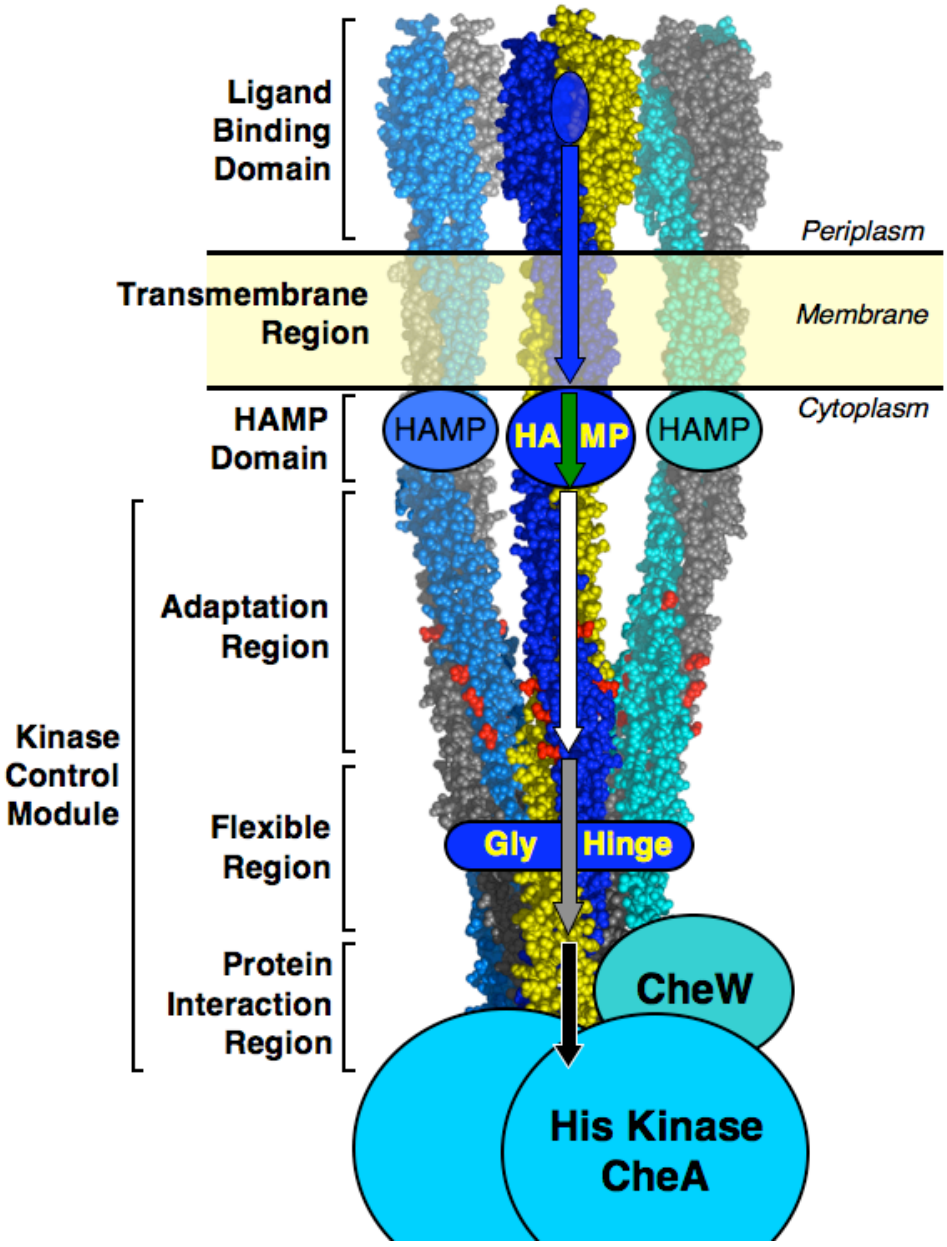

Figure 2. Chemoreceptor core complex.
The receptors are depicted as trimer of chemoreceptor dimers (trimer of dimers), which is believed to be the minimal unit for receptor, regulated kinase activity (Boldog et al., 2006; Hazelbauer et al., 2008). The signal produced by the binding of ligand must travel through the transmembrane region (blue arrow) via a piston displacement mechanism. The signal moves through the HAMP domain where the piston displacement causes a conformational change (green arrow) that travels through kinase control module that includes the adaptation (white arrow), flexible (grey), and protein interaction (black) regions. The signal in turn controls the activity of CheA kinase that is coupled to the receptor with CheW.

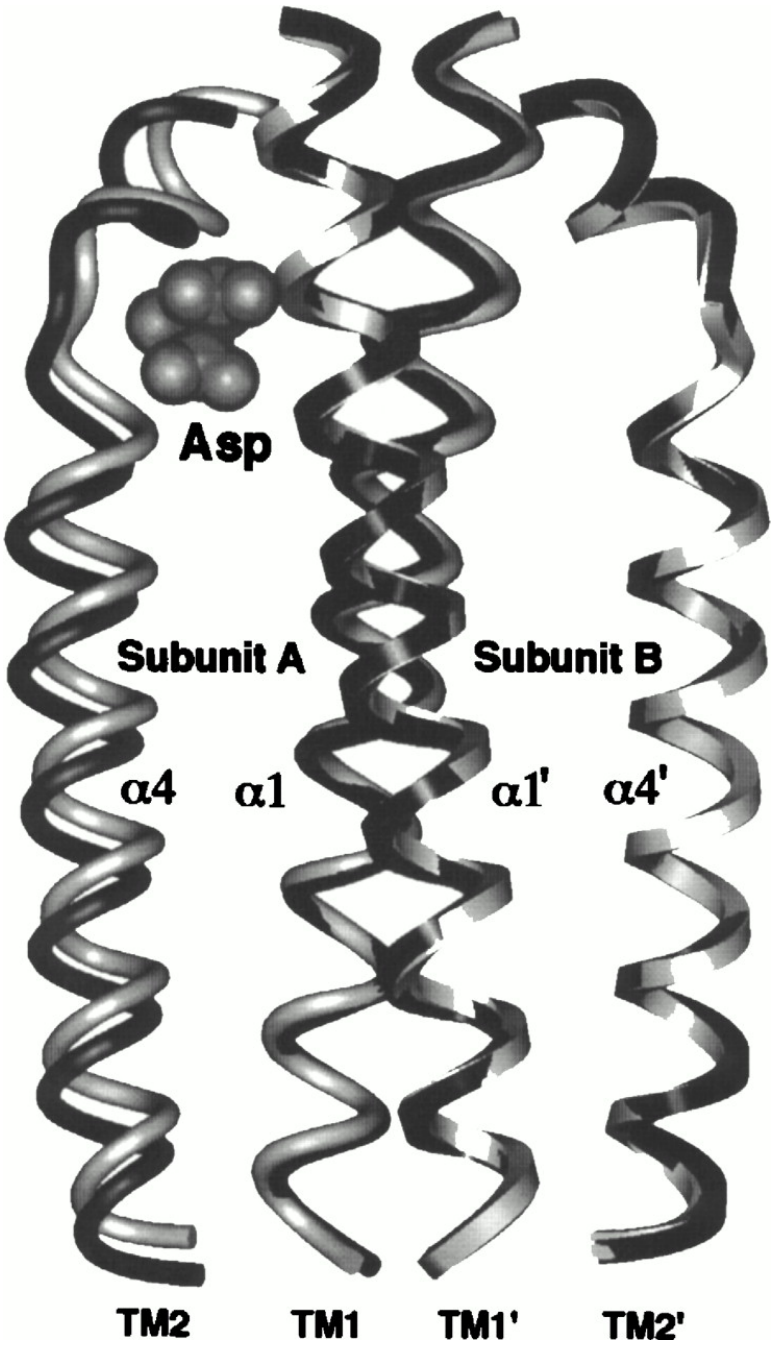

Falke et al. Annu Rev Cell Dev Biol. 1997

Figure 3. Tar chemoreceptor piston displacement.
Two crystal structures have been superimposed to show the difference between the apo state and the aspartate bound state. There is a helical displacement in the signaling helix (TM2) that corresponds to 1.6 Å downward shift toward the cytoplasmic region (Falke et al., 1997).

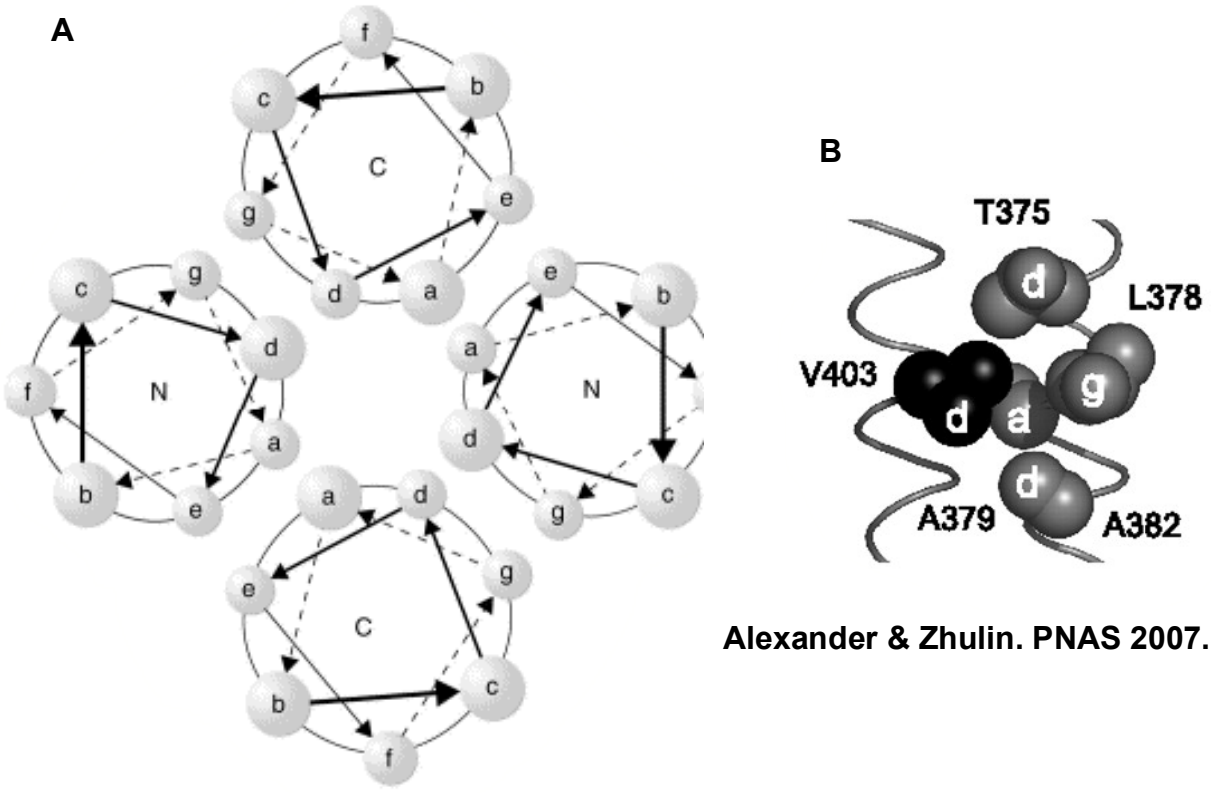

Alexander & Zhulin. PNAS 2007.

Oakley & Hollenbeck. Curr Opin Struct Biol 2001.

Figure 4. Four helix bundles and sockets.
A) Representation of an antiparalell 4-helix bundle. The hydrophobic core of the 4-helix bundle is comprised of interactions between residues placed in the a and d positions in the heptad repeats (Oakley & Hollenbeck, 2001). **B)** Representation of a socket. The sockets are made up of knobs and holes. In the example in **B**, the hydrophobic side chain of valine (black) is accommodated by a hole made up of four resiues (grey) on an adjacent helix (Alexander & Zhulin, 2007).

from the adaptation region to the signaling region is comprised of sockets. The cytoplasmic domain can be divided into four parts: the linker/HAMP, adaptation/methylation, flexible, and signaling region. The HAMP region contains a HAMP motif that is essential for converting mechanical signals between modules in a receptor (Swain & Falke, 2007).The adaptation/methylation region regulates ligand affinity through changes in the methylation state resulting in continuous gradient tracking of attractant through signal re-sensitization. Adaptation occurs at four negatively charged residues: E297, E304, E311 and E493 via adaptation enzymes CheR and CheB (Starrett & Falke, 2005). CheR is a methyltransferase that methylates the adaptation residues, which causes a decreased ligand affinity and subsequently turns CheA on. CheB is a methylesterase, which in the absence of ligand is phosphorylated by CheA and removes methyl groups to increase the affinity of ligand, allowing the detection of weaker gradients during chemotaxis (Falke et al., 1997).

The signaling region, located at the bottom of the chemoreceptor spans about 30 residues. This is the docking site for CheW and CheA. CheW is a small 18 kDa coupling protein that is required for proper CheA activity (Falke et al., 1997). CheA is a 142 kDa histidine kinase dimmer, which is regulated by the receptor. CheA contains two active sites where it uses Mg^{2+}-ATP to autophosphorylate His48 on each subunit (Falke et al., 1997). Phospho-CheA then transfers its phosphate to CheY for flagellar motor regulation.

The flexible region, which is located between the adaptation and signaling region of the receptor requires more extensive studies. This region contains smaller residues such as alanine and glycine, which lack the hydrophobic properties to produce a rigid,

and stable coiled coil structure (Alexander & Zhulin, 2007). One aspect of my proposed project was to obtain more structural information of the four-helix bundle and its importance in signal transduction.

Taken as a whole, the bacterial chemotaxis signaling pathway has been the focus of many studies, yet how the ligand binding signal is transmitted through the cytoplasmic region of the receptor is unknown/not known. Likely, the coiled coil structure of the receptor plays a role in transmitting the signal to the signaling region where CheA is regulated. A Yin-Yang model was proposed whereby destabilizing the coiled coil structure of the adaptation and signaling regions will drive receptor signaling toward the off and on states, respectively. This model is supported by previous “lock-on” cysteine and disulfide studies, which lock the receptor in its kinase “on” state (Danielson et al., 1997; Bass & Falke, 1998; Bass et al., 1999; Bass & Falke, 1999; Winston et al., 2005). These previous studies shown in Figure 5 demonstrate that “lock-on” cysteines exist in the signaling region while “lock-on” disulfides exist in the adaptation region.

The previous studies using cysteine and disulfides to scan the structure of the aspartate receptor (Tar) have allowed us to propose the Yin-Yang model (Danielson et al., 1997; Bass & Falke, 1998; Bass et al., 1999; Bass & Falke, 1999; Winston et al., 2005). This model predicts that weaker sockets in the adaptation region will drive the receptor toward the off-state and that weaker sockets in the signaling region will drive the receptor towards its on-state. In order to determine important conserved sockets I will use the program “SOCKET”. SOCKET is a program that can identify coiled-coil

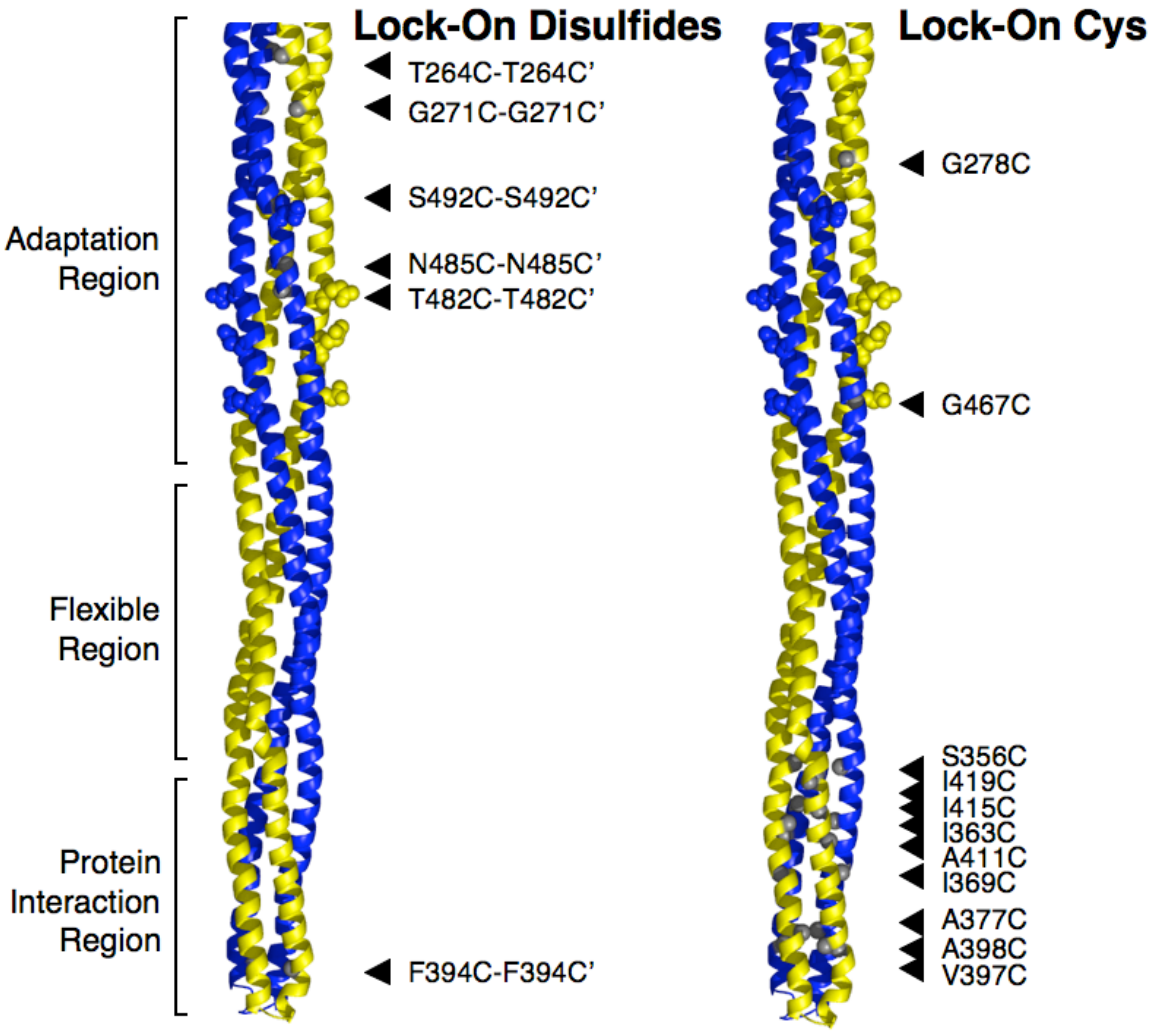

Figure 5. Lock on disulfides and cysteines that support the Yin-Yang hypothesis. Previous studies using disulfide crosslinking and cysteines scanning have identified that a group of lock-on disulfides exist in the adaptation region whereas a group of lock-on cysteines exist in the protein interaction region (Danielson et al., 1997; Bass & Falke, 1998; Bass et al., 1999; Bass & Falke, 1999; Winston et al., 2005).

motifs within a protein structure using atomic coordinates from a pdb file (Walshaw & Woolfson, 2001). In addition, SOCKET can also identify the knobs and holes that form the sockets. Alexander and Zhulin performed sequence analysis on chemoreceptors of the same class as *S. typhimurium* and *E. coli* receptors and they found highly conserved residues (>80%) within the cytoplasmic domain (Alexander & Zhulin, 2007). Using SOCKET we identified which conserved residues are in 'a' and 'd' positions that function as knobs. These sites were the sockets chosen to investigate the specific knob-hole, hydrophobic packing interactions important in four-helix bundle stability.

To test the Yin-Yang prediction it is necessary to weaken conserved sockets in the adaptation and signaling region. In order to weaken the sockets, the conserved knobs were mutated to alanine. Alanine is the smallest hydrophobic residue and should increase the distance between the knob and hole residues, thereby destabilizing the socket.

Mutant receptors were constructed by using site-directed mutagenesis to substitute alanine for select residues on the Tar containing plasmid, pSCF6. The mutant receptors were tested for their *in vivo* effects on aspartate-specific chemotaxis using a swarm assay. The mutant plasmid were transformed into *E. coli* strain RP8611 that lacks all chemoreceptors but contains all other chemotaxis components. Cultures were grown in Luria broth for 6 h and were spotted onto soft agar minimal medium swarm plates with or without aspartate. After an initial 30°C overnight incubation, swarm diameters were taken every 3 h and normalized to wild type to determine the relative rate of chemotaxis (Winston et al., 2005). The results from the swarm assay will demonstrate if the alanine mutation had a robust effect on bacterial chemotaxis.

To test the specific effect of the mutation to the aspartate receptor, two asymmetric assays were used. The receptor must first be expressed in *E. coli* RP3808, which lacks all major chemoreceptors and adaptation enzymes, and isolated in native membranes (Danielson et al., 1997, Winston et al., 2005). The first assay was the *in vitro* receptor-coupled kinase regulation assay. This was used to investigate how changes in the receptor affect the ligand stimulated regulation of CheA kinase activity. Kinase activity was measured by the rate of phosphorylated CheY formation (Winston et al., 2005). Since CheA activity is regulated by the receptor, phospho-CheY formation is directly linked to the receptor's ability to transmit the ligand-binding signal to CheA and prevent autophosphorylation that is transferred to CheY. By incorporating [γ- ^{32} P] ATP as the source of phosphate for CheA autophosphorylation and CheY phosphotransfer, I was able to detect phospho-CheY using SDS-PAGE gel and quantify phospho-CheY by phosphoimaging (Chervitz et al., 1995). The results from the *in vitro* receptor-coupled kinase regulation assay will provide information on how the alanine mutation affects signal transduction and whether the mutation cause a lock-on, lock-off, super activating, inhibiting, or wild-type phenotype. With respect to the Yin-Yang model, alanine mutations in the adaptation region will weaken sockets causing the receptor to switch the kinase off (no phospho-CheY) and alanine mutations in the signaling region will drive the receptor to keep the kinase on (phospho-CheY production).

The second asymmetric assay that was used to test the effect of weakening sockets in the aspartate receptor is the *in vitro* methylation assay. This assay is used to determine the rate at which CheR methylesterifies the adaptation sites using S-adenosyl- [^{3}H-methyl]-L-methionine with or without 1 mM aspartate ligand. The samples

are run on a SDS-PAGE gel where the receptor bands are cut out. The receptor bands are then quantified to observe the extent of methylation using the vapor-phase equilibrium method (Chervitz et al., 1995). If the receptor is methylated, then it will be in its off-state, and if the receptor is not methylated it will be in its on-state. By weakening sockets in the adaptation region, we should see an increase in the rate of methylation between CheA's on and off state where increase methylation will occur in the off-state. Taken all together, the results from this study will provide supporting evidence for the proposed Yin-Yang model using two independent functional assays.

Materials and Methods

Materials.

Reagents were obtained from the following sources: [g-32P]-ATP from Perkin- Elmer; QuickChange site-directed mutagenesis kit from Stratagene; mutagenic oligonucleotides from Integrated DNA Technologies; all other analytical grade chemicals from Sigma unless noted otherwise. *E. coli* strains were provided by Dr. J. S. Parkinson (University of Utah).

Identification of Conserved Sockets Likely to Contribute to Helix-Helix Packing Stability.

To select conserved sockets likely to stabilize helix-helix packing in the kinase control module, the program SOCKET by Derek Woolfson and coworkers (Walshaw & Woolfson, 2001) was used to predict stable sockets in the published atomic structural model for the control module (corresponding to residues 260-520 and 260'-520' of the

aspartate receptor). A cutoff value of 7.8 Å was used to limit the prediction to strong sockets. Subsequently, an alignment of related receptor sequences (Starrett & Falke, 2005) was used to determine which sockets were most conserved, and thus most likely to contribute significantly to helix-helix packing stability. Finally, sockets in which the knob was Ala were eliminated, yielding a library of conserved sockets with knobs all larger than Ala.

***Creation and Isolation of Mutant Aspartate Receptors*.**

Site-directed mutagenesis was performed as previously described (Miller et al., 2006) using the PCR-based QuickChange mutagenesis kit to engineer point mutations into the *Salmonella typhimurium* aspartate receptor gene in plasmid pSF6 (Chervitz et al., 1995). Mutated plasmids were transformed into *E. coli* strain RP3808 lacking the major endogenous receptors and other pathway components, expressed, then receptor-containing membranes were isolated, quantitated and stored as previously described (Starrett & Falke, 2005) except that EDTA was reduced from 10 mM to 0.1 mM in the high salt buffer. The final membranes were resuspended at a receptor concentration of ~50 μM in EDTA-free final buffer (20 mM sodium phosphate, pH 7.0 with NaOH, 10% glycerol, and 0.5 mM phenylmethylsulfonylfluoride).

***Receptor Activity Kinase Assay*.**

Mutant receptors were assessed for their ability to bind, activate, and regulate CheA kinase by reconstituting receptor- containing, isolated membranes with purified CheA, CheW and CheY (Cysless constructs as previously described (Miller et al., 2006)), then

quantitating receptor-regulated kinase activity in the standard *in vitro* assay under conditions where the kinase activity of CheA is rate-determining (Miller et al., 2006).

Standard Deviation.

Error ranges represent the standard deviation of the mean for n > 3.

Results

Development of the Yin-Yang model for cytoplasmic domain signaling.

The observation that lock-on Cys residues are highly concentrated in the protein interaction region, while lock-on disulfides are located primarily in the adaptation region, has led us to propose the Yin-Yang hypothesis. In this model, signals generated by the transmembrane signaling and HAMP domains are transmitted through the 4-helix bundle of the kinase control module to the kinase via changes in helix-helix packing. In the adaptation region, tighter packing of helices within the 4-helix bundle is proposed to activate CheA kinase, and looser packing is proposed to inhibit the kinase. This feature of the model explains the observation that multiple lock-on disulfides can be generated in the adaptation region, each of which covalently stabilizes a helix-helix contact (Fig. 5). Moreover, multiple, native negative charges found in this region at the subunit helix-helix interface inhibit kinase activity via charge repulsion across the interface. Neutralization of these negative charges activates the kinase, presumably via stabilization of helix-helix packing (Starrett & Falke, 2005). By contrast, the Yin-Yang model proposes that in the protein interaction region tighter helix packing within the bundle inhibits kinase activity, and looser packing activates the kinase. This feature explains the observation that multiple Cys substitutions located at helix-helix interfaces

lock the receptor in the kinase-activating state, presumably by weakening the native helix-helix packing (Fig. 5). The Yin-Yang hypothesis is testable, as illustrated by studies described below.

Testing Strategy for the Yin-Yang model by weakening sockets at helix-helix interfaces.

To test the Yin-Yang model for signaling in the kinase control module, a strategy to weaken local helix-helix interactions and to determine the resulting effects on receptor signaling state was devised. As typical for antiparallel 4-helix bundles, the helix-helix interactions in the kinase control module are stabilized by local socket structural elements, in which a knob residue on one helix inserts into a cavity formed by four hole residues on an adjacent helix (Walshaw & Woolfson, 2001). The component helices exhibit the usual heptad repeating heptad pattern in which the “a” and “d” positions are buried, “b”, “c” and “f” are exposed, and “e” and “g” are interfacial. The knob residues are located at “a” and “d” positions, while the holes residues are typically positions “d”, “g”, “a”, “d”; or positions “a”, “d”, “e”, “a”, respectively. The strongest sockets possess large, hydrophobic knob and hole residues, although a diversity of residues are found at both the knob and hole positions in typical sockets. A selected socket can be weakened by introduction of a small side chain at one or more of its positions, thereby decreasing the number of stabilizing knob-hole contacts.

Here we test the Yin-Yang model by introducing point mutations that truncate selected knob side chains to the smaller Ala side chain, thereby perturbing the corresponding conserved sockets and weakening helix-helix interactions in specific

locations. Subsequently, the effect of each knob truncation on the receptor signaling state is determined using the anti-symmetric activity assay. The Yin-Yang model predicts that knob truncations in the adaptation and protein interaction regions will often generate lock-off and lock-on receptors, respectively. An example is illustrated in Figure 6, where a hydrophobic knob (L415) in the known structure of the protein interaction region contacts a hydrophobic hole (I359', I362', I363', I366') in the opposite subunit. Truncation of the Leu to Ala is predicted to significantly reduce the contacts of the knob with its hole residues and weaken the socket. Since the mutation would weaken helix-helix packing in the protein interaction region, the Yin-Yang model predicts a higher-than-random probability that the mutant receptor will be locked in the kinase-activating, methylation-inhibiting on-state.

To select a library of suitable knob side chains for truncation to Ala, the program SOCKET was used to predict the strongest sockets in the published atomic structural model for the control module (corresponding to residues 260-520 and 260'-520' of the aspartate receptor; see Methods). Subsequently, an alignment of related receptor sequences was used to determine which sockets were most conserved, and thus most likely to contribute significantly to helix-helix packing stability (Alexander & Zhulin, 2007). Finally, sockets in which the knob was already Ala were eliminated. This procedure yielded the library of 32 conserved aspartate receptor sockets targeted for knob truncation, as summarized in Table 1. The library included 16 sockets in the adaptation region, 8 in the flexible region, and 8 in the protein interaction region. Some knobs insert into a hole on the adjacent helix in the same subunit, while others insert into a hole on an adjacent helix in the other subunit, yielding intra- and inter-subunit

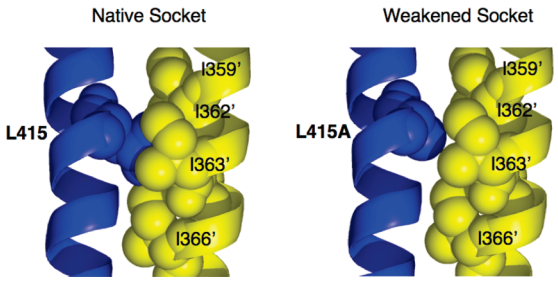

Figure 6. Weakening sockets to destabilize helix-helix interactions.
To locally reduce the strength of helix-helix packing, in principle one can truncate the side chain of a selected knob to Ala, thereby decreasing the knob-in-hole packing of a native, inter-helix socket. Shown is a representative socket (left) in which L415 is the knob that inserts into a hole comprised by I359', I362', I363', and I366' on an adjacent helix provided by the other subunit. Truncating the knob side chain from Leu to Ala, a mutation termed a knob truncation, significantly decreases the knob-hole contacts (right) (Swain et al., 2009).

sockets, respectively (Table 1, where the hole residues of inter-subunit sockets are indicated by a prime). All but 4 of the 32 knobs are hydrophobic, and the four exceptions are all neutral, hydrogen-bonding side chains (Ser, Asn, Gln) that insert into holes containing at least one other hydrogen bonding side chain. In some cases, a knob residue is also a hole residue for a different conserved socket (Table 1); in principle, truncation of such a residue to Ala will thus weaken two sockets simultandously and thereby have an even greater destabilizing effect on the local helix-helix packing interactions.

It should be noted that the atomic model of the kinase control module (Kim et al., 1999; Falke & Kim, 2000) used in the SOCKET analysis is constructed from high-resolution crystallographic data for the flexible and protein interaction regions, but no such data is available for the adaptation region. Instead, the adaptation region is based on molecular modeling constrained by a lower resolution, chemically derived structure of the kinase control module (Winston et al., 2005; Bass & Falke, 1999). The latter chemical structure was elucidated in the full-length, membrane-bound receptor, and it provides strong evidence that the atomic model of the kinase control module, including the adaptation region, closely represents the native structure of the extended 4-helix bundle. This fact, together with sequence conservation, ensures that most or all of the 32 selected sockets are correctly identified structural features of the native, membrane-bound receptor.

Table 1

knob (heptad position)	hole residue (n1, n4, n5, n8)	hole type[a]	kinase activity without Asp	kinase activity with Asp
		Adaptation Region (amino acids 260−320, 461−520)		
WT			1.00 ± 0.07	0.04 ± 0.02
V265A (**a**)	510 (V, F, R, S)	4	0.02 ± 0.01	0.01 ± 0.01
V268A (**d**)	506′ (L, A, V, F)	4	0.44 ± 0.05	0.05 ± 0.01
I282A (**d**)	492′ (S, A, A, L)	4	0.02 ± 0.01	0.01 ± 0.01
N286A (**a**)	489 (V, S, A, A)	2	0.02 ± 0.01	0.01 ± 0.01
Q296A (**d**)	478′ (M, V, T, N)	2	1.13 ± 0.02	0.05 ± 0.01
L300A (**a**)	475 (V, M, D, T)	4	0.02 ± 0.01	0.01 ± 0.01
T303A (**d**)	471′ (V, A, V, M)	4	1.03 ± 0.08	0.01 ± 0.01
V314A (**a**)	461 (S, Q, S, I)	2	0.02 ± 0.01	0.01 ± 0.01
(N317A)(**d**)	459′ (I, A, S, Q)	2		
S461A (**a**)	314 (V, N, A, A)	2	0.02 ± 0.01	0.01 ± 0.01
I468A (**a**)	307 (M, L, T, V)	2	0.02 ± 0.01	0.01 ± 0.01
(V471A) (**d**)	305′ (T, S, M, L)	2		
(V475A) (**a**)	302 (L, T, A, M)	4		
M478A (**d**)	296′ (Q, A, L, T)	4	0.02 ± 0.01	0.01 ± 0.01
V510A (**a**)	265 (V, V, R, S)	4	0.65 ± 0.12	0.00 ± 0.01
F513A (**d**)	261′ (L, T, V, V)	4	0.05 ± 0.01	0.01 ± 0.01
N379F	(disrupts trimer)		0.01 ± 0.01	0.01 ± 0.01
		Protein Interaction Region (amino acids 363−419)		
WT			1.00 ± 0.07	0.04 ± 0.02
I363A (**a**)	412 (A, I, R, I)	1	1.20 ± 0.07	1.06 ± 0.05
I366A (**d**)	408 (S, A, A, I)	3	0.02 ± 0.01	0.01 ± 0.01
L376A (**d**)	397′ (V, E, V, L)	4	0.03 ± 0.01	0.02 ± 0.01
V397A (**d**)	376′ (L, N, A, E)	2	0.25 ± 0.02	0.16 ± 0.01
(V401A) (**d**)	375 (T, L, A, A)	4		
L404A (**d**)	369′ (I, Q, T, L)	2	0.49 ± 0.03	0.33 ± 0.02
I415A (**d**)	359′ (I, I, I, I)	3	0.88 ± 0.10	0.68 ± 0.06
I419A (**a**)	356 (S, I, A, I)	2	0.95 ± 0.08	0.91 ± 0.01
N379F	(disrupts trimer)		0.01 ± 0.03	0.01 ± 0.01

Abbreviations. [a]NS, not standard.
(low yield), < 1% total membrane protein.

Construction of weakened-socket receptor library.

To create a library of mutant aspartate receptors possessing weakened sockets in the kinase control module, PCR site-directed mutagenesis of the aspartate receptor gene *tar* was used to introduce Ala substitutions at the 32 selected knob positions. The resulting point mutations were confirmed by DNA sequencing. Mutant receptors were expressed in an *E. coli* strain lacking all major components of the chemotaxis pathway, including the aspartate receptor and adaptation enzymes (CheB, CheR). The absence of adaptation enzymes ensured that each mutant receptor population possessed identical adaptation sites and thus was homogeneous.

Effects of weakened sockets on receptor-regulated CheA kinase activity.

To analyze the effects of the 28 remaining weakened sockets on the receptor signaling state, the behavior of each modified receptor was tested in the anti-symmetric activity assay (Miller & Falke, 2004). Of special interest are modifications that lock the receptor in its on- or off-state. In the kinase assay, wherein the receptor is reconstituted with CheA and CheW to generate the functional, membrane-bound signaling complex, lock-on modifications trap the signaling complex in the kinase activating state such that it becomes insensitive to attractant binding. By contrast, lock-off modifications trap the complex in the kinase-inhibiting state. Although I began the testing of the weakened sockets on kinase activity, Kalin Swain aided in completing the mutants that I did not test.

Table 1 and Figure 7 summarize the effects of weakened sockets on receptor-regulated CheA kinase activity. Strikingly, the effects can be grouped into three distinct

classes (Fig. 7). One class (V268A, Q296A, T303A, V447A, V510A) exhibits wild type-like kinase activity, including nearly complete inhibition by attractant aspartate. A second class (I359A, I363A, V397A, L404A, I415A, I419A, V426A, V450A, M454A) exhibits potential lock-on character since super-physiological levels (1 mM) of aspartate do not fully inhibit kinase activity; instead, the remaining kinase activity is at least 4-fold that of the wild type receptor in its aspartate-occupied state. A third class (V265A, I282A, N286A, L300A, V314A, M349A, I352A, I366A, L376A, I457A, S461A, I468A, M478A, F513A) exhibits potential lock-off activity, since little or no kinase activation is observed even in the absence of aspartate.

Discussion

During my time in the Falke lab my contributions included developing the Yin-Yang model, devising a strategy to test this model, constructing mutant chemoreceptors, and performing the initial kinase assays. I was able to identify weakened sockets that produced a lock-on or lock-off phenotype (Figure 8). Although my contributions support the predictions of the Yin-Yang model further testing was necessesary. I was not able to test the methylation rates or the effect on live cell chemotaxis of the mutant receptors.

This project was ultimatley finished by Kalin Swain who perfermed the receptor methylation experiments, the live cell chemotaxis assays, and completed the CheA kinase assays. Our work was combined and written as a manuscript titled “Engineered Socket Study of Signaling through a Four-Helix Bundle: Evidence for a Yin-Yang Mechanism in the Kinase Control Module of the Aspartate Receptor.” Additional findings are discussed in the paper (Swain et al., 2009).

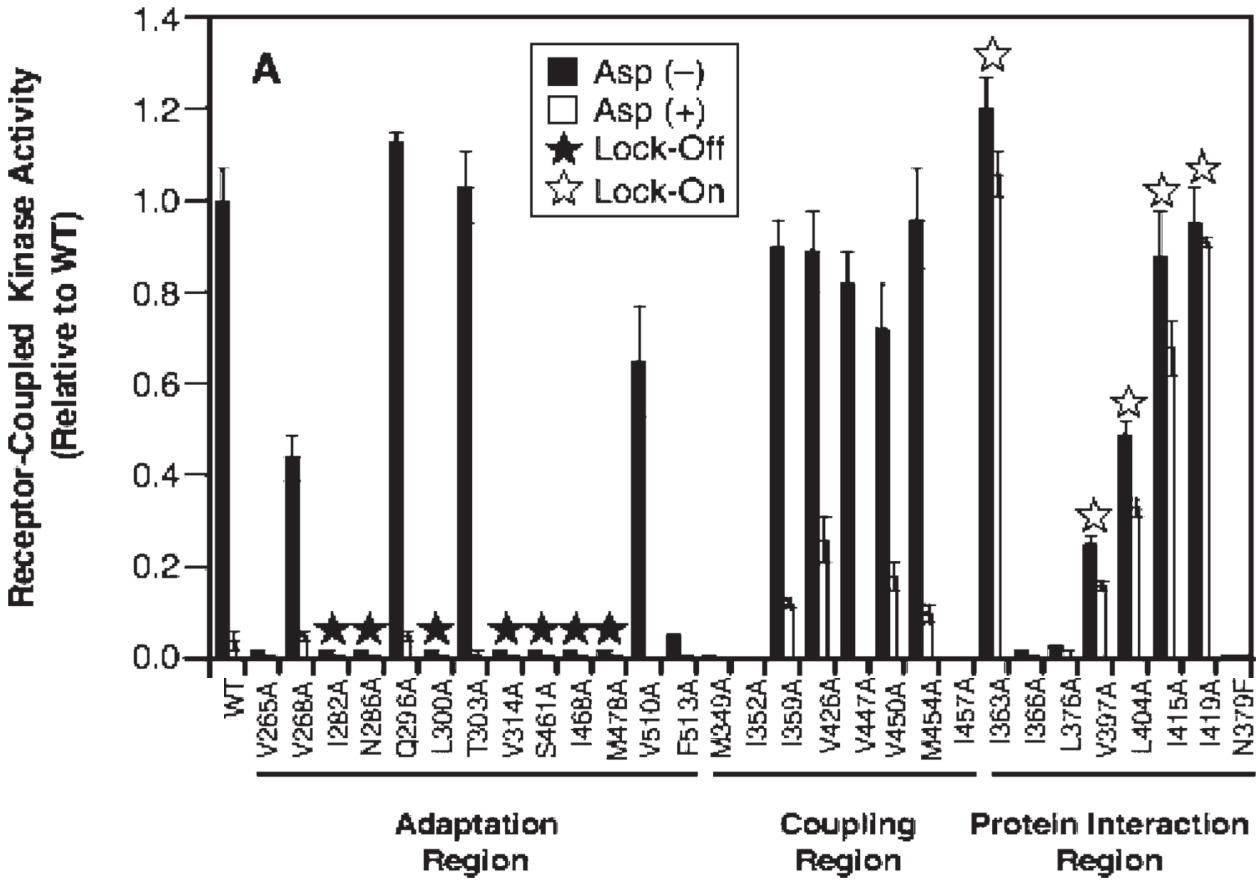

Figure 7. Effects of weakened sockets on receptor function in vitro.
Effects of knob truncations (defined in Fig. 6) on receptor-regulated kinase activity in the reconstituted receptor-CheA-CheW signaling complex. Shown are CheA kinase activities for signaling complexes containing each knob truncation mutant in both the apo and attractant-occupied (1 mM aspartate) states. All kinase activities are normalized to that of the signaling complex containing the apo wild type receptor. Notably, a high percentage of knob truncations in the adaptation region inhibit kinase activity, while a high percentage in the protein interaction region prevent normal attractant inhibition of kinase activity (Swain et al., 2009).

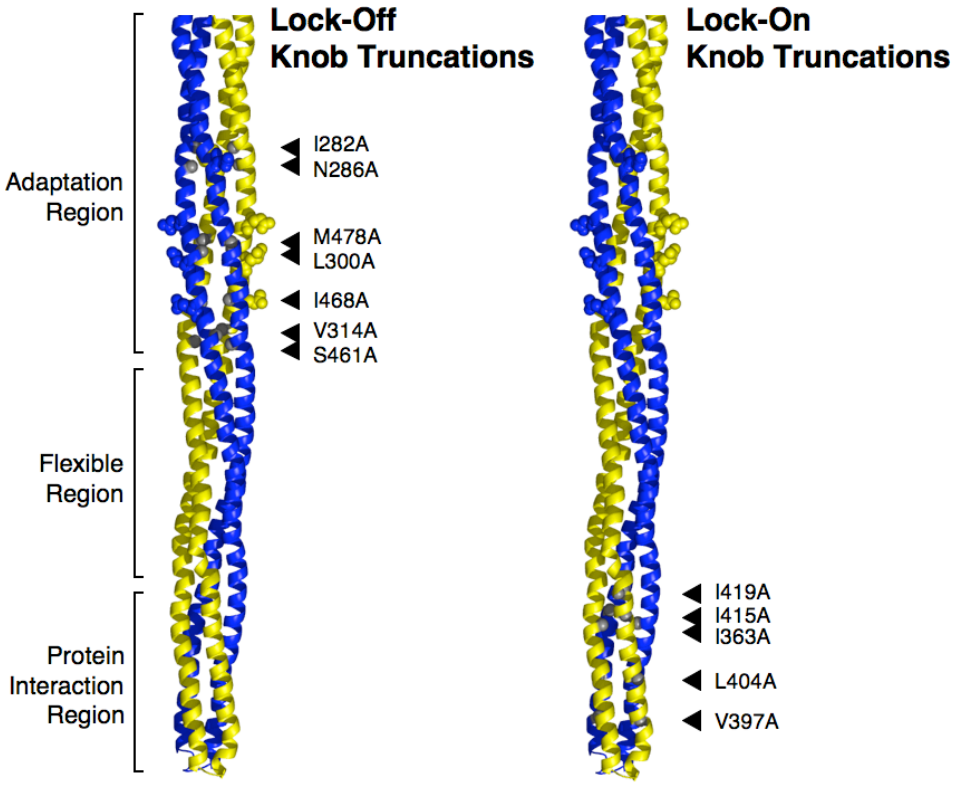

Figure 8. Locations of lock-on and lock-off knob truncations.
Shown is the kinase control module of the receptor (Hazelbauer et al., 2008), illustrating the locations of the signal-locking knob truncations identified using the anti-symmetric activity method. Each label (arrow) highlight the position of a pair of symmetric mutations in the homodimer. Lock-on knob truncations are operationally defined by high rates of receptor-regulated CheA kinase activity, even in the presence of attractant that normally turns the kinase off, as well as low CheR methylation activity regardless of the attractant concentration. Lock-off knob truncations are defined by low rates of receptor-regulated CheA kinase activity, and high rates of CheR methylation activity, regardless of the attractant concentration (Swain et al., 2009).

Chapter 2. Structural and Functional Studies of EBV Latent Membrane Protein 1 (LMP-1) Signaling Complexes.

Introduction

Epstein-Barr virus (EBV) is the causative agent of infectious mononucleosis that is transmitted through saliva. EBV is a human γ-herpesvirus that is present in >90% of all adults. Upon infection, the virus will maintain a life long persistent infection within the host. EBV is also a human tumor virus associated with Burkitt's lymphoma (Wilson et al., 1990), Hodgkin's lymphoma (Kuppers & Rajewsky, 1998), post transplant lymphoproliferative disease (Knowles et al., 1995), and nasopharyngeal carcinoma (Sixbey et al., 1987). EBV alone is not sufficient to cause cancer. Secondary factors such as immunosuppression or environmental factors are required.

EBV targets naïve B-cells and hijacks their maturation process. Normally, a naïve B-cell comes into contact with an antigen through its B-cell receptor (BCR) and becomes activated. The activated B-cell proliferates and migrates to a follicle to create a germinal center. Infected cells can then differentiate to memory B-cells. Normal B cells require engagement of CD40 by CD40L on T cells to survive the germinal center reaction and differentiate into memory. Memory B cells leave the germinal center and enter the peripheral circulation. Viral proteins in EBV infected cells mimic the signals produced by the antigen binding BCR and CD40 to drive the B cell through EBV mediated survival, proliferation, and differentiation. This allows EBV to maintain a life long infection in the host as an infected memory B-cell that can become activated in order to replenish the infected memory pool or create virus particles to infect new hosts.

The two EBV proteins that mimic signals produced by the BCR and CD40 are latent membrane protein 2a (LMP-2a) and latent membrane protein 1 (LMP-1) respectively. LMP-2a is a membrane protein with 12 transmembrane helices and contains the same ITAM motif present in BCR that is required for signaling (Beaufils et al., 1993). LMP-1 mimics CD40 signaling and will be discussed in greater detail.

Latent membrane protein 1 is a membrane protein with an N-terminal cytoplasmic region, six transmembrane helices, and an unordered cytoplasmic region (Wang et al., 2003). LMP-1's amino acid sequence is 386 residues long with residues 1-24 in the N-terminal cytoplasmic region, 25-186 in the transmembrane region, and 187-386 in the cytoplasmic C-terminal region (Liebowitz et al., 1986). The cytoplasmic N-terminus is required for LMP-1 insertion into the membrane (Coffin et al., 2001, Martin & Sugden, 1991). The transmembrane region is required for LMP-1 oligomerization and lipid raft association (Clausse et al., 1997; Higuchi et al., 2001). The transmembrane region is also required for the constitutive activity of LMP-1 (Kaykas et al., 2001). The cytoplasmic C-terminal region of LMP-1 is required for signaling. LMP-1 activates the NF-κB, JNK, and STAT signaling pathways to trigger survival and proliferation. This results from LMP-1's ability to bind tumor necrosis factor receptor associated factors (TRAFs) to its C-terminal activation regions (CTARs) (Bishop et al., 2007; Brodeur et al., 1997; Devergne et al., 1996; Eliopoulos & Young, 1998; Huen et al., 1995; Kulwichit et al., 1998; Sandberg et al., 1997). LMP-1 possesses 3 CTARs in its cytoplasmic C-terminal region: CTAR1, CTAR2, and CTAR3 (Figure 1). CTAR1 and CTAR2 bind TRAFs and TRADD and activate NF-κB (Li & Chang, 2003). CTAR1 activates Akt signaling (Dawson et al., 2003). CTAR2 is required for JNK signaling, while CTAR3 is

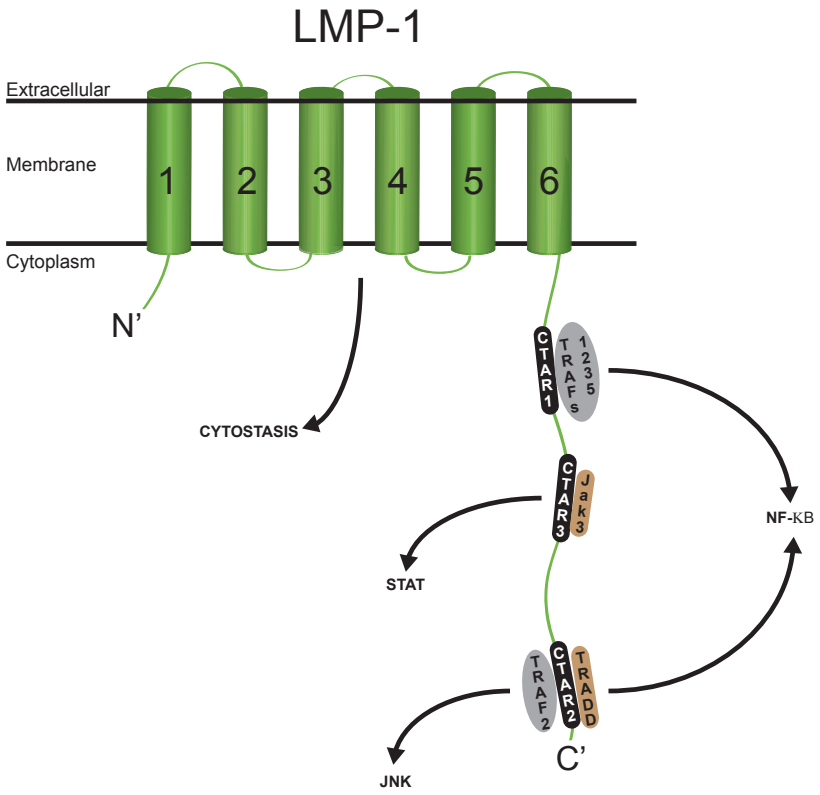

Figure 1. Structure of LMP-1
LMP-1 possesses a cytoplasmic N-terminus followed by six transmembrane helices and a cytoplasmic C-terminus. LMP-1 is involved in activating the NF-κB, JNK, and STAT pathways as well as being involved in cytostasis.

involved in STAT signaling (Gires et al., 1999). LMP-1 also possesses a non-TRAF signaling activity mediated by its transmembrane region where Tyk2 interaction leads to decreased interferon-alpha (IFN-α) signaling to promote survival (Geiger et al., 2006). LMP-1 inhibits IFN-α signaling in a TRAF independent manner. This activity requires an interaction with Tyk2.

LMP-1 signals through various pathways that are involved in B-cell survival and proliferation (NF-κB and JNK) and IFN-α inhibition. LMP-1 also has been linked to the unfolded protein response involved in cellular stress and cytostasis (Lee et al., 2009; Coffin et al., 2003; Floettmann et al., 1996; Kaykas & Sugden, 2000; Sandberg et al., 2000). How does LMP-1 interact with multiple signaling pathways? Of special interest, how does LMP-1 promote survival and proliferation while also triggering cytostasis?

The work described in this chapter is the results of studies designed to determine if LMP-1 is coupled to its multiple signaling outputs via formation of one large heterogeneous signaling complex (Mothership) or via formation of multiple distinct signaling complexes (Swarm) (Figure 2). A biochemical approach was taken in which lysates from EBV-positive lymphoblastoid cells were fractionated by size using size exclusion chromatography and LMP-1 containing the samples were affinity purified and sent for Multidimensional Protein Identification Technology (MudPIT) analysis. Concurrently, 2-D crystallographic approaches were employed to probe LMP-1's structure with the goal of better understanding LMP-1's pleotropic signaling activity.

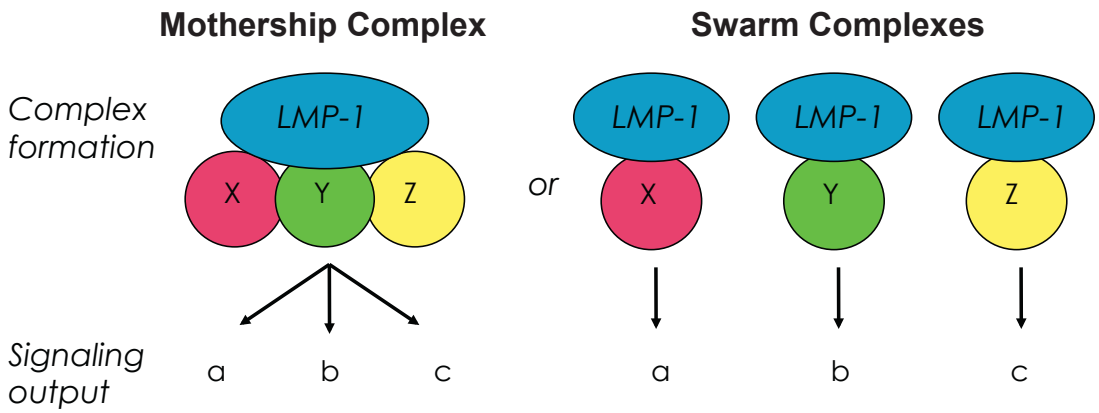

Figure 2. LMP-1 Signaling Complex or Signaling Complexes
The Mothership Complex model predicts that LMP-1 may function as a complex with multiple signaling outputs. The Swarm Complexes model predicts LMP-1 is involved in unique signaling complexes where each has their own signaling output.

Materials and Methods

Cells.

721 is an *in vitro* transformed EBV-positive lymphoblastoid cell line (Kavathas). The cell line was grown in RPMI supplemented with 10% bovine calf serum (R10C) and maintained at 37°C, in high humidity, with 5% CO_2.

Antibodies and reagents.

Anti-LMP-1 antiserum is an affinity-purified polyclonal rabbit serum raised against the C-terminus (residues 188-352) of LMP-1 fused to glutathione-S-transferase. CS1-4 is a pool of monoclonal antibodies recognizing epitopes in the LMP-1 C-terminus (Dako). Anti-LMP-1 antibodies were used at a dilution of 1:2500 (Rabbit) 1:1000 (mouse) for Western blotting. Horseradish peroxidase conjugated secondary antibodies were from Promega.

NEM treatment.

721 cells were pretreated with the membrane permeable, irreversible alkylating agent N-ethylmaleimide (NEM; 20 mM)(Pierce) at 10^6 cells/ml in R10C for 30 minutes at 37°C prior to harvest.

SDS-PAGE and Western blotting.

Samples were solubilized in 4X nonreducing SDS-sample buffer (100mM TrisHCL pH6.8, 5%SDS, 10% Glycerol, 0.02g Bromophenol Blue), sonicated, and heated to 85°C for 30 minutes. Samples were then resolved on a 10% acrylamide gel at 80V for

10 minutes and 220V for 1 hour and transferred to Immobilon (Millipore) membranes at 100V for 75 minutes. Proteins were visualized on blots following staining with primary and anti-rabbit or anti-mouse HRP- conjugated secondary antibody using ECL Plus Western Blotting Detection System (GE Healthcare). Protein standards were BenchMark Pre-Stained (Invitrogen).

Size Exclusion Chromatography.

$3x10^8$ 721 cells were treated with NEM and harvested by centrifugation, washed twice with 1xPBS, resuspended in 2 mLs of Syn 7 Buffer (50 mM NaPO4, pH 7.4, 150 mM NaCl, 25 mM sucrose, 5% glycerol, 1% Triton X-100), and lysed by vortexing for 45 minutes at 4°C. Insoluble material was removed at 13,000 RPM in a microcentrifuge for 15 min. Lysates were passed through glass wool and loaded onto a HiPrep 16/60 Sephacryl S-400 HR FPLC column (120 mL column volume) and resolved using an ÄKTApurifier chromatography system and were run at a flow rate of 0.5mL/min. Fractions were 0.681mL.

Immunoprecipitation of Column Fractions for MudPIT.

Column fractions from 721 cells were used as the starting material, precleared with protein-G agarose beads and antibody was added to the precleared supernatant for 30 minutes on ice. Immune complexes were recovered with Protein-G agarose (Roche). Beads were washed 5 times in column buffer and the protein was eluted in 50µl of 8M urea + 100 mM DTT while boiling for 30 min. Samples were allowed to cool and TCA precipitated (Sigma) to a final TCA concentration of 6.5%. Samples were pelleted and

washed with ice-cold 100% acetone (1mL) two times at 4°C. Pellets were air dried and shipped to the Yates lab for MudPIT analysis.

Baculovirus generation and Flag-LMP-1-6xHis purification.

Baculovirus vectors: Flag-LMP-1-6xHis/pFastBac1 was generated by the addition of a 6xHis tag to the LMP-1 C-terminus in FLAG-LMP-1 by PCR and then the FLAG-LMP-1-6xHis cassette was cloned into pFastBac1 (Invitrogen). Flag-LMP-1-6xHis/pFastBac1 was transformed into DH10 Bac E. coli (Invitrogen) for recombination into its resident bacmid. FLAG-LMP-1-6xHis-bacmid was purified from DH10 Bac cells and transfected into Sf9 cells to generate Flag-LMP-1-6xHis expressing baculovirus. FLAG-LMP-1-6xHis baculovirus stocks were used to infect Sf9 cells and recombinant LMP-1 was purified as described below.

Recombinant Flag-LMP-1-6xHis expression and purification: 120mLs of Sf9 cells at $2x10^6$ cells/mL were infected with FLAG-LMP-1-6xHis baculovirus and incubated for 72 hours at 27°C with shaking at 130 revolutions/min. Harvested cells were washed twice with 1xPBS and lysed in 4mL Syn7 lysis buffer (50 mM $NaPO_4$, pH 7.4, 150 mM NaCl, 25 mM sucrose, 5% glycerol, 1% Triton X-100) with 1 mM DTT and P8849 Protease Inhibitor Cocktail (Sigma) at 4°C by vortex for 45 min. Lysate was centrifuged in a refrigerated microfuge at 20,000x g for 15 min. Supernatant was filtered through a 0.45µm filter and filtered lysate was purified over a Ni-NTA column according to manufacturers directions (Qiagen). Ni-NTA column-purified eluate was then purified over a FLAG M2 affinity column according to manufacturer's directions except the

column buffers contained 0.65% Triton X-100 (Sigma). Column eluate (purified Flag-LMP-1-6xHis) was snap frozen in liquid nitrogen and stored at -80°C until use. Purification of Flag-LMP-1-6xHis was verified by Silver stain and Western blot for LMP-1.

Lipid Layer Method for Crystallizing Recombinant LMP-1.

This method is a modified version of the protocol described in Levy et al., 1999. Prior to experiments, custom Teflon plates were made with wells that measure 4mm in diameter and 2mm deep with a smaller injection hole added to the side of each well. A 27µl drop of detergent free buffer was placed in each well. 0.5µl of 1,2-dioleoyl-*sn*-glycero-3-[(N-(5-amino-1-carboxypentyl)iminodiacetic acid)succinyl] (nickel salt) (DOGS-NTA) (Avanti Polar Lipids) at 0.1 mg/mL in chloroform/methanol 9:1 (v/v) was spread on top of the droplet and left to incubate overnight at room temperature. A 3µl sample of detergent solubilized rLMP-1 in a 1:1 ratio with 1,2-dioleoyl-*sn-glycero-3-phosphocholine* (DOPC) (Avanti Polar Lipids) at 0.1 mg/mLwas injected underneath the lipid layer of DOGS-NTA using the injection hole (Figure 3A). The solution was gently mixed with a small magnetic stir bar for 1 hr at room temperature. To remove detergent and induce crystallization, 5 mg of BioBeads (BioRad) were injected into the well and allowed to incubate overnight at room temperature (Figure 3B).

Electron Microscopy of Lipid Layers

The interfacial lipid surfaces were transferred to carbon coated grids and negatively stained with 1% (w/v) uranyl acetate (Figure 3C-3D). Images were collected on a Philips CM 10 transmission electron microscope operating at 80kV.

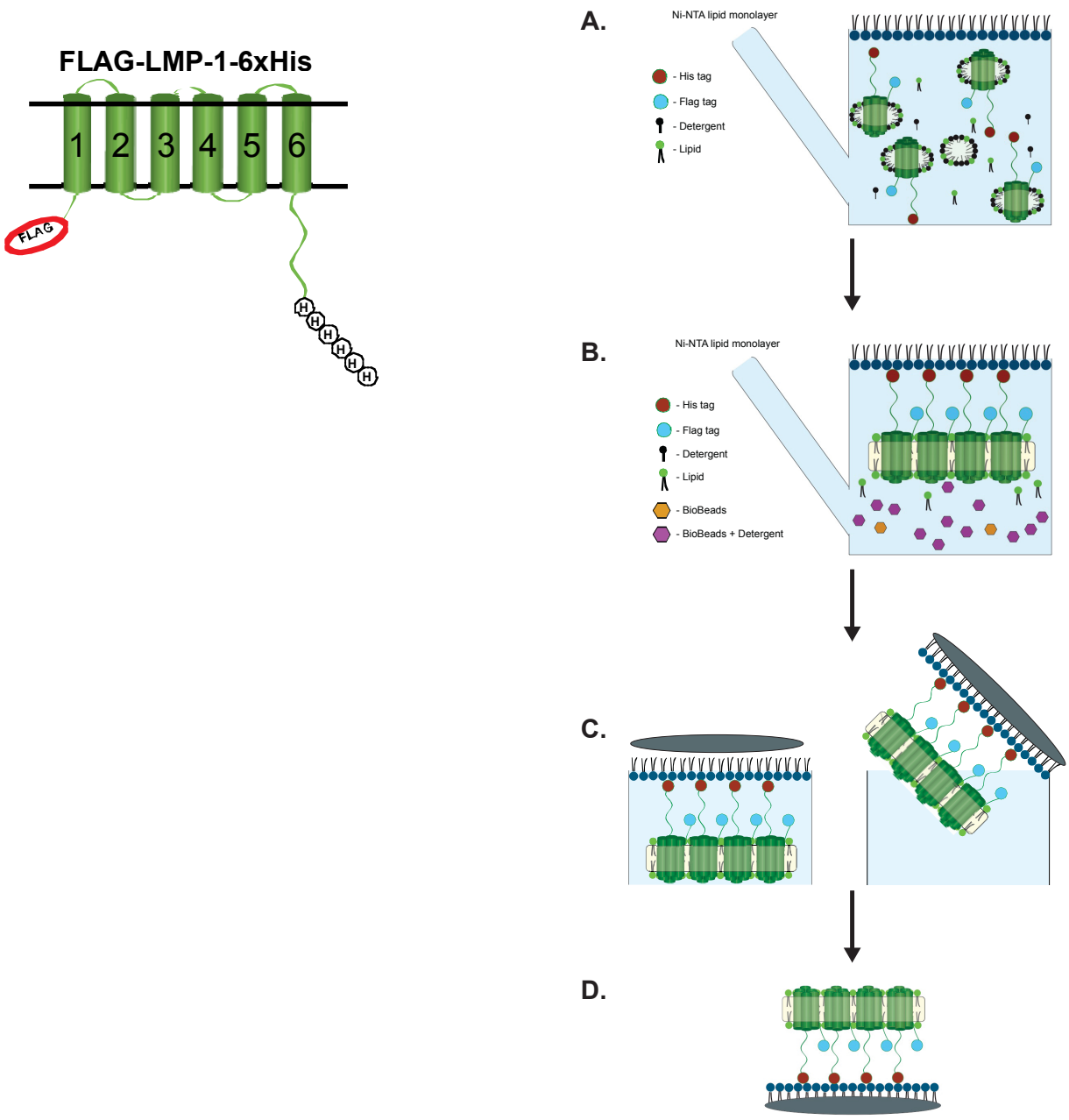

Figure 3. Lipid Layer Method for Crystallizing Membrane Proteins
This method was originally described in Lévy et al., 1999. Teflon wells were made on a plate. The wells have an injection hole to inject material underneath the lipid layer. **A)** A sample containing rLMP-1/TX-100/lipid are injected into a drop of detergent-free buffer with a Ni-NTA lipid monolayer on top. **B)** The His tag on the C-terminus binds to the Ni-NTA head group of the monolayer and concentrates rLMP-1 at the surface. BioBeads are added to remove TX-100, which will induce the reconstitution and crystallization of rLMP-1. **C)** The crystalized rLMP-1 can be collected by adhering the monolayer on to a hydrophobic carbon coated EM grid. **D)** The collected sample can then be used for negative staining and EM imaging.

Results

CHARACTERIZATION OF LMP-1 INTERACTIONS

Fractionating 721 Lysates using Size Exclusion Chromatography.

Lysates obtained from an EBV positive cell line (721) were used to identify unique LMP-1 signaling complexes. The lysate was resolved over a Sephacryl S400 column and fractionated samples were probed by SDS-PAGE and Western blot analysis to identify the samples containing LMP-1. LMP-1 was found in fractions containing markers ranging from 232 kDa to >2MDa. Western blot analysis of a fractionated 721 lysate (Figure 4) shows the typical LMP-1 elution profile. The intensities of each LMP-1 band were quantified. The intensities of each band were used to generate a graph of LMP-1 peaks after normalizing each blot using the loaded LMP-1 marker (Figure 5A). LMP-1 is present in multiple fractions. Western blot analysis of the fractions using antibodies to other signaling proteins was performed (Figures 5B-5G). Some of the signaling proteins co-elute with LMP-1 in certain fractions, while others do not. Of interest are the LMP-1 interactors CD40, Traf3, and Tyk2. In Figure 5B, CD40 is found in a single peak eluting earlier than the 440 kDa marker. The majority of Traf3 is in fractions that also contain CD40 (Figure 5E), while smaller amounts of Traf3 are also present in other LMP-1 containing fractions. Tyk2 is found in the fastest eluting LMP-1 fractions (>2MDa) (Figure 5G). These results suggest unique LMP-1 signaling complexes (swarm complexes) exist and that only one CD40/Traf3 signaling complex is present in B cells.

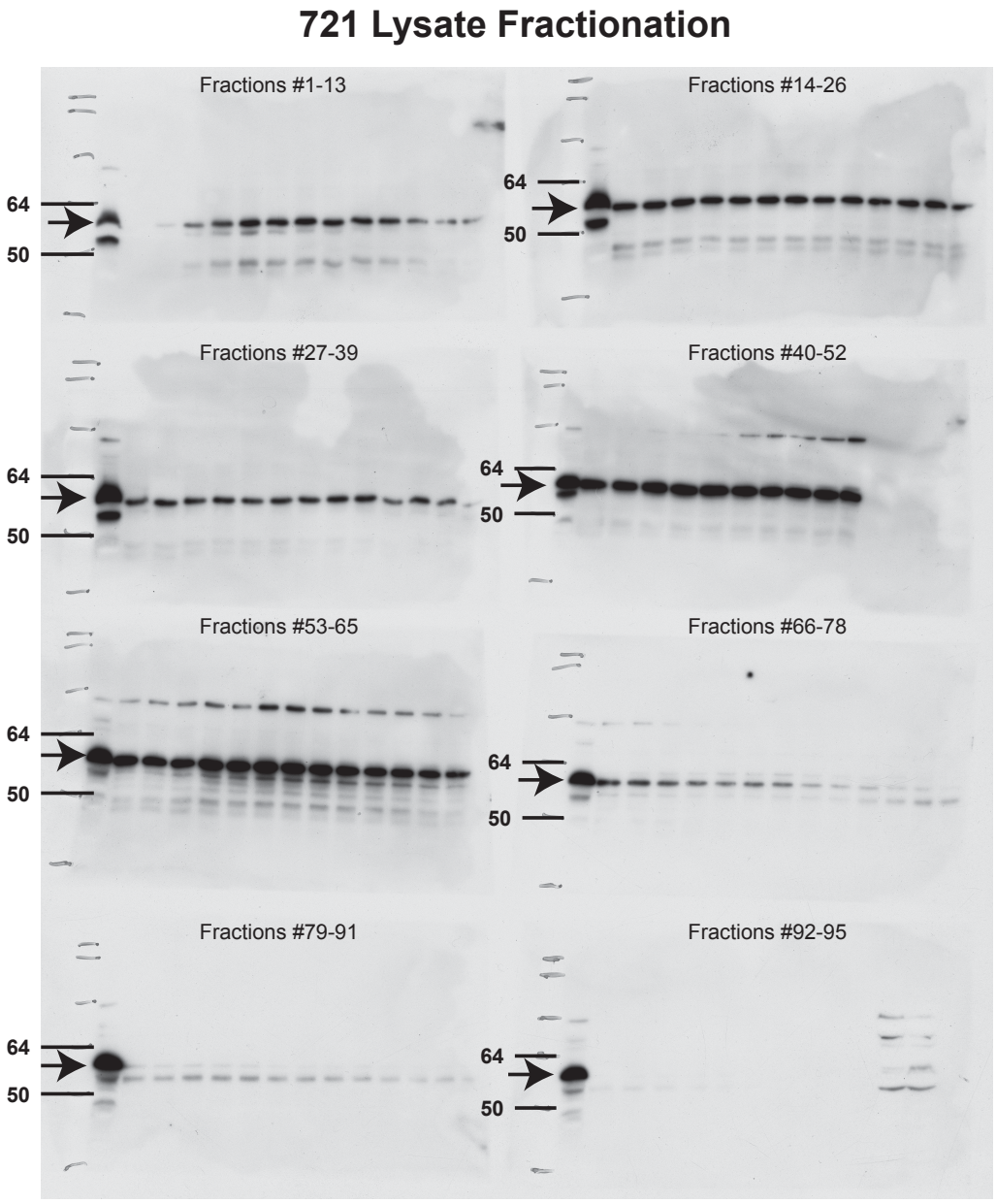

Figure 4. Size exclusion chromatography of 721 lysates.
Western blot analysis of fractionated 721 lysates. Fractions were analyzed for LMP-1 by SDS-PAGE and Western blot (anti-LMP-1). Molecular weight markers are shown on the left of each blot and fraction numbers above. The arrow identifies the location of the LMP-1 band, which is approximately 62kDa.

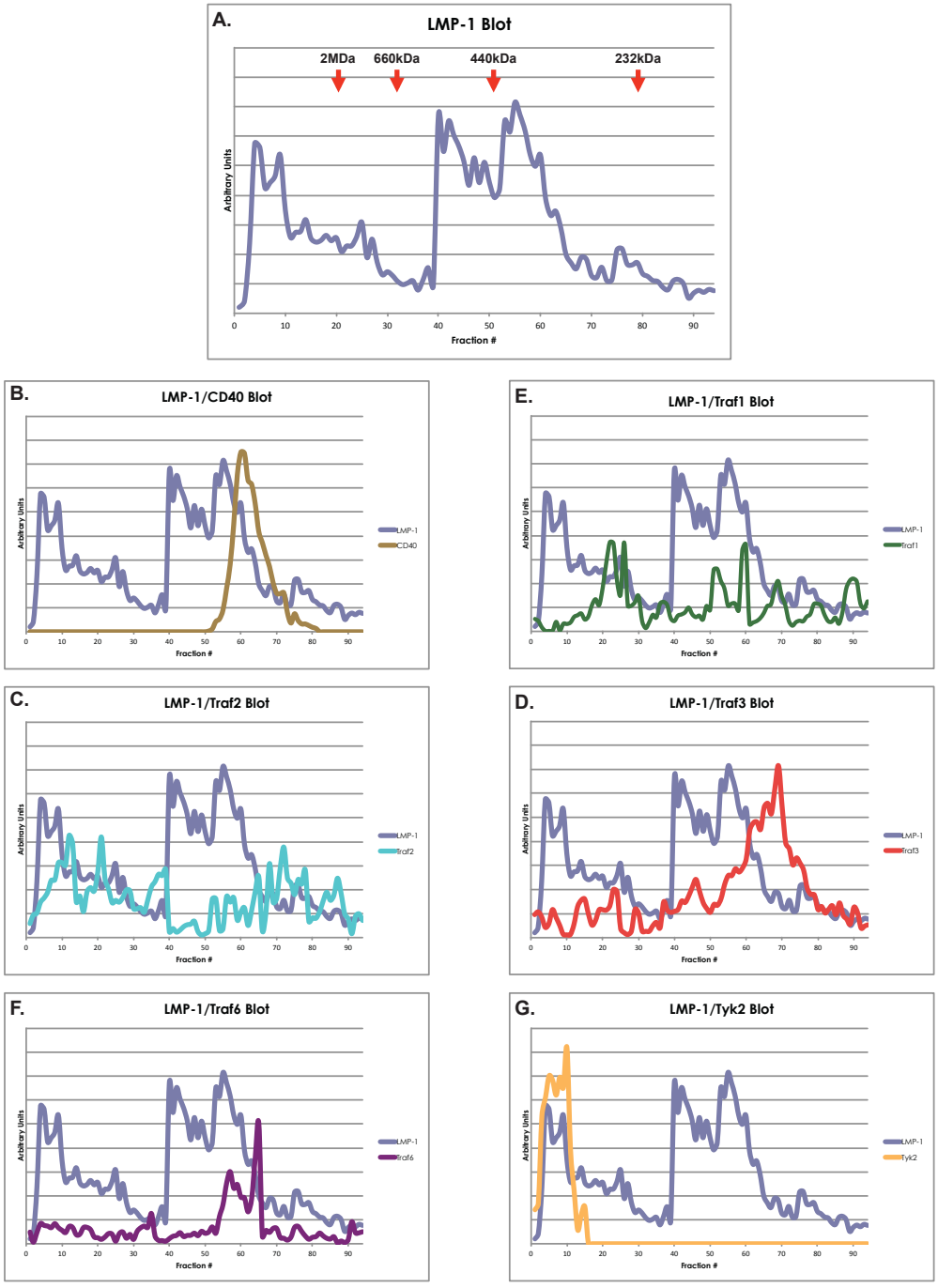

Figure 5. Identification of LMP-1 and known signaling partners in 721 lysates
LMP-1 bands in the blots shown in Fig. 4 were normalized and quantified. Results are shown in graphical form. The x-axis corresponds to the fraction number and the y-axis corresponds to band intensity. **A)** LMP-1 **B)** CD40, **C)** Traf1, **D)** Traf2, **E)** Traf3, **F)** Traf6, and **G)** Tyk2. Red arrows with their corresponding molecular weights designate elutions of molecular weight standards.

MudPIT Analysis of Selected LMP-1 Containing Fractions.

The identification multiple LMP-1 containing fractions ranging from 232 kDa to >2 MDa suggest LMP-1 may form multiple signaling complexes. To test this, peak LMP-1 containing fractions were selected for MudPIT analysis. MudPIT was performed in collaboration with the Yates lab at Scripps. Peak fractions that were selected for MudPIT analysis are shown in Figure 6A. Results of Blue Native Page analysis of samples selected for MudPIT (C.W. Figure 6B) are consistant with size exclusion data and show the molecular weight range of LMP-1 complexes. Selected fractions were immuno-affinity purified (IP and a mock-IP) and sent for MudPIT analysis in order to exclude false positives (Figure 7).

LMP-1 was identified in each sample but no interacting proteins were found. Keratin contamination was likely a contributing factor.

STRUCTURAL ANALYSIS OF LMP-1

Expressing Recombinant LMP-1 using Baculovirus Expression System.

2-D crystallographic analysis of LMP-1 requires large amounts of pure LMP-1 protein. A recombinant LMP-1 (rLMP-1) expression vector (FLAG-LMP-1-6xHis) was employed for baculovirus expression (engineered by Aaron Robitaille). rLMP-1 expression from this vector possesses an N-terminal FLAG tag and a C-terminal 6x His tag (Figure 8A). This baculovirus expression system generates large amounts of rLMP-1 in Sf9 insect cells (Figure 8B). Overexpressed LMP-1 was purified sequentially with Ni-NTA affinity resin and FLAG affinity resin (Figure 8C-8D). This method produced 500 ul of 0.1mg/mL of rLMP-1. Purified recombinant LMP-1 was used in preliminary 2-D

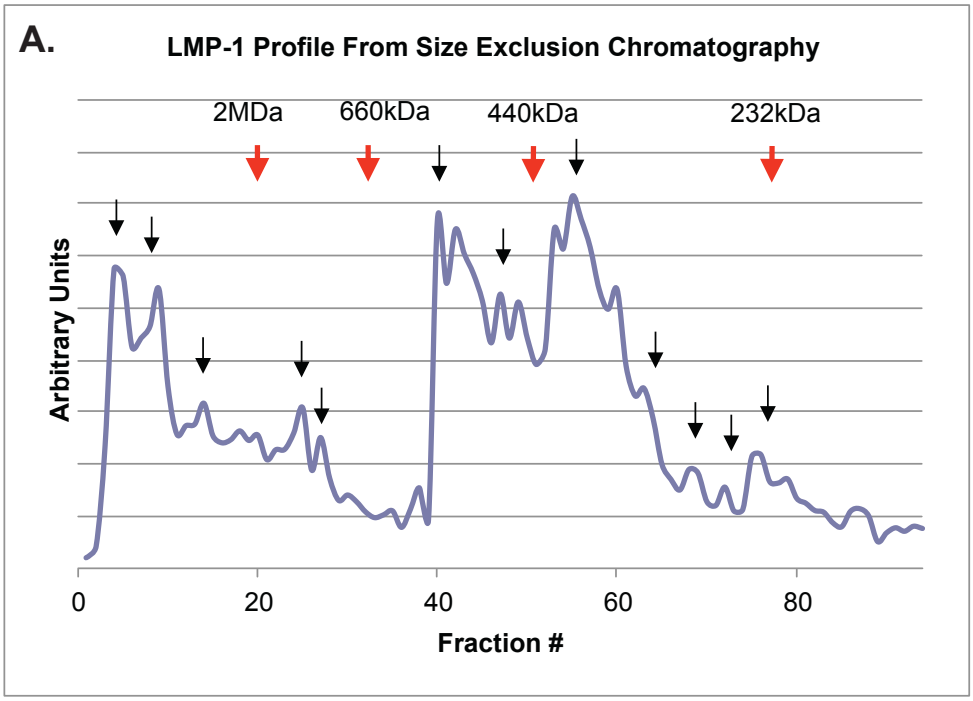

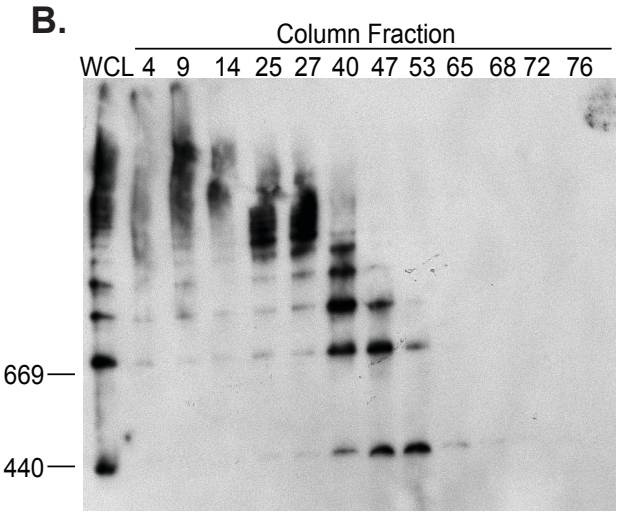

Figure 6. Selecting LMP-1 enriched samples for MudPIT
Fractions from the column elution shown in Figure 5A **(A)** were analyzed by Blue Native PAGE **(B)**. Black arrows in **A** mark the fractions analyzed by Blue Native PAGE in **B** and subsequently analyzed by MudPIT.

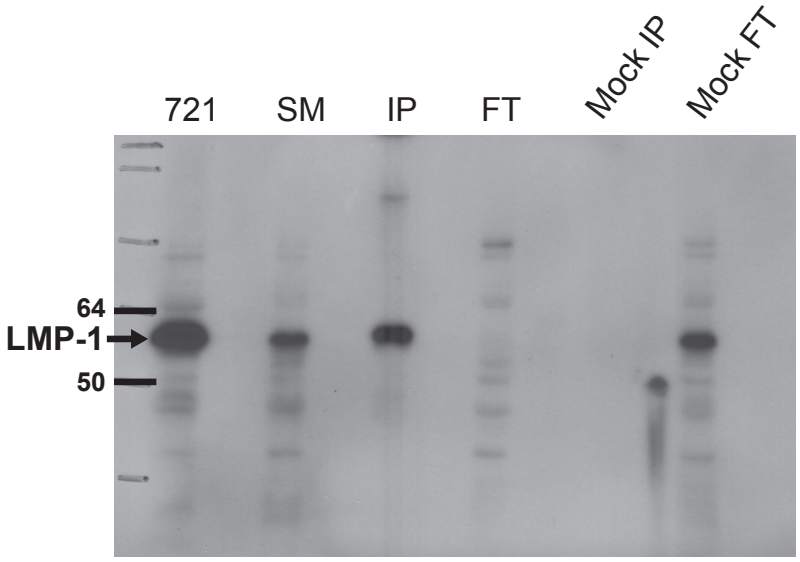

Figure 7. Immunoprecipitation of LMP-1 Enriched Fractions
A representative Western blot showing an LMP-1 IP sample and a mock IP sample analyzed by MudPIT.

crystallization experiments (results not shown). Further work was required to optimize crystallization conditions.

Discussion

My project was aimed at identifying unique LMP-1 signaling complexes. Size exclusion chromatography revealed multiple high molecular weight complexes (ranging from 232kDa to >2MDa). LMP-1 containing fractions were selected and affinity purified by immunoprecipitation and analyzed by MudPIT. Unfortunately, the only protein detectable was LMP-1 itself and keratin. Keratin contamination may have masked the signal of other proteins present but it was not possible to know with certainty. Another possibility is that the conditions of the immunoprecipitation were too stringent and LMP-1 interactors were lost during purification. Optimization of IP conditions would be helpful in determining if this was the cause of the negative MudPIT results.

By using a LMP-1 baculovirus expression system I was able to produce rLMP-1 in amounts necessary for 2D electron crystallography. This project required a time investment to become proficient with 2D crystallization techniques, training on the electron microscope (EM) for both cryo-electron microscopy and negative staining, and learning how to use the software for data analysis. Several attempts were made to form 2D crystals but ultimately there was not enough time to finish this project.

Ultimately, I enjoyed working on this project very much. It was very challenging and required the ability to merge different areas of science. Although I was unable to obtain publishable results during the time I devoted to the project, I believe the reagents and methodology are sufficiently developed so that this project results yield important if pursued further.

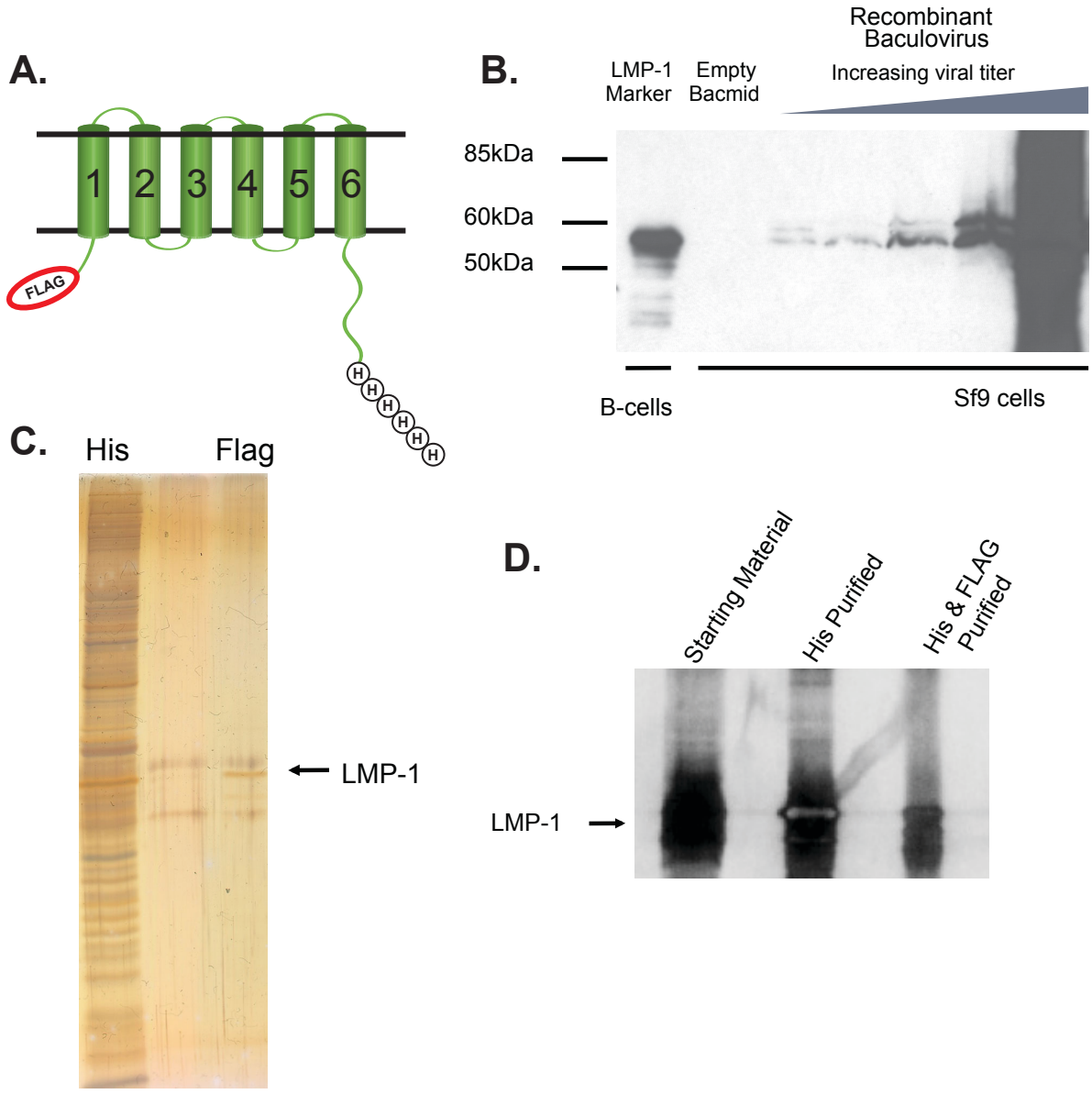

Figure 8. Recombinant LMP-1 Expression and Purification for 2D Electron Crystallography

A) rLMP-1 possesses an N-terminal FLAG tag and a C-terminal 6x His tag. **B)** Abundant amounts of rLMP-1 were expressed using the baculovirus expression system. **C)** Purified rLMP-1 analyzed by SDS-PAGE and silver staining. **D)** The presence of rLMP-1 was verified by Western blot analysis.

Chapter 3. Structural Studies of Kar3Cik1 using Cryo-Electron Microscopy and Helical Reconstruction.

Introduction

Microtubules are an essential element of eukaryotic cells. They are involved in many aspects of the cell's cytoskeleton and organelles including but not limited to flagella, cilia, and centrioles. They are a key player during mitosis and are involved in moving vesicles, granules, organelles, and chromosomes during interphase as well as mitosis (reviewed in: McIntosh et al., 2002). Microtubules are formed from tubulin heterodimers, which are comprised of α-tubulin and β-tubulin. The tubulin dimers polymerize into protofilaments and multiple protofilaments form a microtubule (Figure 1). Protofilaments are long linear strings of subunits joined end to end. In the cell, typically 13 protofilaments come together to form a hollow tube, which is the microtubule with a diameter of 25 nm. Microtubules are polar structures with a highly dynamic plus-end, exhibiting rapid grow and shrinking rates, (Mandelkow & Mandelkow, 1985) whereas the minus-end is less dynamic and often anchored in so-called microtubule-organizing centers (MTOCs). During interphase the minus end points towards the cell center (nucleus) and the plus-end is oriented towards the periphery. During mitosis the plus-ends contact kinetochores, and are oriented towards the spindle mid region. In cells, a GTP cap stabilizes the microtubules plus-ends, when the cap is hydrolyzed to GDP it leads to microtubule depolymerization (Mandelkow & Mandelkow, 1985; Kirschner & Mitchison, 1986; reviewed in: Desai & Mitchison, 1997).

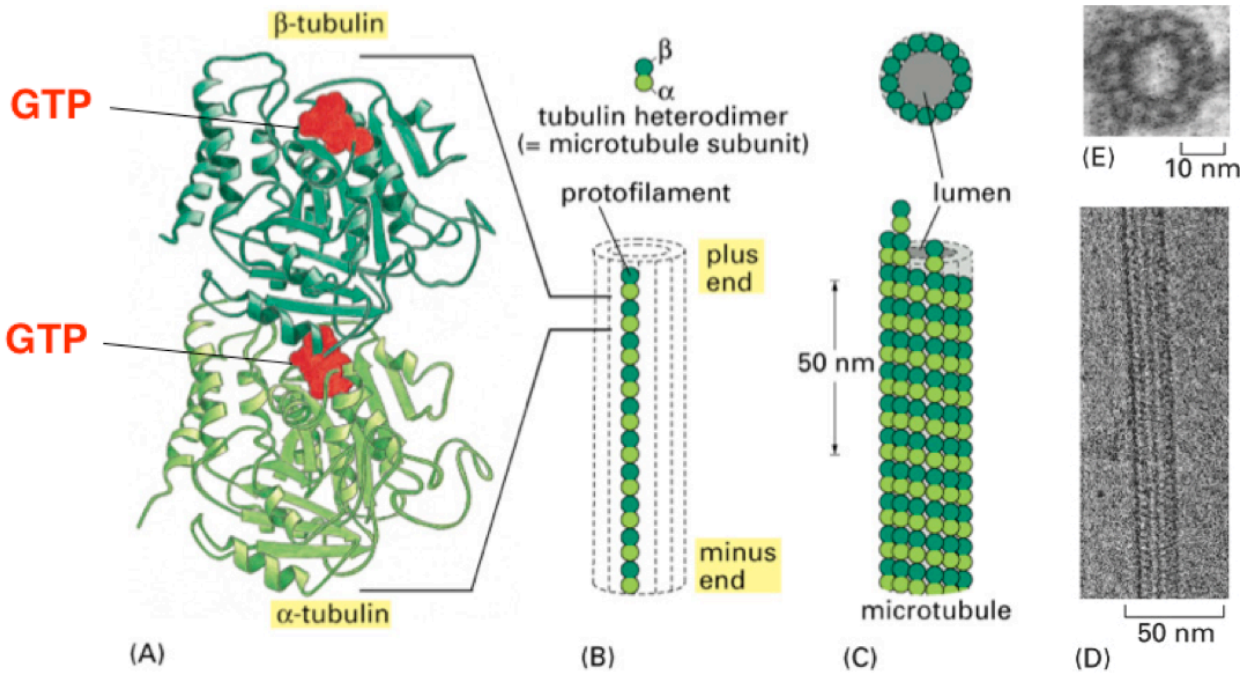

Figure 16–6. Molecular Biology of the Cell, 4th Edition.

Figure 1. Microtubule Structure.
Microtubules are assembled from αβ-tubulin heterodimers **(A)**. **B)** The tubulin dimers come together to form protofilaments, which resemble strings of dimers. **C)** The strings come together to form a hollow tube that is the microtubule. **D)** An EM micrograph of a microtubule, the tubulin is visible in the image. **E)** A cross-sectional view shows the protofilaments that form the hollow tube.

In *Saccharomyces cerevisiae*, microtubules are involved in nuclear migration, chromosome segregation, and karyogamy (nuclear fusion: Neff et al., 1983; Huffaker et al., 1988; Stearns, 1990). Microtubules originate at the cell's MTOC's or spindle pole bodies (SPB). During nuclear migration, cytoplasmic microtubules ensure that the mother and daughter cell get a single SPB as well as one complete copy of the genome (Figure 2). During chromosomal segregation nuclear microtubules attach to the kinetochores of the chromosomes and separate them so each cell get a single copy of the genome. During karyogamy, cytoplasmic microtubules from each nuclear envelope interdigitate to bring the nucleus of each cell together for nuclear fusion (reviewed in: Rose, 1996). Microtubules alone are not capable of performing these functions; these processes require a tightly regulated interaction between microtubules, molecular motors and other microtubule-associated proteins (MAPs) (reviewed in Molk & Bloom, 2006).

Molecular motors of the kinesin family (for a standardized nomenclature see: Lawrence et al., 2004) interact with microtubules and drive the functions described above. In budding yeast, there are six kinesin genes and one dynein gene (Meluh & Rose 1990). Kinesin motors consist of a motor domain, an α-helical coiled coil, and a cargo binding tail. The majority of kinesins form homodimeric coiled-coil interactions, some form hetero-dimers, and a few act as monomers (reviewed in Vale, 2003). The motor domain consists of two major parts: a globular catalytic core consisting of six helices with three covering either side of an eight-stranded β-sheet and a neck region required for directionality and movement (Vale & Fletterick, 1997; Case et al., 1997). The globular region contains a nucleotide pocket for ATP binding and a microtubule-

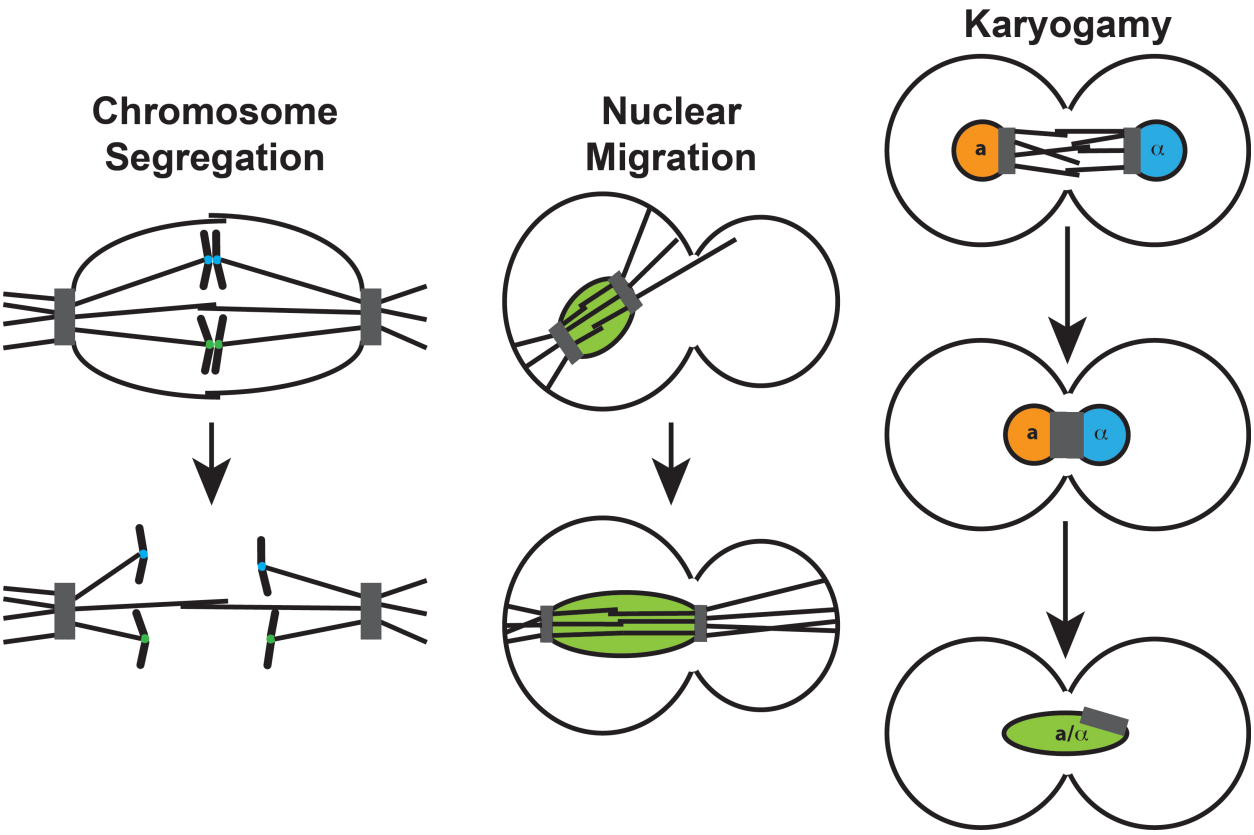

Figure 2. Microtubule Functions in *Saccharomyces Cerevisiae*.
In eukaryotes, microtubules are involved in many cellular roles. In budding yeast, microtubules play three specific roles: chromosome segregation, nuclear migration, and karyogamy.

binding site (Vale & Fletterick, 1997). Directionality of the motor appears to be linked to the neck region that connects the motor domain to the coiled-coil stalk consist of 13 residues (Sablin et al., 1998). Mutational analysis of the neck region has shown that it is essential for directionality and generating force in kinesin-14s (Henningsen & Schliwa, 1997; Sablin et al., 1998; Endow & Waligora, 1998; Endres et al., 2006; Cross, 2010).

Kinesin-1 (previously called conventional kinesin) was the first discovered kinesin (Vale et al., 1985; Brady, 1985) among the currently 14 families. It is involved in transporting organelles and lysosomes in cells. Kinesin-1 is a homodimeric plus end directed motor with a heavy chain composed of N-terminal motor domain and a coiled coil stalk region, and a light chain forming the C-terminal cargo-binding domain (reviewed in Vale, 2003; Figure 3A). It functions as a homodimer where it used both motor heads to move along microtubules in a processive manner at a rate ~45 μm/min (Hancock et al., 1998).

Of the six kinesins found in *S. cerevisiae*, only one of them belongs to the kinesin-14 family. Kinesin-14s are so far the only kinesins we know that have their motor domain at the C-terminal end of the polypeptide chain, and all of them seem to be non-processive, retrograde motors. Hence, kinesin-14s contribute to an inward directed force towards the minus-end of the microtubules (Saunders & Hoyt, 1992; Sharp et al., 1999; Gardner et al., 2008). Probably the most extensively studied kinesin-14 has been ncd from *Drosophila melanogaster* (McDonald et al., 1990), which plays a role in meiosis and mitosis (for structural investigations see: Sablin et al., 1996; Wendt et al., 2002; Fink et al., 2009). It is required for proper chromosome distribution and may have

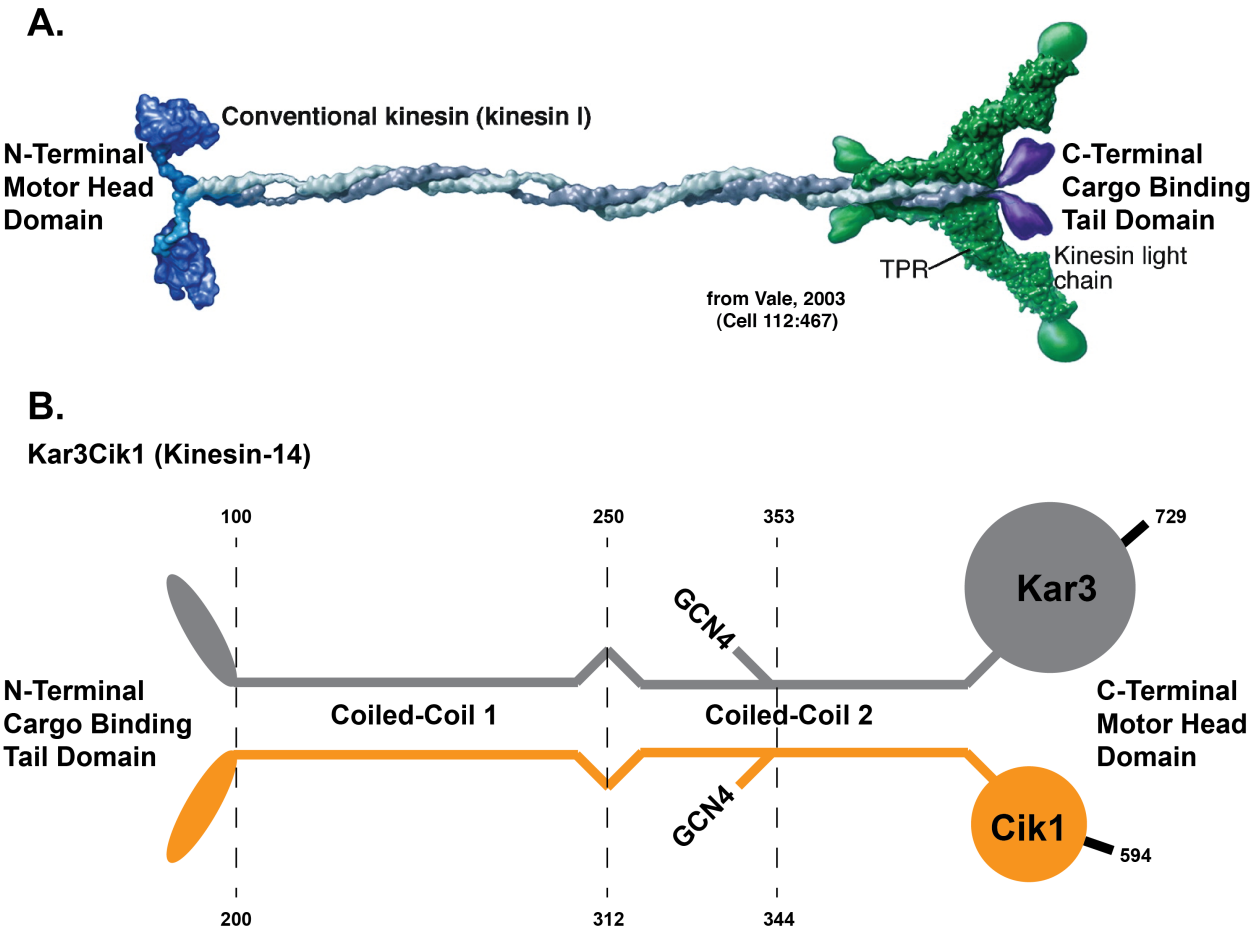

Figure 3. Kinesin Structure.
A) Kinesin-1 was the first identified kinesin (Vale et al., 1985; Brady 1985). It forms a homodimer and possesses an N-terminal motor domain followed by a coiled-coil region connecting it to a C-terminal cargo-binding region. The homodimer appears to be held together by the coiled-coil region. Kar3Cik1 possesses a similar structure to kinesin-1 with certain exceptions. **B)** Kar3Cik1 is a heterodimer comprised of Kar3 and Cik1. Kar3 possesses a motor head with ATPase activity while Cik1's motor head has none. Kar3Cik1 has an N-terminal cargo-binding region followed by a coiled-coil region that connects to a C-terminal motor domain. For the experiments described in this chapter, a truncated version of Kar3Cik1 was used where Kar3 and Cik1 begin in coiled-coil 2 and the heterodimer is held together with the help of a GCN4 leucine zipper motif (provided by Ivan Rayment, University of Wisconsin, Madison).

a role in spindle assembly, maintenance and spindle pole formation in meiosis (Endow et al., 1994; Oladipo et al., 2007). Ncd crosslinks antiparallel microtubules with its microtubule-binding site on the cargo-binding end, and translocate them toward the minus ends at a rate between 4-15 μm/min (Walker et al., 1990; Endow et al., 1994).

The kinesin-14 found in budding yeast is Kar3. Kar3 like ncd and all other kinesin-14s is a COOH-terminal motor that crosslinks microtubules similar to ncd, and Kar3 is involved in karyogamy and mitosis (Meluh & Rose, 1990; Rose, 1996). Kar3 is essential for yeast nuclear fusion during mating. Its expression is induced by an α-factor, and is not essential for mitotic growth (Meluh & Rose, 1990). The structure of Kar3 has been solved and like all other kinesin motor domains exhibits eight stranded β-sheet with six helices where three are on either side (Gulick et al., 1998).

Kar3 functions as a heterodimer with either Cik1 or Vik1, depending on the circumstances (Figure 3B). Kar3Vik1 is involved in mitotic cells (Manning et al., 1999) and an EM structure has previously been reported; Cope et al., 2010) as well as a X-ray crystal structure (Rank et al., 2012). In contrast to Kar3Vik1 Kar3Cik1 participates in spindle formation and karyogamy in mating cells. Upon pheromone treatment, Kar3Cik1 localize to spindle pole bodies (SPB) and cytoplasmic microtubules via Cik1 localization (Page et al., 1994). Kar3Cik1 depolymerizes microtubules from their plus ends and promotes minus end directed microtubule gliding (Page & Snyder, 1992; Sproul et al., 2005). Karyogamy is facilitated in part by Kar3Cik1's ability to depolymerize microtubule plus ends attached to the shmoo tip (Page et al., 1994; Maddox et al., 2003). A shmoo is a projection of the cell during mating that gives rise to a pear-like appearance. Cik1 is not essential for mitotic growth (Page et al., 1994; Manning et al., 1999). In mitotic cells,

Kar3Cik1 is localized at the mitotic spindle and may have a role in chromosome segregation and spindle assembly (Meluh & Rose, 1990; Page et al., 1994).

Here we report an intermediate resolution 3-D structure of Kar3Cik1 obtained by cryo-electron microscopy and 3-D image reconstruction based on the helical symmetry of microtubules composed of 15 protofilaments (Arnal et al., 1996; reviewed in Hoenger and Gross, 2008). The most common form of microtubule, composed of 13 protofilaments is not helical and carries a so-called seam between two protofilament (directly visualized by Kikkawa et al., 1994; McIntosh et al., 2009) that interrupts the symmetry of the B-lattice (Amos & Klug, 1974). We have studied the conformation of a heterodimeric Kar3Cik1 motor domain construct (provided by Dr. Ivan Rayment, University of Wisconsin, Madison) in the presence of ADP and AMP-PNP (mimicking an ATP state) as well as in the absence of nucleotides. Our results show that when ADP is bound to Kar3Cik1 it has a reduced affinity for microtubules, which is a quite common observation for most kinesin motor domains studied so far. In the nucleotide-free state, Kar3Cik1 decorates microtubules with a very high affinity, filling every available binding site with one dimeric motor construct. Consequently Kar3 is in contact with the microtubule, while Cik1 is oriented away. Therefore the coiled coil stalk points towards the plus end of the microtubule. In the ATP state, Kar3Cik1 completely decorates microtubules with a very high affinity. Again Kar3 is in contact with the microtubule whereas Cik1 is oriented outward. However, there is a significant conformational difference to the nucleotide-free state. The stalk rotates approximately 65° and now points toward the minus end of the microtubule. Comparing the structures of Kar3Cik1 and Kar3Vik1 shows that both dimeric constructs act very similarly and show almost

identical 3-D conformations and binding patterns. The question of how Kar3Cik1 and Kar3Vik1 can perform completely different functions in the cell and have the same structure and mechanism of force transduction still needs to be addressed.

Material & Methods

Microtubule polymerization

Microtubules were polymerized *in vitro* from 45 μM bovine brain tubulin (Cytoskeleton, Inc., Denver, CO) with BRB80 (80 mM PIPES, pH 6.8, 1 mM $MgCl_2$, 1 mM EGTA) in the presence of 15% (v/v) DMSO as described previously (Cope, Thesis Dissertation).

Expression and purification of WT GCN4-Kar3Cik1

GCN4-Kar3Cik1 was expressed and purified in the lab of Ivan Rayment at the University of Wisconsin, Madison WI similarly to previously reported methods (Sproul et al., 2005, Allingham et al., 2007). GCN4-Kar3Cik1 is a truncation of Kar3Cik1 containing residues Lys_{353} - Lys_{729} of Kar3, and Asn_{344} – Asp_{594} of Cik1. The complete C-terminal globular domains of Kar3 and Cik1 plus part of native coiled-coil stalk through which Kar3 and Cik1 heterodimerize were included. A GCN4 leucine zipper sequence was encoded onto the N-terminus of the truncated Kar3Cik1, which was used to initialize dimerization.

Vitrification of GCN4-Kar3Cik1-MT complexes for cryo-EM

GCN4-Kar3Cik1-MT complexes were assembled directly on holey carbon C-flat grids (Protochips, Inc., Raleigh, NC) as described (Cope, Thesis Dissertation) with the following exceptions. Polymerized MTs were diluted to 2.25 μM with BRB80. 13.55 μM GCN4-Kar3Cik1 in ATPase buffer (20 mM HEPES pH 7.2, 5 mM magnesium acetate,

50 mM potassium acetate, 0.1 mM EDTA, 0.1 mM EGTA, 1 mM DTT) or BRB80 was added to the MTs for 90-120 s.

ADP state

GCN4-Kar3Cik1 at a final concentration of 13.55 μM in ATPase buffer with 5% sucrose and 1 mM ADP was incubated at room temperature for 10 min. MTs at a final concentration of 2.25 μM were added to the GCN4-Kar3Cik1-ADP and incubated for a further 15 min. A droplet of GCN4-Kar3Cik1-ADP - MT complexes was applied to a holey carbon grid and vitrified as described above.

Nucleotide-free state

The nucleotide-free state was obtained as previously described (Cope, Thesis Dissertation). GCN4-Kar3Cik1 was diluted to 13.55 μM with ATPase buffer and 1 unit of apyrase.

ATP state

ATP bound GCN4-Kar3Cik1 was obtained using the non-hydrolyzable ATP analog adenylyl imidodiphosphate tetralithium salt (AMP-PNP) (Sigma, St. Louis, MO) as previously described (Cope, Thesis Dissertation) with the following exception, GCN4-Kar3Cik1 was at a final concentration of 13.55 μM.

Cryo-EM data collection

Data collection was done as previously described (Cope, Thesis Dissertation) using an FEI Tecnai F20 (FEI-Company, Eindhoven, The Netherlands) and 4K x 4K Gatan Ultrascan CCD (Gatan, Inc, Pleasanton, CA).

Results

Structure of Kar3Cik1 in Complex with Microtubules

Polymerized and taxol-stabilized microtubules were mixed 1:6 with Kar3Cik1 heterodimers that were incubated with either ADP, apyrase to generate the nucleotide-free state, or AMP-PNP a non-hydrolyzable ATP analog to generate the ATP bound state. AMP-PNP has been widely used in the past to induce ATP-like conformations into kinesins (e.g. see Sosa et al., 1997; Hoenger et al., 1998) and myosins (e.g. see Jontes et al., 1995; reviewed in Vale & Milligan, 2000) Vitrified samples were obtained by plunge freezing Kar3Cik1 and microtubules in liquid ethane on holey carbon grids. Images of samples were collected using cryo-electron microscopy (Kar3Vik1 by Julia Cope) (Figure 4). The collected images were screened for 15 protofilament microtubules that are decorated with motor proteins, which can be used for helical reconstruction using the PHOELIX/SUPRIM image-processing package (Whittaker et al., 1995; Schroeter & Bretaudiere, 1996). For cryo-EM experiments the samples that were incubated in the presence of excess ADP (10 mM) resulted in empty microtubules with no Kar3Cik1 decoration (Figure 5A). The lack of decoration with ADP can also be seen in the Fourier transform with the presence of the 4 nm layer line corresponding to the tubulin repeat but the lack of an 8 nm layer line which corresponds to the motor repeats, binding to each αβ-tubulin dimer (Figure 5A).

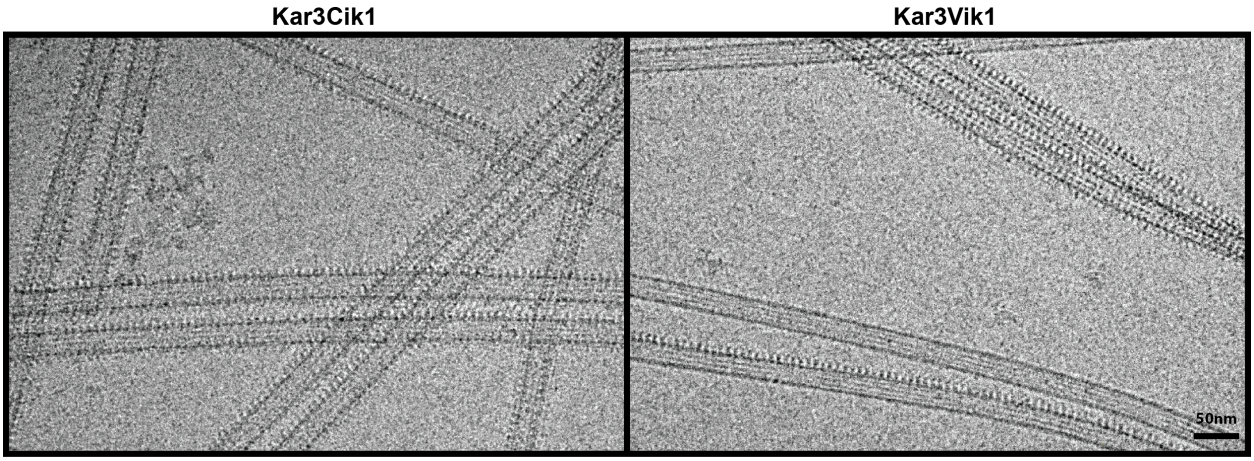

Figure 4. Cryo-EM Raw Images.
Images were collected on a Tecnai F20 TEM running at 200kV with a magnification of 29,000x using a Gatan 4k x 4k Ultracam. Microtubules in the image were incubated with apyrase to generate the nucleotide-free state. Kar3Cik1heterodimers can be seen in contact with the microtubules. In the apyrase state, Kar3Cik1 has a stronger affinity for microtubules as can be seen by complete decoration. Kar3Vik1in comparison appears to have more cooperative binding than Kar3Cik1. Individual microtubules are selected for further processing using PHOELIX. Kar3Vik1 image courtesy of Julia Cope.

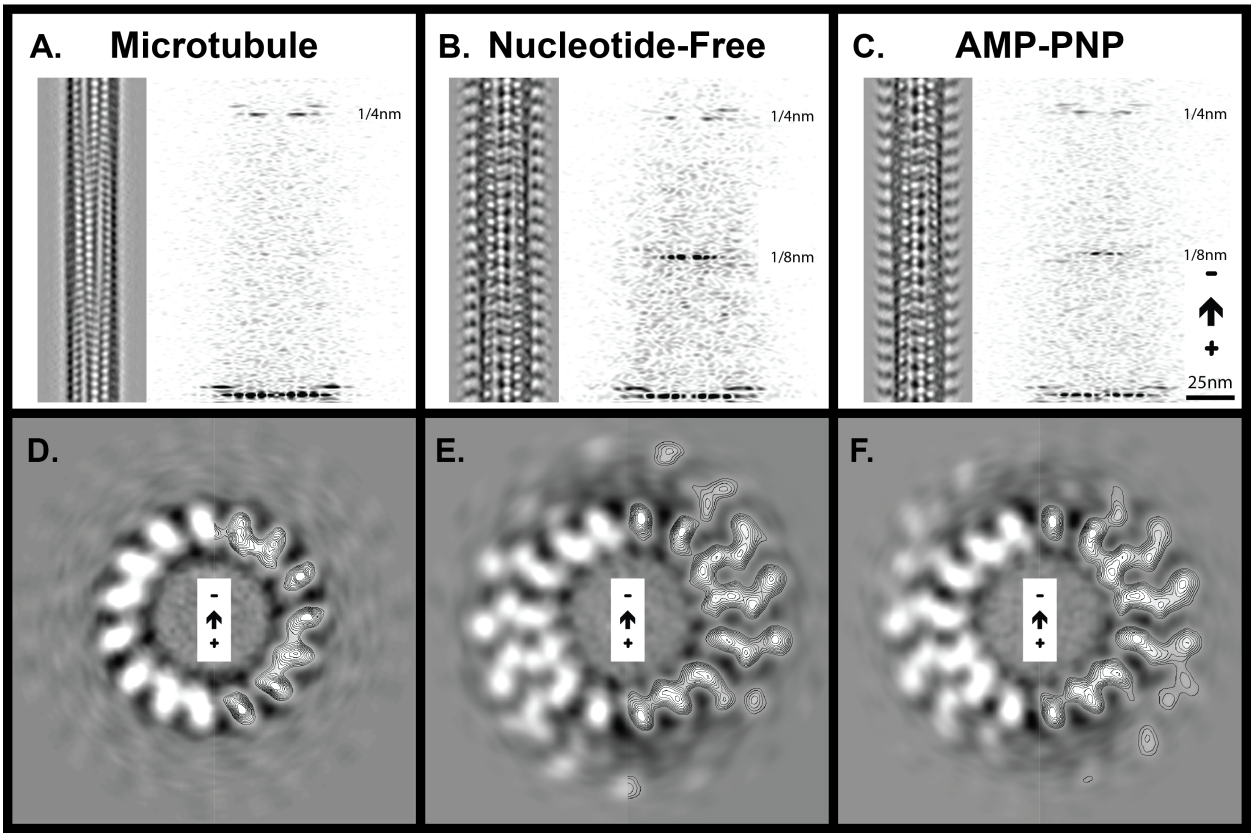

Figure 5. 3-D Helical Reconstruction of Decorated and Undecorated Microtubules. PHOELIX was used to process individual microtubules obtained from cryo-EM images(compare Fig. 4). Individual microtubules were straightened and analyzed to determine if they were 15 protofilament microtubules. Data collected was put into datasets that were averaged and used to reconstruct a 3-D microtubule. **A)** Reconstruction of a microtubule obtained by incubating Kar3Cik1 motors with ADP prior to addition to microtubules. A Fourier transform of the 3D reconstructed microtubule is to the right. The 4 nm layer line, which corresponds to the tubulin repeats, is clearly visible. **B)** Reconstruction of a Kar3Cik1 decorated microtubule in the nucleotide-free state. Two dark spots are visible at each motor subunit corresponding to Kar3 and Cik1. The Fourier transform reveals that along with the 4 nm layer line (tubulin repeats) there is also an 8 nm layer line, this corresponds to the motor repeat which happens every 8 nm. **C)** Reconstruction of the ATP state using the non-hydrolyzable ATP analog AMP-PNP. The microtubule is fully decorated with Kar3Cik1 as in (B). The Fourier transform shows that the 4 nm and 8 nm layer lines are present. A cross-sectional view of the reconstructed microtubules can be seen below **D)** naked microtubule, **E)** nucleotide-free, and **F)** ATP. On the right side of each image contour lines are shown depicting densities observed from tubulin and Kar3Cik1.

However, while cryo-EM data essentially revealed empty tubes there is some sparse decoration detectable with high-resolution surface metal shadowing (Figure 6A). The data from ADP-Kar3Cik1 is compared to ADP-Kar3 homodimers and ADP-ncd (Figure 6B-6C). In all of these cases (as well as with ADP-Kar3Vik1 (Rank et al., 2012, in press) it appears as if all of these kinesin-14 dimers adopt a dimeric binding configuration that bridges two adjacent protofilaments. While this configuration is not always obvious, it becomes clear that all of these kinesin-14 dimers (including the Kar3 homodimer) exhibit a very different binding conformation from motors such as dimeric kinesin-1 or kinesin-5 (Eg5; see Krzysiak et al., 2006). At least in the presence of AMP-PNP, or in a nucleotide-free state, these anterograde motor constructs clearly bind with both motors along one single protofilament.

Incubation of kinesin motors with apyrase creates a nucleotide free state as the nucleotides are digested to AMP and phosphate. In the nucleotide-free state of Kar3Cik1, the microtubules are completely decorated. The Fourier transform confirms full decoration through the presence of a strong 8 nm layer line corresponding to the motor repeats. As for undecorated microtubules, the 4 nm layer line corresponding to the tubulin monomer repeat is very strong as well (Figure 5B). In the ATP state of the Kar3Cik1 generated by the use of AMP-PNP, the microtubules are again completely decorated and the completeness on decoration can be confirmed from the layer line intensities in the Fourier transform (Figure 5C). By displaying a single cross-sectional slice with ~0.5 nm thickness and a pixel size of 3.8 Å through the reconstructed microtubules we can see the different densities corresponding to tubulin (Figure 5D), tubulin-Kar3Cik1 in the nucleotide-free state (Figure 5E), and tubulin-Kar3Cik1 in the

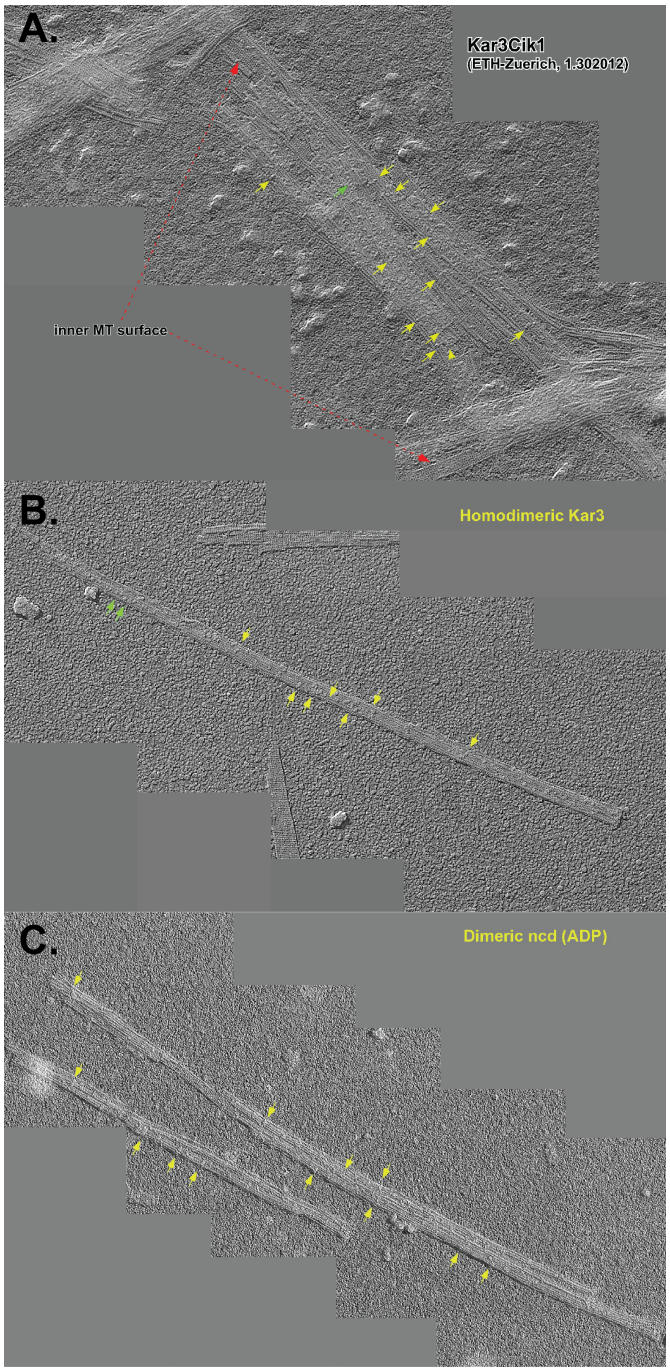

Figure 6. High-Resolution Surface Metal Shadowing of Kinesin Motors.
Kinesin motors bound to ADP were incubated with microtubules at sub stoichiometric levels and coated in a heavy metal. Kinesin motors are identified by a yellow arrow **A)** Kar3Cik1, **B)** Kar3 homodimer, **C)** dimeric ncd. The kinesin-14s motors appear to bind sparsely along the microtubules and bridge adjacent protofilaments.

ATP bound state (Figure 5F). On the right half of the images the densities are depicted with contour lines outlining different density levels that correspond either to tubulin and to Kar3Cik1 radially protruding away from the microtubule outer surface.

The three different 3-D density maps described above were used to generate isosurface renderings of the reconstructed microtubules at a density cutoff that included roughly 90% of the projected protein mass, and excluding excess noise-related densities (Figure 7). Unlike the contour maps described above, isosurface representations do not give any information about internal density distributions, but they facilitate looking at the entire 3-D complex and deliver a better perception of the overall structure. In particular, smaller details such as the 3-D extend of the α-helical coiled-coil stalk regions, and the conformational changes therein between the different maps can be better appreciated in the isosurface representation. As outlined above, Kar3Cik1 motor constructs incubated in ADP prior to adding to microtubules produced undecorated microtubules (Figure 7A & 7B). Hence, the individual protofilaments can be seen in their full 3-D shape and in the cross-sectional view 15 undecorated protofilaments can be counted. In the nucleotide-free state, the microtubule is fully decorated (Figure 7C & 7D). Based on previous date from Kar3Vik1-microtubule complexes (Rank et al., in press; Cope et al., in preparation) it is most likely that in both, ATP and nucleotide-free state the Kar3 motor domain appears to be one that is in contact with the microtubule, while Cik1 is oriented away (Figure 8: Cope et a., in preparation).

The stalk region that stabilizes the heterodimer can be seen as a relatively well defined elongated density that with its N-terminal end is tilting toward the plus end of the

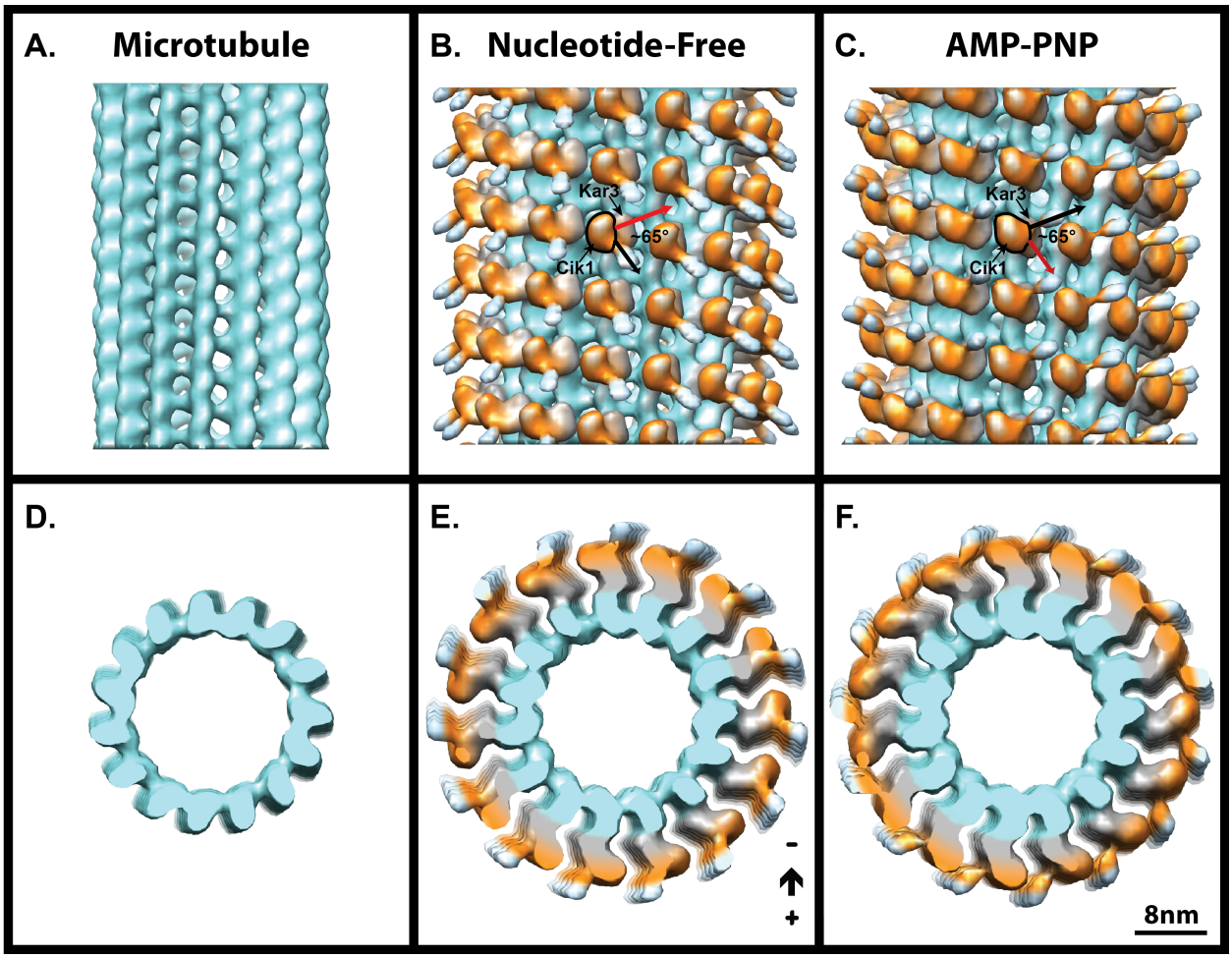

Figure 7. Isosurface Rendering of Density Maps after helical reconstruction. Chimera (Pettersen et al., 2004) was utilized to visualize the 3-D helical reconstructed datasets. **A)** Isosurface of naked 15-protofilament microtubule showing the orientation of tubulin (turquoise). **B)** In the nucleotide-free Kar3Cik1is in complex with the microtubule. It appears that Kar3 (grey) is in contact with the microtubule while Cik1 (orange) is oriented away from the microtubule. The coiled coil stalk (light blue) connecting Kar3 and Cik1 is pointed toward the plus end of the microtubule. **C)** In the ATP state Kar3Cik1 is also in complex with the microtubule with Kar3 in contact with the microtubule and Cik1 oriented away. Interestingly, there is a change in Kar3Cik1's conformation that is equivalent to a ~65° rotation in the stalk region that causes it to point toward the minus end of the microtubule. Other subtle differences can be seen when comparing the orange globular region corresponding to Cik1. A cross-sectional view of **D)** naked microtubule, **E)** nucleotide-free, **F)** ATP shows how Kar3Cik1 is in contact with the tubulin subunits of the microtubules.

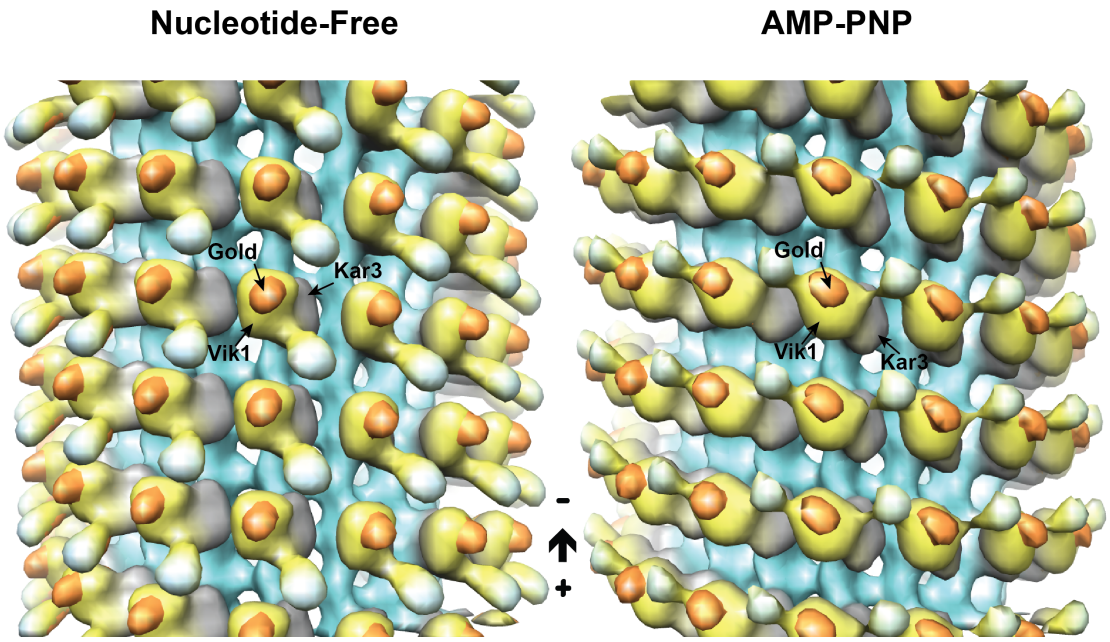

Figure 8. Nano-Gold Labeling of Kar3Vik1.
In experiments described in Cope et al. (in preparation), a Kar3Vik1 construct was made with a cysteine engineered into Vik1. This cysteine could then be modified by covalently binding a Nano-gold particle to Kar3Vik1, specifically Vik1. If Kar3 is in contact with the microtubule and Vik1 is oriented away, then the gold particle should be clearly visible on the outer surface of Kar3Vik1. If Vik1 came into contact with the microtubule the density corresponding to the gold particle would be visible near the microtubule surface. In both the nucleotide-free and AMP-PNP states, the density corresponding to the gold particle appeared on the outer surface of Kar3Vik1 away from the microtubule, this suggest that Kar3 and not Vik1 is in contact with the microtubule.

microtubule. The cross-sectional view allows us to study in great detail how Kar3Cik1 interacts with the tubulin subunits of the microtubule (see the molecular docking data below, carried out with the crystal structures of Kar3 motor domain and the Vik1 motor-homology domain, in lieu of the non-existing Cik1 crystal structure).

As pointed out above, in the ATP state, the microtubule is again fully decorated with a stoichiometry of one Kar3Cik1 dimer per αβ -tubulin dimer (Figure 7E & 7F). Similarly to the nucleotide-free state, Kar3 is in contact with the microtubule while Cik1 is oriented away. However, in contrast to the nucleotide-free state, the stalk has now rotated ~65° and is pointing toward the minus end of the microtubule. The cross-sectional view again shows the interaction between Kar3Cik1 and the tubulin of the microtubule. These results suggest that Kar3Cik1 operates with a nucleotide-dependent molecular mechanism of movement that seems very similar to Kar3Vik1 (Rank et al., in press; Cope et al., in preparation), as well as Ncd (Wendt et al., 2002; Endres et al., 2006), the kinesin-14 family member of Drosophila melanogaster (McDonald et al., 1990).

Docking X-ray crystal structures into the 3-D EM scaffold

So far, despite numerous attempts no kinesin-motor domain has been crystalized in complex with an αβ -tubulin dimer. Hence, the structure of the motor-tubulin interface can only be modeled by docking the atomic-resolution X-ray or electron crystal structures of kinesin motor domains (X-ray crystallography: kinesin-1: Kull et al., 1996; Kar3: Gulick et al., 1998), motor homology domains (e.g. Vik1: Allingham et al., 2007) and the αβ -tubulin dimer (Nogales et al., 1998; electron crystallography; Löwe et. al.,

2001) into 3-D cryo-EM scaffolds (first attempt: Sosa et al., 1997; highest resolution so far: Hirose et al., 2006 (Kar3) and Sindelar & Downing, 2010 (kinesin-1)) using Chimera (Pettersen et al., 2004). The tubulin high-resolution structure has been docked according to Nogales et al., 1999.

By depicting the isosurface renderings as a mesh we could dock the near-atomic resolution X-ray crystal structures of Kar3 (Gulick et al., 1998) and Vik1 structures (Allingham et al., 2007), as well as a predicted model of Cik1 into them. In Figure 9A, the near-atomic resolution structures αβ-tubulin, Kar3, and GCN4 are docked into the nucleotide-free state. The refined tubulin dimer structure (Löwe et. al., 2001; PDB: 1JFF) has been placed into the microtubule region. The structure of Kar3 (Gulick et al., 1998; PDB: 3KAR) has been docked into the globular region that is in contact with the microtubule (see also Hirose et al., 2006). The α-4 helix of Kar3 (shown in red) is part of the so-called switch-II region (see Vale & Milligan, 2000) and is positioned to be in contact the highly negatively charged C-terminal helix of β-tubulin. The structure of GCN4 (O'Shea et al., 1991; PDB: 1ZTA) is docked into the stalk region.

In the nucleotide-free state, the stalk is pointed toward the plus end of the microtubule. To date, there is no high-resolution structure available for Cik1, neither by electron or X-ray crystallography, nor by NMR-spectroscopy. Hence I resorted to a predicted structural model of Cik1 (Figure 10A). Such a predicted structure was obtained using the protein structure prediction software Phyre2 (Kelley & Sternberg, 2009) that generates a 3-D tertiary-structure model based on the protein sequence, 3-D structures of similar proteins, and fold recognition. The predicted Cik1 structure was constructed by blasting its sequence against other sequences with known structures.

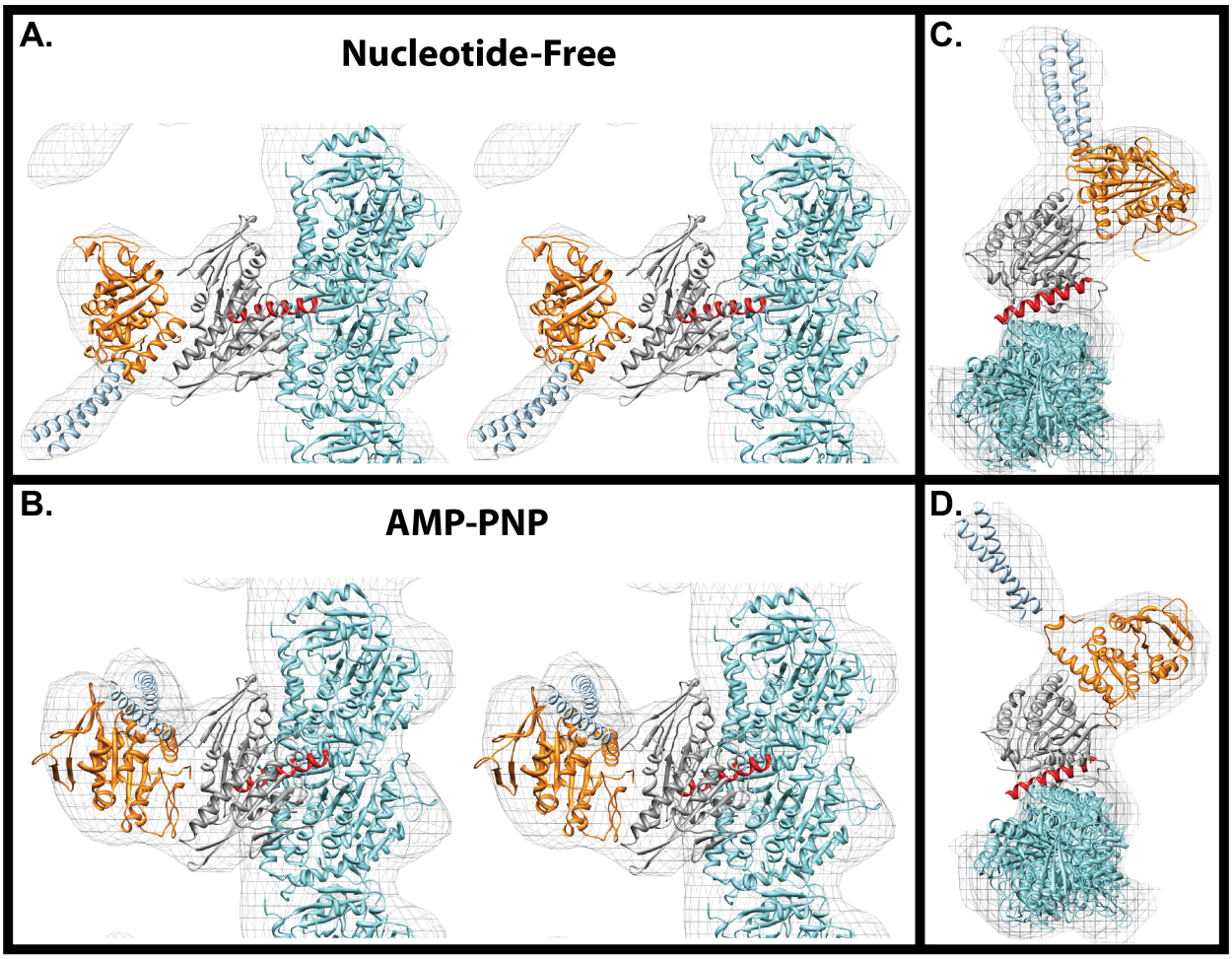

Figure 9. Structure Docking into Isosurfaces.
By turning the isosurface into a mesh it is possible to visualize how protein atomic structures fit into the volume of the EM structure. **A)** In the nucleotide-free state, the structure of tubulin (turquoise, PDB: 1JFF) is shown, the Kar3 (grey, PDB: 3KAR) structure is positioned in the globular region in contact with the B-tubulin. Kar3's helix α-4 (red) is at the interface of where Kar3 meets tubulin. There is currently no known structure for Cik1; a predicted structure obtained using Phyre 2 (Kelley & Sturnberg 2009). This predicted Cik1 (orange) structure is positioned in the globular region oriented away from the microtubule. The structure of GCN4 (light blue, PDB: 2ZTA) is located in the stalk region. In the nucleotide-free state the stalk is pointing toward the plus end of the microtubule. **B)** In the ATP state, there is a conformational change in Kar3Cik1 that leads to a ~65° rotation that results in the stalk pointing toward the minus end of the microtubule. A top view of Kar3Cik1 in complex with microtubules is shown in the **C)** nucleotide-free and **D)** ATP states. The atomic structures fit the EM structures very well and the changes in the stalk region can be clearly seen.

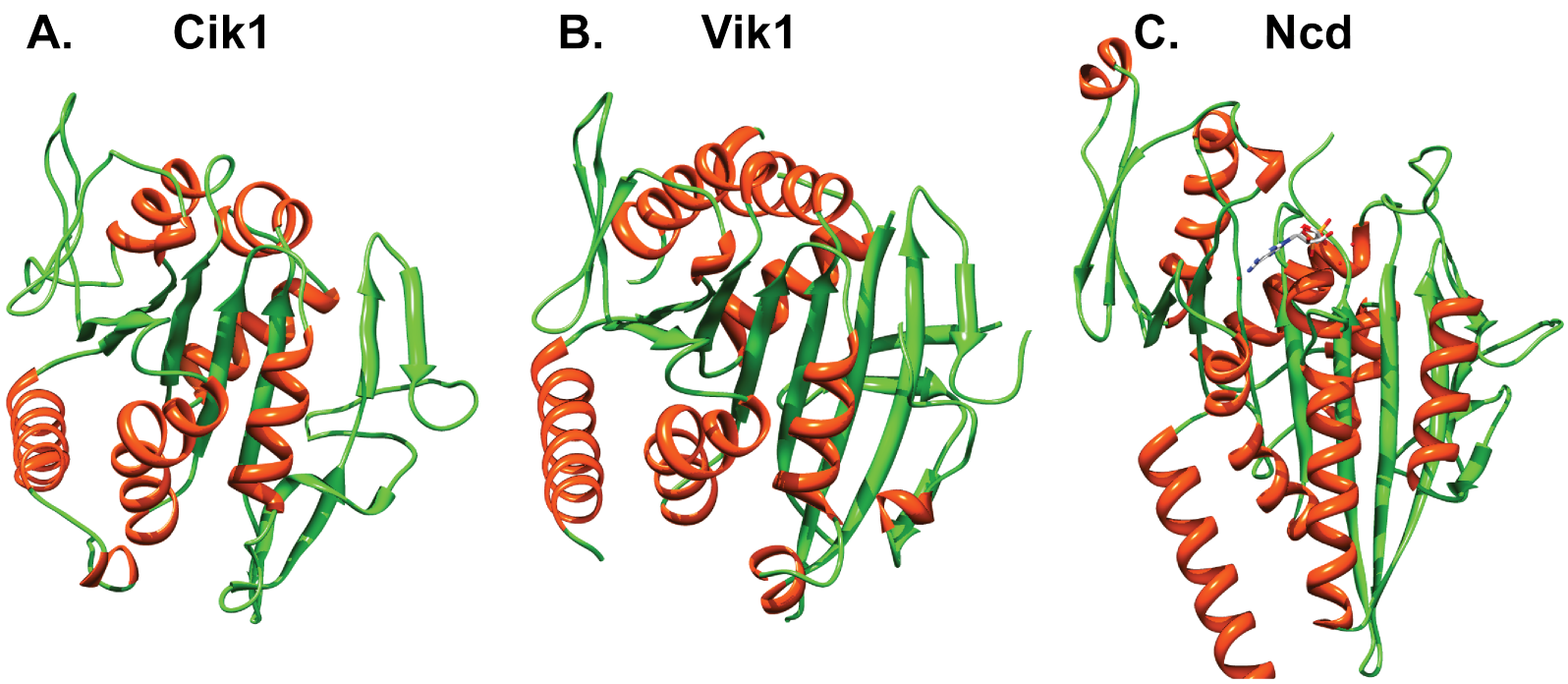

Figure 10. Phyre2 predicted structure of Cik1.

A) Predicted Cik1 structure was obtained using the protein prediction software Phyre2 (Kelley & Sternberg, 2009). This predicted Cik1 structure can be compared to other kinesin-14s **B)** Kar3Vik1 and **C)** Ncd. All three structures have a central β-sheet that is surrounded by α-helices.

Obviously the most important two sequences that were used were Vik1 (25% identity to Cik1) (Allingham et al., 2007; PBD: 2O0A) and Ncd (Sablin et al., 1998; PDB: 2NCD) (Figure 10B-10C). By comparing the structures of Cik1, Vik1, and Ncd, they all have a central β-sheet surrounded by α-helices. All of the structures appear to fit the helical 3-D cryo-EM structure very well supporting the validity of the EM structure.

In both, nucleotide free and ATP state, the known and predicted structures both fit the EM structure with remarkable precision (Figure 9B). However, there are some significant rearrangements from the nucleotide-free configuration upon ATP uptake. Most importantly the ATP-bound conformation has the stalk pointing toward the minus end of the microtubule. This is in good agreement with a minus-end directed powerstroke of this kinesin-14 family member and strongly resembles the situation in Kar3Vik1 (Rank et al., 2012 in press; Cope et al., in preparation). Figures 9A & 9B show stereo pairs of the specific conformations and allow the structure docking to be viewed in 3D. A top view of the nucleotide-free and ATP state is also shown (Figure 9C & 9D).

Structural Comparisons between the nucleotide-dependent 3-D Conformations of Kar3Cik1 and Kar3Vik1

Given the close relationship between the budding yeast (*S. cerevisiae*) Kar3Cik1 and Kar3Vik1, it is imperative to carefully explore the structural differences between these two heterodimers as they might give a hint as of why these two alternative configurations exit in yeast in the first place, and why only one of them alone seem not sufficient. The heterodimeric nature of Kar3Cik1/Vik1 is different from metazoan cells, where kinesin-14 occurs as a homodimer (e.g. *Drosophila melanogaster* ncd:

McDonald et al., 1990). Interestingly, with regard to cryo-EM microtubule-decoration experiments under various nucleotide conditions, not only does Kar3Vik1 and Kar3Cik1 behave quite similar, ncd bears some striking similarities as well. The similarities already begin with a striking cooperative microtubule-decoration property, evident in all three kinesin-14's. All three decorate an individual microtubule protofilament with enormous cooperativity, while lateral decoration appears less affected (Figure 11). Further structural comparisons are described below.

Helical reconstructions of 15-protofilament microtubules decorated with Kar3Vik1 have been reported (Cope et al., 2010; Cope et al., in preparation). A thorough comparison between the reconstructions of Kar3Cik1 and Kar3Vik1 in both, the nucleotide-free as well as the ATP state revealed many strong similarities, and the isosurfaces do not seem to differ much, (Figure 12). This is not surprising given the strong structural similarities of the two heterodimers.

In the nucleotide-free state, both motors decorate microtubules with a 1:1 stoichiometry (Kar3Cik1 and Kar3Vik1 heterodimer : tubulin dimer). For both dimers Kar3 is in contact with the microtubule while Cik1 or Vik1 are oriented away from the microtubule with both stalk regions pointing toward the plus end of the microtubule (Figure 12A & 12B). In the ATP state, both motors decorate the microtubule with Kar3 in contact with, and Cik1 or Vik1 oriented away from the microtubule. However in the ATP state the motor has undergone a conformational change that has the coiled coil stalk pointed toward the minus end of the microtubule (Figure 12C & 12D) reminiscent for a minus-end directed power stroke. Hence, Kar3Cik1 and Kar3Vik1 appear to exhibit a structurally identical microtubule binding conformation in the nucleotide-free as well as

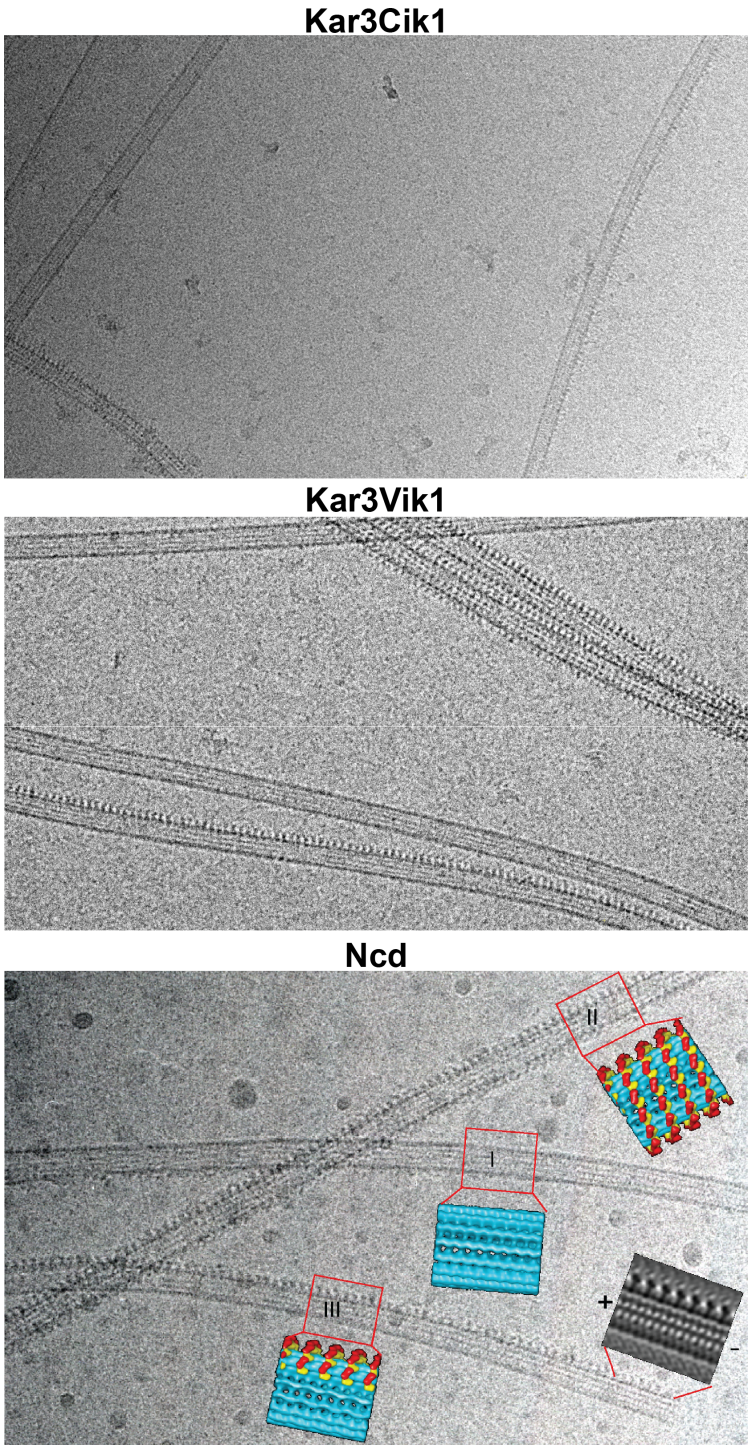

Wendt et al., 2002

Figure 11. Kinesin-14 Binding Cooperativity.
All three of the kinesin-14s mentioned in this chapter exhibit high cooperativity: **A)** Kar3Cik1, **B)** Kar3Vik1, **C)** Ncd. In **C)** examples of cooperative binding are illustrated with 3-D reconstructions of the microtubule: I) shows a naked microtubule, II) shows a fully decorated microtubule, and III) shows a partially decorated microtubule. Kar3Vik1 image courtesy of Julia Cope.

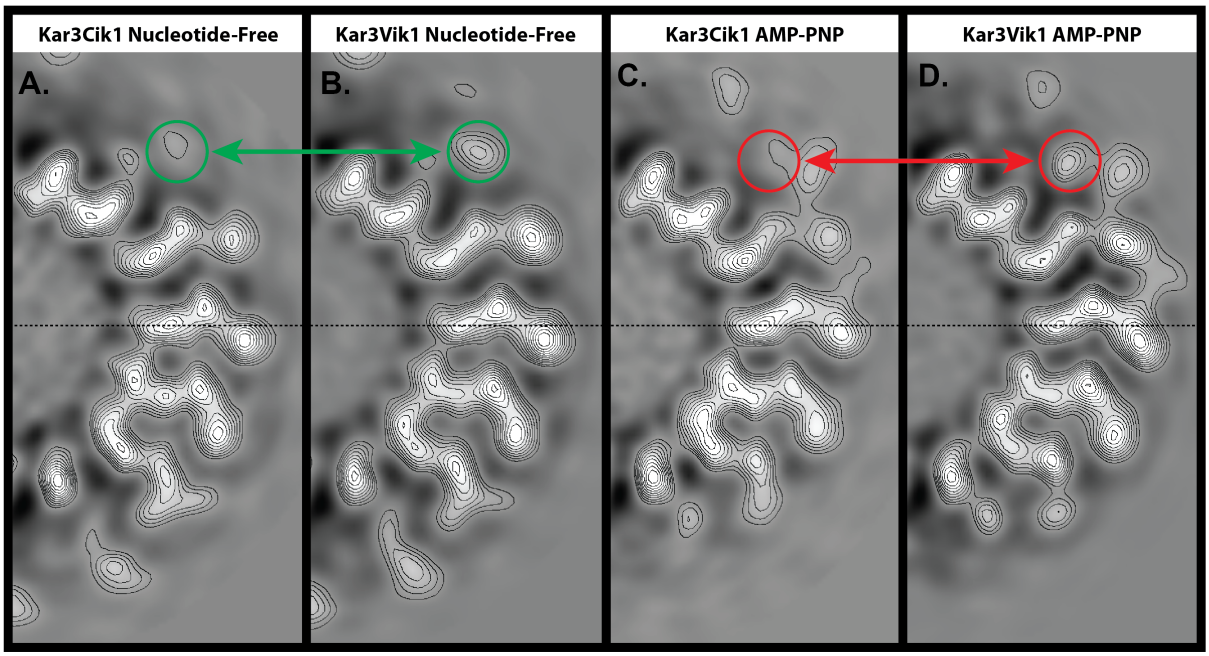

Figure 12. Structural Comparison of Kar3Cik1 and Kar3Vik1.
By comparing the density map of a single slice of **A)** Kar3Cik1 and **B)** Kar3Vik1 in the nucleotide-free state we can see a difference in the density of the motors. Cik1 appears to have less density present than Vik1; this may suggest that Cik1 has a more mobile structure than Vik1. The same observation is seen when comparing **C)** Kar3Cik1 and **D)** Kar3Vik1 in the ATP state. Cik1 again appears to have less density than Vik1. Interestingly, Kar3Cik1 and Kar3Vik1 appear structurally identical and it seems that they utilize the same mechanism of movement to perform different functions in the cell. Green circle identify differences in the density of Cik1 and Vik1 in the nucleotide-free state while the red circles show the differences in the bound ATP state. Kar3Vik1 images courtesy of Julia Cope.

the ATP state. This suggests that both motor use the same mechanism of movement to perform their unique functions within the cell. One difference that is noticeable when comparing the density maps of Kar3Cik1 and Kar3Vik1 is that Kar3Vik1 appears to have more density than Kar3Cik1in both heads, especially in the ATP state. This may be evidence of Kar3Cik1 being more mobile or flexible than Kar3Vik1, in particular between the tightly bound Kar3 motor domain and the protruding Vik1 motor homology domain.

Discussion

The first kinesin has been discovered over twenty-seven years ago (Vale et al., 1985; Brady, 1985), and ever since kinesins have been the focus of intense cell and structural biology investigations. Nowadays we classify kinesins into fourteen different subfamilies (Lawrence et al., 2004), starting with the previously called conventional kinesin as kinesin-1. The focus of this work has been on a member of the kinesin-14 family. The longest known member of that family is ncd (Walker et al., 1990; McDonald et al., 1990). So far the kinesin-14 members are the only kinesins we know of that move towards the microtubule minus-end, however, mostly in a non-processive fashion (reviewed in Cross, 2010). The key elements for directionality in kinesins are the so-called neck-linker regions (reviewed in Vale & Milligan, 2000), i.e. the region that connects the head domain with the α-helical stalk (kinesin-1: Kozielski et al., 1997; Kinesin-14: Sablin et al., 1998; Yun et al., 2003). In kinesin-1 and other anterograde kinesins this region is mostly random coil, or forms a b-sheet in its locked (ATP-bound) configuration (Kozielski et al., 1997). For kinesin-1 the conformational changes

associated with the lock-in mechanism has been demonstrated by FRET (Rice et al., 1999). In kinesin-14's the neck-linker is part of the coiled-coil stalk (Sablin et al., 1998; Yun et al., 2003). Site-directed mutations into the stalk regions of kinesin-14's (ncd) demonstrated its importance for the minus-end directionality (Endow & Waligora, 1998; Endow & Higuchi, 2000). So far all of the structural work on kinesin-14's has been done on ncd.

Here we are now focusing onto the 3-D structure and nucleotide-dependent walking cycle of a different member of the kinesin-14 subfamily, Kar3Cik1. Unlike ncd this motor is a heterodimer with Kar3 as its ATP-binding motor domain, and Cik1 an associate motor-homology domain (Chu et al., 2005; Chen et al., 2011). Kar3Cik1 is a facultative heterodimer (similar to some kinesin-2's; e.g. see: Muresan et al., 1998; Yang & Goldstein, 1998; De Marco et al., 2001), and depending on the state of cell cycle Kar3 may also dimerize with Vik1 (Cope et al., 2010).

By using cryo-EM I was investigating the structure of Kar3Cik1 in complex with microtubules under different nucleotide conditions. I obtained images of frozen-hydrated motor-microtubule complexes and performed 3-D reconstructions by helical averaging (De Rosier & Klug, 1968), with the help of the PHOELIX/Suprim software (Whittaker et al., 1995/ Schroeter & Bretaudiere, 1996). Our version of PHOELIX is specifically optimized for 15-protofilament microtubules and allows for a straightforward and unambiguous identification of the 15-protofilament microtubule configuration, which unlike others exhibit true helical symmetry (the most relevant helical paths that define the helical symmetry have Bessel orders -2 (left-handed helix that follows the motors laterally) and +15 (the right-handed protofilament supertwist)).

By incubating Kar3Cik1 with ADP its microtubule affinity was so low that we recorded essentially empty microtubules (Fig. 5A). Only the high-resolution shadowing approach shown in Figure 6 revealed the presence of sparse decoration and individual dimers could be seen either sticking out from the surface or crossing over sideward over two adjacent protofilaments. However, such low occupancy would not have produced any reasonable helical reconstruction from cryo-EM data. The shadowing revealed a potential conformation of dimeric-surface binding of Kar3Cik1, similar to what has been proposed for Kar3Vik1 in the presence of ADP (Allingham et al., 2007; Chen et al., 2011;Rank et al., in press). These authors claim that in the presence of ADP the Vik1 motor homology domain plays an active role in binding to the microtubule surface, initiating the first contact (see also below). However, one has to be clear that the images obtained in Figure 6 do not allow to unambiguously determine an active surface binding conformation from a random overlay without actual surface-binding affinity. Hence, while these data agree with the postulations of Chen et al. (2011) and Rank et al. (in press) they are no hard proof for them.

The low-occupancy picture obtained with ADP changed dramatically for Kar3Cik1 decorated microtubules when using apyrase (generates nucleotide-free Kar3Cik1) or the ATP analog AMP-PNP. Under these conditions motor-microtubule complexes showed complete decoration and revealed excellent helical 3-D maps. These maps were very suggestive of a conformation where Kar3Cik1 appears to be in contact with the microtubule via Kar3 while Cik1 is oriented away. There is a clearly detectable conformational change that occurs between the nucleotide-free and ATP-bound states that is most noticeable from the orientation of the coiled-coil stalk with respect to the

polarity of the motor-microtubule complex. After ATP uptake the stalk goes from being pointed to the plus-end of the microtubule to being pointed toward the minus-end, respectively. This type of binding is also seen in other kinesin-14s such as Kar3Vik1 (Rank et al., in press; Cope et al., in preparation) and ncd (Wendt et al., 2002; Endres et al., 2006), but was not obvious from structural studies on monomeric Kar3-microtubule complexes, despite much higher resolution (Hirose et al., 2006).

When comparing helical 3-D reconstructions from Kar3Cik1 and Kar3Vik1 microtubule complexes they are very similar. They appear to have the same binding configurations when treated ADP, apyrase, and AMP-PNP. How is it that these two molecular motors have the same mechanism of movement while having completely different cellular functions? Kar3's localization is completely dependent its binding partner (Manning & Synder, 2000). Kar3Cik1 localizes to the plus ends of microtubules and along spindle microtubules during mitosis possibly aiding in proper spindle assembly, while Kar3Vik1 is found at the spindle pole bodies where it produces an inward directed to prevent spindle collapse from the outward directed for created by kinesin-5s. It appears that Cik1 and Vik1's ability to determine Kar3's localization may be the key to understand the functional differences between Kar3Cik1 and Kar3Vik1's ability to crosslink and slide microtubules. Even though it appears that Kar3Cik1 and Kar3Vik1 have the same mechanism of movement, the location of the movement may dictate the function.

Recently, a study on Kar3Cik1 was published where a novel model of movement was reported. Chen et al (2011), performed equilibrium, microtubule association kinetics, and microtubule•Kar3Cik1 dissociation experiments to come up with a hypothetical

Kar3Cik1 stepping model. As outlined in Figure 13, Cik1 collides with a microtubule where Kar3•ADP comes into contact with the microtubule and thereby acts as the first initiator for microtubule contact. Once the motor is firmly associated with the protofilament outer surface ADP is released from the Kar3 motor domain at a very rapid pace, resulting in the nucleotide-free state (E0-E3). Kar3 can then binds ATP, which induces a conformational change causing a rotation of the neck and stalk leading to Cik1 coming off the microtubule and the stalk going from the plus-end to the minus-end (E4). Upon hydrolysis of ATP to ADP Kar3Cik1 comes off the microtubule where it can repeat the cycle in a non-processive manner (E5). This process in Kar3Vik1 as well as other kinesin-14's is very different from kinesin-1 and other processive kinesins where one of the heads always remains in tight contact with the microtubule surface, preventing it from being washed away (Hackney, 1994; Hoenger et al., 1998).

Unfortunately, the results from the Gilbert lab are not supported by the data I produced here, although we cannot claim that they are entirely incompatible due to the nature of our negative results, which might have been caused by unknown circumstances. As it has already been the case with Vik1 (Julia Cope: unpublished results), one of the key differences between the Gilbert lab and our data are the very different observations we made with regard to the binding affinity of a single-headed Cik1 construct. Our cryo-EM investigations indicate that similar to single-headed Vik1, of Cik1 motor homology domains do not bind to microtubules with any detectable affinity. In contrast, the Gilbert lab reported a 38 nM microtubule-binding affinity for Vik1 (Allingham et al., 2007), and 320 nM for the isolated Cik1 motor homology domain (Chen et al., 2011). Hence, there is no structural evidence for an initiation of Kar3Cik1

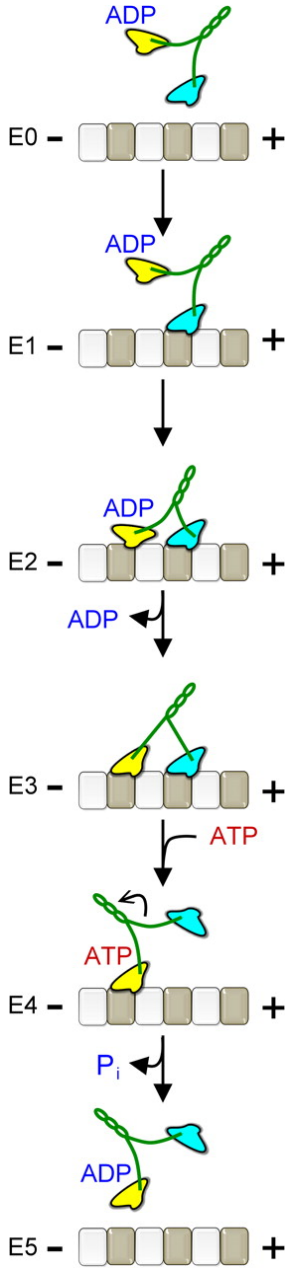

Chen et al. J. Biol. Chem. 2011

Figure 13. Previously Reported Model of Kar3Cik1 Movement Along Microtubules. Based on the results from equilibrium binding, microtubule association kinetics, and MT-Kar3Cik1 dissociation experiments Chen et al. introduced this model for Kar3Cik1 movement along microtubules. Cik1 collides with the microtubule and allows Kar3 to come in contact with the microtubule where ADP is released and the nucleotide-free state is generated. ATP binds to Kar3 and causes a conformational change where Cik1 is pulled off the microtubule. ATP is hydrolysed and Kar3Cik1 come off the microtubule and can begin the cycle again in a non-processive manner (Chen et al., 2011).

– microtubule binding by the Cik1 domain. We only detected the Kar3 motor domain in contact with tubulin.

My results suggest a walking model as presented in Figure 14. When ADP is bound to Kar3, Kar3Cik1 is not (or only very loosely: see shadowing) associated with microtubules (A). Upon release of ADP the nucleotide-free state is produced and Kar3 binds to the microtubule with Cik1 tethered to Kar3 and the coiled-coil stalk pointed toward the plus-end of the microtubule (B). The binding of ATP to Kar3 results in a conformational change that causes a rotation of about 65° leading to the coiled-coil stalk being pointed toward the minus-end of the microtubule (C), reminiscent for a minus-end directed powerstroke of a retrograde kinesin motor. After hydrolysis of the ATP to ADP, Kar3 loses its affinity for the microtubule and Kar3Cik1 comes off the microtubule where it may repeat the cycle in a non-processive manner (D-E). Even though Kar3Cik1 is a non-processive motor it is still beneficial to the cell. A single Kar3Cik1 motor is not able to crosslink or move microtubules, but when many Kar3Cik1s are bound to microtubules and work as one, they are able to produce enough force to drive the microtubule crosslinking and sliding need for Kar3Cik1's role in mating and vegetative cells.

The future directions of this project are three fold. First, I would like to determine which motor head is in contact with the microtubule Kar3 or Cik1. To perform this I will use Kar3 and Cik1 homodimers to obtain reconstructions using cryo-EM. By performing this experiment I should be able to determine if Kar3 and/or Cik1 is in contact with the microtubule surface. Second, the experiments describe in this chapter were performed in the presence of excess Kar3Cik1 protein, therefore to determine the binding surface configurations of Kar3Cik1 at substoichometric conditions high resolution heavy metal

shadowing will be used. Metal shadowing will allow me to observe how Kar3Cik1 arranges itself on microtubules and identify cooperative binding. Finally, ADP bound Kar3Cik1 when added to microtubules produce naked tubes using helical reconstruction methods, it is necessary to determine if there is low levels of binding that would not be visible using helical reconstruction. Using more extensive metal shadowing experiments I should be able to determine if ADP bound Kar3Cik1 comes into contact with microtubules.

There are many next steps in the field of kinesin research. Several diseases and disorders have been linked to malfunctions in kinesins including Alzheimer's, amyotropic lateral sclerosis (ALS), polycystic kidney disease (PKD), and tau aggregation on microtubules (Mandelkow & Mandelkow, 2002; Pazour & Rosenbaum, 2002; Stokin & Goldstein, 2006). Understanding the structure and function of kinesins should provide insight toward the development of specific drugs and therapies. There is also a need to take the studies performed here and take them to the next level where structural information is obtained at a physiological level. By combining atomic structures with kinetic studies and cryo-EM structures on physiologically relevant conditions should guide us toward a better understanding of kinesin function.

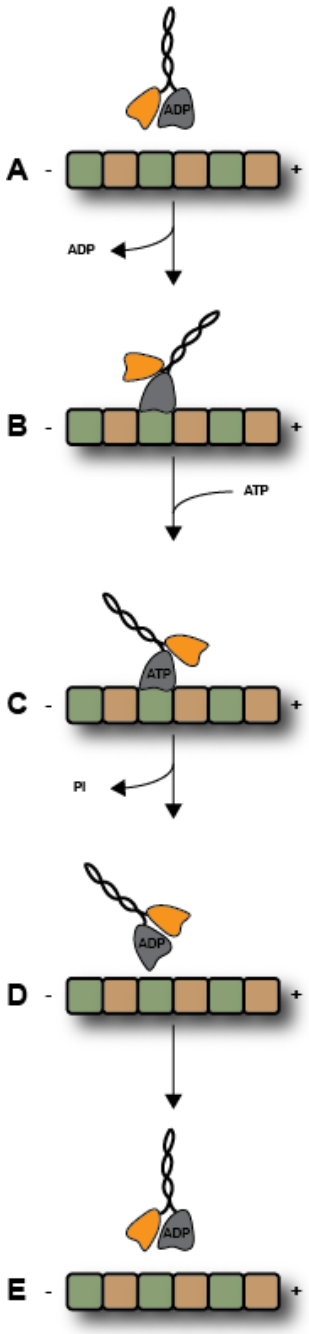

Figure 14. Model of Kar3Cik1 Movement Along Microtubules.
When ADP is bound to Kar3, Kar3Cik1 is not associated with microtubules **(A)**. Upon release of ADP the nucleotide-free state is produced and Kar3 binds to the microtubule with Cik1 oriented away and the coiled-coil stalk pointed toward the plus-end of the microtubule **(B)**. The binding of ATP to Kar3 results in a conformational change that causes a rotation of about 65° leading to the coiled-coil stalk being pointed toward the minus-end of the microtubule **(C)**. After hydrolysis of the ATP to ADP, Kar3 losses its affinity for the microtubule and Kar3Cik1 comes off the microtubule where it may repeat the cycle in a non-processive manner **(D-E)**.

Thesis Summary

This Ph.D. thesis combines three different topics in structural biology, *in vitro* and *in silico*. By using a wide spectrum of techniques ranging from molecular biology, biochemistry, and biophysics I was able to perform structural and functional studies on the macromolecules of different origin, function and composition.

In Chapter 1, using structural biology methods such as computer modeling, I was developing a so-called Ying-Yang model for bacterial chemoreceptor signaling. The Ying-Yang model gets its name from the prediction that a change in one part of the chemoreceptor with cause an equal but opposite change in another part of the chemoreceptor. This model predicts that stabilization of the 4-helix bundle in the chemoreceptor protein interaction region which binds to signaling partners CheA and CheW will cause a destabilization in the adaptation region and vice versa. After devising a strategy for testing this model, I constructed mutant chemoreceptors and tested them for kinase activity. My studies identified weakened helix-helix interactions that produce a lock-on or lock-off phenotype, which support the Ying-Yang model of signaling. The importance of this work is in understanding the mechanism of chemoreceptor signaling and bacterial chemotaxis so that we may provide the basis for the next generation of antibiotics to protect us from bacteria, which is no longer as susceptible to conventional antibiotics.

In Chapter 2, using protein purification and proteomics, I probed the question of whether Epstein-Barr virus' latent membrane protein 1 (LMP-1) functions as a single signaling complex or as multiple signaling complexes with unique signaling partners. Size exclusion chromatography and Western blot analysis revealed that LMP-1 is found

in multiple high molecular weight complexes ranging from 232 kDa to >2MDa. LMP-1 containing fractions were immuno-precipitated and analyzed by MudPIT but no other LMP-1 associated signaling partners were identified due to keratin contamination. This work provided a good starting point for identifying proteins that are involved in LMP-1 containing signaling complexes. By understanding how LMP-1 is able to produce multiple signals in B cells, we may be able to contribute to the development of more effective treatments for LMP-1 associated diseases such as Burkitt's lymphoma. This work may also contribute to the general understanding of human tumor viruses.

In Chapter 3, using cryo-electron microscopy and helical 3-D image reconstruction, I was able to investigate the structure of the heterodimeric, minus-end directed motor-head construct of the S. cerevisiae kinesin-14 Kar3Cik1 in complex with microtubules. By incubating Kar3Cik1 with ADP, I found that Kar3Cik1's affinity for microtubules was much too low to regularly decorate the surface of microtubules forbidding helical 3-D analysis. The only way I could see sparse MT-binding of Kar3Cik1 dimers was with so-called surface metal shadowing. However, when Kar3Cik1 was pre-treated with apyrase (to generate nucleotide-free Kar3Cik1) or soaked with the ATP analog AMP-PNP, the microtubules were completely decorated with Kar3Cik1. 3-D helical reconstruction of the nucleotide-free and ATP states revealed that each tubulin dimer was decorated by one Kar3Vik1 dimer, of which the Kar3 domain contacted the microtubule surface while the Vik1 motor-homology domain was pointing outwards. I could observe a significant conformational change that occurs upon nucleotide uptake and hydrolysis. The α-helical coiled-coil stalk (the key dimerization motive in many dimeric kinesins) rotates about 65 degrees causing the

stalk from being pointed toward the plus-end of the microtubule (nucleotide-free) to being pointed toward the minus-end of the microtubule (ATP). My studies also revealed that Kar3Cik1's mechanism of movement along microtubules is very similar to other well-studied kinesin-14s such as Kar3Vik1 and ncd, which are all minus-end directed and not processive. All of them are very different to the mechanisms of movement of kinesin-1's and other plus-end directed, processive kinesins.

Taken as a whole, structural biology has proven to be a very useful tool that allowed me to perform structural and functional studies on three completely different and unrelated proteins. My work has only scratched the surface of fully understanding the macromolecules discussed in this thesis. By continuing to integrate molecular biology, biochemistry, and biophysics we should be able to shed light to the questions still surrounding bacterial chemoreceptors oncogenic viral membrane proteins, and molecular motors.

References

Alberts B, Johnson A., Lewis J., Raff M., Roberts K., and Walter P. (2002). *Molecular Biology of the Cell. 4th edition.* New York: Garland Science.

Alexander, R.P., and Zhulin, I.B. (2007). Evolutionary genomics reveals conserved structural determinants of signaling and adaptation in microbial chemoreceptors. Proc Natl Acad Sci U S A 104, 2885-2890.

Allingham, J.S., Sproul, L.R., Rayment, I., and Gilbert, S.P. (2007). Vik1 modulates microtubule-Kar3 interactions through a motor domain that lacks an active site. Cell 128, 1161-1172.

Amos, L., and Klug, A. (1974). Arrangement of subunits in flagellar microtubules. J Cell Sci 14, 523-549.

Arnal, I., Metoz, F., DeBonis, S., and Wade, R.H. (1996). Three-dimensional structure of functional motor proteins on microtubules. Curr Biol 6, 1265-1270.

Bass, R.B., Coleman, M.D., and Falke, J.J. (1999). Signaling domain of the aspartate receptor is a helical hairpin with a localized kinase docking surface: cysteine and disulfide scanning studies. Biochemistry 38, 9317-9327.

Bass, R.B., and Falke, J.J. (1998). Detection of a conserved alpha-helix in the kinase-docking region of the aspartate receptor by cysteine and disulfide scanning. J Biol Chem 273, 25006-25014.

Bass, R.B., and Falke, J.J. (1999). The aspartate receptor cytoplasmic domain: in situ chemical analysis of structure, mechanism and dynamics. Structure 7, 829-840.

Beaufils, P., Choquet, D., Mamoun, R.Z., and Malissen, B. (1993). The (YXXL/I)2 signalling motif found in the cytoplasmic segments of the bovine leukaemia virus envelope protein and Epstein-Barr virus latent membrane protein 2A can elicit early and late lymphocyte activation events. EMBO J 12, 5105-5112.

Bishop, G.A., Moore, C.R., Xie, P., Stunz, L.L., and Kraus, Z.J. (2007). TRAF proteins in CD40 signaling. Adv Exp Med Biol 597, 131-151.

Boldog, T., Grimme, S., Li, M., Sligar, S.G., and Hazelbauer, G.L. (2006). Nanodiscs separate chemoreceptor oligomeric states and reveal their signaling properties. Proc Natl Acad Sci U S A 103, 11509-11514.

Brady, S.T. (1985). A novel brain ATPase with properties expected for the fast axonal transport motor. Nature 317, 73-75.

Brodeur, S.R., Cheng, G., Baltimore, D., and Thorley-Lawson, D.A. (1997). Localization of the major NF-kappaB-activating site and the sole TRAF3 binding site of LMP-1 defines two distinct signaling motifs. J Biol Chem 272, 19777-19784.

Case, R.B., Pierce, D.W., Hom-Booher, N., Hart, C.L., and Vale, R.D. (1997). The directional preference of kinesin motors is specified by an element outside of the motor catalytic domain. Cell 90, 959-966.

Chen, C.J., Rayment, I., and Gilbert, S.P. (2011). Kinesin Kar3Cik1 ATPase pathway for microtubule cross-linking. J Biol Chem 286, 29261-29272.

Chervitz, S.A., and Falke, J.J. (1996). Molecular mechanism of transmembrane signaling by the aspartate receptor: a model. Proc Natl Acad Sci U S A 93, 2545-2550.

Chervitz, S.A., Lin, C.M., and Falke, J.J. (1995). Transmembrane signaling by the aspartate receptor: engineered disulfides reveal static regions of the subunit interface. Biochemistry 34, 9722-9733.

Chu, H.M., Yun, M., Anderson, D.E., Sage, H., Park, H.W., and Endow, S.A. (2005). Kar3 interaction with Cik1 alters motor structure and function. EMBO J 24, 3214-3223.

Clausse, B., Fizazi, K., Walczak, V., Tetaud, C., Wiels, J., Tursz, T., and Busson, P. (1997). High concentration of the EBV latent membrane protein 1 in glycosphingolipid-rich complexes from both epithelial and lymphoid cells. Virology 228, 285-293.

Coffin, W.F., 3rd, Erickson, K.D., Hoedt-Miller, M., and Martin, J.M. (2001). The cytoplasmic amino-terminus of the Latent Membrane Protein-1 of Epstein-Barr Virus: relationship between transmembrane orientation and effector functions of the carboxy-terminus and transmembrane domain. Oncogene 20, 5313-5330.

Coffin, W.F., 3rd, Geiger, T.R., and Martin, J.M. (2003). Transmembrane domains 1 and 2 of the latent membrane protein 1 of Epstein-Barr virus contain a lipid raft targeting signal and play a critical role in cytostasis. J Virol 77, 3749-3758.

Cope, J. (2011) Structural insights into the mechanism of movement of the heterodimeric kinesin KAR3VIK1. Doctoral Dissertation, University of Colorado, Boulder, Colorado.

Cope, J., Gilbert, S., Rayment, I., Mastronarde, D., and Hoenger, A. (2010). Cryo-electron tomography of microtubule-kinesin motor complexes. J Struct Biol 170, 257-265.

Cross, R.A. (2010). Kinesin-14: the roots of reversal. BMC Biol 8, 107.

Danielson, M.A., Bass, R.B., and Falke, J.J. (1997). Cysteine and disulfide scanning reveals a regulatory alpha-helix in the cytoplasmic domain of the aspartate receptor. J Biol Chem 272, 32878-32888.

Dawson, C.W., Tramountanis, G., Eliopoulos, A.G., and Young, L.S. (2003). Epstein-Barr virus latent membrane protein 1 (LMP1) activates the phosphatidylinositol 3-kinase/Akt pathway to promote cell survival and induce actin filament remodeling. J Biol Chem 278, 3694-3704.

De Marco, V., Burkhard, P., Le Bot, N., Vernos, I., and Hoenger, A. (2001). Analysis of heterodimer formation by Xklp3A/B, a newly cloned kinesin-II from Xenopus laevis. EMBO J 20, 3370-3379.

DeRosier, D.J., and A. Klug. (1968). Reconstruction of three dimensional structures from electron micrographs. *Nature*. 217:130-134.

Desai, A., and Mitchison, T.J. (1997). Microtubule polymerization dynamics. Annu Rev Cell Dev Biol 13, 83-117.

Devergne, O., Hatzivassiliou, E., Izumi, K.M., Kaye, K.M., Kleijnen, M.F., Kieff, E., and Mosialos, G. (1996). Association of TRAF1, TRAF2, and TRAF3 with an Epstein-Barr virus LMP1 domain important for B-lymphocyte transformation: role in NF-kappaB activation. Mol Cell Biol 16, 7098-7108.

Eliopoulos, A.G., and Young, L.S. (1998). Activation of the cJun N-terminal kinase (JNK) pathway by the Epstein-Barr virus-encoded latent membrane protein 1 (LMP1). Oncogene 16, 1731-1742.

Endow, S.A., Chandra, R., Komma, D.J., Yamamoto, A.H., and Salmon, E.D. (1994). Mutants of the Drosophila ncd microtubule motor protein cause centrosomal and spindle pole defects in mitosis. J Cell Sci 107 (Pt 4), 859-867.

Endow, S.A., and Higuchi, H. (2000). A mutant of the motor protein kinesin that moves in both directions on microtubules. Nature 406, 913-916.

Endow, S.A., Kang, S.J., Satterwhite, L.L., Rose, M.D., Skeen, V.P., and Salmon, E.D. (1994). Yeast Kar3 is a minus-end microtubule motor protein that destabilizes microtubules preferentially at the minus ends. EMBO J 13, 2708-2713.

Endow, S.A., and Waligora, K.W. (1998). Determinants of kinesin motor polarity. Science 281, 1200-1202.

Endres, N.F., Yoshioka, C., Milligan, R.A., and Vale, R.D. (2006). A lever-arm rotation drives motility of the minus-end-directed kinesin Ncd. Nature 439, 875-878.

Falke, J.J., Bass, R.B., Butler, S.L., Chervitz, S.A., and Danielson, M.A. (1997). The two-component signaling pathway of bacterial chemotaxis: a molecular view of signal transduction by receptors, kinases, and adaptation enzymes. Annu Rev Cell Dev Biol 13, 457-512.

Falke, J.J., and Hazelbauer, G.L. (2001). Transmembrane signaling in bacterial chemoreceptors. Trends Biochem Sci 26, 257-265.

Falke, J.J., and Kim, S.H. (2000). Structure of a conserved receptor domain that regulates kinase activity: the cytoplasmic domain of bacterial taxis receptors. Curr Opin Struct Biol 10, 462-469.

Fennewald, S., van Santen, V., and Kieff, E. (1984). Nucleotide sequence of an mRNA transcribed in latent growth-transforming virus infection indicates that it may encode a membrane protein. J Virol 51, 411-419.

Fink, G., Hajdo, L., Skowronek, K.J., Reuther, C., Kasprzak, A.A., and Diez, S. (2009). The mitotic kinesin-14 Ncd drives directional microtubule-microtubule sliding. Nat Cell Biol 11, 717-723.

Floettmann, J.E., Ward, K., Rickinson, A.B., and Rowe, M. (1996). Cytostatic effect of Epstein-Barr virus latent membrane protein-1 analyzed using tetracycline-regulated expression in B cell lines. Virology 223, 29-40.

Gardner, M.K., Bouck, D.C., Paliulis, L.V., Meehl, J.B., O'Toole, E.T., Haase, J., Soubry, A., Joglekar, A.P., Winey, M., Salmon, E.D., et al. (2008). Chromosome congression by Kinesin-5 motor-mediated disassembly of longer kinetochore microtubules. Cell 135, 894-906.

Geiger, T.R., and Martin, J.M. (2006). The Epstein-Barr virus-encoded LMP-1 oncoprotein negatively affects Tyk2 phosphorylation and interferon signaling in human B cells. J Virol 80, 11638-11650.

Gires, O., Kohlhuber, F., Kilger, E., Baumann, M., Kieser, A., Kaiser, C., Zeidler, R., Scheffer, B., Ueffing, M., and Hammerschmidt, W. (1999). Latent membrane protein 1 of Epstein-Barr virus interacts with JAK3 and activates STAT proteins. EMBO J 18, 3064-3073.

Gulick, A.M., Song, H., Endow, S.A., and Rayment, I. (1998). X-ray crystal structure of the yeast Kar3 motor domain complexed with Mg.ADP to 2.3 A resolution. Biochemistry 37, 1769-1776.

Gulick, A.M., Song, H., Endow, S.A., and Rayment, I. (1998). X-ray crystal structure of the yeast Kar3 motor domain complexed with Mg.ADP to 2.3 A resolution. Biochemistry 37, 1769-1776.

Hackney, D.D. (1994). Evidence for alternating head catalysis by kinesin during microtubule-stimulated ATP hydrolysis. Proc Natl Acad Sci U S A 91, 6865-6869.

Hancock, W.O., and Howard, J. (1998). Processivity of the motor protein kinesin requires two heads. J Cell Biol 140, 1395-1405.

Hazelbauer, G.L., Falke, J.J., and Parkinson, J.S. (2008). Bacterial chemoreceptors: high-performance signaling in networked arrays. Trends Biochem Sci 33, 9-19.

Henningsen, U., and Schliwa, M. (1997). Reversal in the direction of movement of a molecular motor. Nature 389, 93-96.

Higuchi, M., Izumi, K.M., and Kieff, E. (2001). Epstein-Barr virus latent-infection membrane proteins are palmitoylated and raft-associated: protein 1 binds to the cytoskeleton through TNF receptor cytoplasmic factors. Proc Natl Acad Sci U S A 98, 4675-4680.

Hirose, K., Akimaru, E., Akiba, T., Endow, S.A., and Amos, L.A. (2006). Large conformational changes in a kinesin motor catalyzed by interaction with microtubules. Mol Cell 23, 913-923.

Hoenger, A., and Gross, H. (2008). Structural investigations into microtubule-MAP complexes. Methods Cell Biol 84, 425-444.

Hoenger, A., Sack, S., Thormahlen, M., Marx, A., Muller, J., Gross, H., and Mandelkow, E. (1998). Image reconstructions of microtubules decorated with monomeric and dimeric kinesins: comparison with x-ray structure and implications for motility. J Cell Biol 141, 419-430.

Huen, D.S., Henderson, S.A., Croom-Carter, D., and Rowe, M. (1995). The Epstein-Barr virus latent membrane protein-1 (LMP1) mediates activation of NF-kappa B and cell surface phenotype via two effector regions in its carboxy-terminal cytoplasmic domain. Oncogene 10, 549-560.

Huffaker, T.C., Thomas, J.H., and Botstein, D. (1988). Diverse effects of beta-tubulin mutations on microtubule formation and function. J Cell Biol 106, 1997-2010.

Jontes, J.D., Wilson-Kubalek, E.M., and Milligan, R.A. (1995). A 32 degree tail swing in brush border myosin I on ADP release. Nature 378, 751-753.

Kaykas, A., and Sugden, B. (2000). The amino-terminus and membrane-spanning domains of LMP-1 inhibit cell proliferation. Oncogene 19, 1400-1410.

Kaykas, A., Worringer, K., and Sugden, B. (2001). CD40 and LMP-1 both signal from lipid rafts but LMP-1 assembles a distinct, more efficient signaling complex. EMBO J 20, 2641-2654.

Kelley, L.A., and Sternberg, M.J. (2009). Protein structure prediction on the Web: a case study using the Phyre server. Nat Protoc 4, 363-371.

Kikkawa, M., Ishikawa, T., Nakata, T., Wakabayashi, T., and Hirokawa, N. (1994). Direct visualization of the microtubule lattice seam both in vitro and in vivo. J Cell Biol 127, 1965-1971.

Kilger, E., Kieser, A., Baumann, M., and Hammerschmidt, W. (1998). Epstein-Barr virus-mediated B-cell proliferation is dependent upon latent membrane protein 1, which simulates an activated CD40 receptor. EMBO J 17, 1700-1709.

Kim, K.K., Yokota, H., and Kim, S.H. (1999). Four-helical-bundle structure of the cytoplasmic domain of a serine chemotaxis receptor. Nature 400, 787-792.

Kirschner, M.W., and Mitchison, T. (1986). Microtubule dynamics. Nature 324, 621.

Knowles, D.M., Cesarman, E., Chadburn, A., Frizzera, G., Chen, J., Rose, E.A., and Michler, R.E. (1995). Correlative morphologic and molecular genetic analysis demonstrates three distinct categories of posttransplantation lymphoproliferative disorders. Blood 85, 552-565.

Kozielski, F., Sack, S., Marx, A., Thormahlen, M., Schonbrunn, E., Biou, V., Thompson, A., Mandelkow, E.M., and Mandelkow, E. (1997). The crystal structure of dimeric kinesin and implications for microtubule-dependent motility. Cell 91, 985-994.

Krzysiak, T.C., Wendt, T., Sproul, L.R., Tittmann, P., Gross, H., Gilbert, S.P., and Hoenger, A. (2006). A structural model for monastrol inhibition of dimeric kinesin Eg5. EMBO J 25, 2263-2273.

Kull, F.J., Sablin, E.P., Lau, R., Fletterick, R.J., and Vale, R.D. (1996). Crystal structure of the kinesin motor domain reveals a structural similarity to myosin. Nature 380, 550-555.

Kulwichit, W., Edwards, R.H., Davenport, E.M., Baskar, J.F., Godfrey, V., and Raab-Traub, N. (1998). Expression of the Epstein-Barr virus latent membrane protein 1 induces B cell lymphoma in transgenic mice. Proc Natl Acad Sci U S A 95, 11963-11968.

Kuppers, R., and Rajewsky, K. (1998). The origin of Hodgkin and Reed/Sternberg cells in Hodgkin's disease. Annu Rev Immunol 16, 471-493.

Lawrence, C.J., Dawe, R.K., Christie, K.R., Cleveland, D.W., Dawson, S.C., Endow, S.A., Goldstein, L.S., Goodson, H.V., Hirokawa, N., Howard, J., et al. (2004). A standardized kinesin nomenclature. J Cell Biol 167, 19-22.

Lee, J.W., Liu, P.F., Hsu, L.P., Chen, P.R., Chang, C.H., and Shih, W.L. (2009). EBV LMP-1 negatively regulates expression and pro-apoptotic activity of Par-4 in nasopharyngeal carcinoma cells. Cancer Lett 279, 193-201.

Levy, D., Mosser, G., Lambert, O., Moeck, G.S., Bald, D., and Rigaud, J.L. (1999). Two-dimensional crystallization on lipid layer: A successful approach for membrane proteins. J Struct Biol 127, 44-52.

Li, H.P., and Chang, Y.S. (2003). Epstein-Barr virus latent membrane protein 1: structure and functions. J Biomed Sci 10, 490-504.

Liebowitz, D., Wang, D., and Kieff, E. (1986). Orientation and patching of the latent infection membrane protein encoded by Epstein-Barr virus. J Virol 58, 233-237.

Lowe, J., Li, H., Downing, K.H., and Nogales, E. (2001). Refined structure of alpha beta-tubulin at 3.5 A resolution. J Mol Biol 313, 1045-1057.

Maddox, P.S., Stemple, J.K., Satterwhite, L., Salmon, E.D., and Bloom, K. (2003). The minus end-directed motor Kar3 is required for coupling dynamic microtubule plus ends to the cortical shmoo tip in budding yeast. Curr Biol 13, 1423-1428.

Mandelkow, E., and Mandelkow, E.M. (2002). Kinesin motors and disease. Trends Cell Biol 12, 585-591.

Mandelkow, E.M., and Mandelkow, E. (1985). Unstained microtubules studied by cryo-electron microscopy. Substructure, supertwist and disassembly. J Mol Biol 181, 123-135.

Manning, B.D., Barrett, J.G., Wallace, J.A., Granok, H., and Snyder, M. (1999). Differential regulation of the Kar3p kinesin-related protein by two associated proteins, Cik1p and Vik1p. J Cell Biol 144, 1219-1233.

Manning, B.D., and Snyder, M. (2000). Drivers and passengers wanted! the role of kinesin-associated proteins. Trends Cell Biol 10, 281-289.

Martin, J., and Sugden, B. (1991). Transformation by the oncogenic latent membrane protein correlates with its rapid turnover, membrane localization, and cytoskeletal association. J Virol 65, 3246-3258.

McDonald, H.B., Stewart, R.J., and Goldstein, L.S. (1990). The kinesin-like ncd protein of Drosophila is a minus end-directed microtubule motor. Cell 63, 1159-1165.

McIntosh, J.R., Grishchuk, E.L., and West, R.R. (2002). Chromosome-microtubule interactions during mitosis. Annu Rev Cell Dev Biol 18, 193-219.

McIntosh, J.R., Morphew, M.K., Grissom, P.M., Gilbert, S.P., and Hoenger, A. (2009). Lattice structure of cytoplasmic microtubules in a cultured Mammalian cell. J Mol Biol 394, 177-182.

Meluh, P.B., and Rose, M.D. (1990). KAR3, a kinesin-related gene required for yeast nuclear fusion. Cell 60, 1029-1041.

Miller, A.S., and Falke, J.J. (2004). Side chains at the membrane-water interface modulate the signaling state of a transmembrane receptor. Biochemistry 43, 1763-1770.

Miller, A.S., Kohout, S.C., Gilman, K.A., and Falke, J.J. (2006). CheA Kinase of bacterial chemotaxis: chemical mapping of four essential docking sites. Biochemistry 45, 8699-8711.

Molk, J.N., and Bloom, K. (2006). Microtubule dynamics in the budding yeast mating pathway. J Cell Sci 119, 3485-3490.

Muresan, V., Abramson, T., Lyass, A., Winter, D., Porro, E., Hong, F., Chamberlin, N.L., and Schnapp, B.J. (1998). KIF3C and KIF3A form a novel neuronal heteromeric kinesin that associates with membrane vesicles. Mol Biol Cell 9, 637-652.

Neff, N.F., Thomas, J.H., Grisafi, P., and Botstein, D. (1983). Isolation of the beta-tubulin gene from yeast and demonstration of its essential function in vivo. Cell 33, 211-219.

Nogales, E., Whittaker, M., Milligan, R.A., and Downing, K.H. (1999). High-resolution model of the microtubule. Cell 96, 79-88.

Nogales, E., Wolf, S.G., and Downing, K.H. (1998). Structure of the alpha beta tubulin dimer by electron crystallography. Nature 391, 199-203.

O'Shea, E.K., Klemm, J.D., Kim, P.S., and Alber, T. (1991). X-ray structure of the GCN4 leucine zipper, a two-stranded, parallel coiled coil. Science 254, 539-544.

Oakley, M.G., and Hollenbeck, J.J. (2001). The design of antiparallel coiled coils. Curr Opin Struct Biol 11, 450-457.

Oladipo, A., Cowan, A., and Rodionov, V. (2007). Microtubule motor Ncd induces sliding of microtubules in vivo. Mol Biol Cell 18, 3601-3606.

Page, B.D., Satterwhite, L.L., Rose, M.D., and Snyder, M. (1994). Localization of the Kar3 kinesin heavy chain-related protein requires the Cik1 interacting protein. J Cell Biol 124, 507-519.

Page, B.D., and Snyder, M. (1992). CIK1: a developmentally regulated spindle pole body-associated protein important for microtubule functions in Saccharomyces cerevisiae. Genes Dev 6, 1414-1429.

Pazour, G.J., and Rosenbaum, J.L. (2002). Intraflagellar transport and cilia-dependent diseases. Trends Cell Biol 12, 551-555.

Pettersen, E.F., Goddard, T.D., Huang, C.C., Couch, G.S., Greenblatt, D.M., Meng, E.C., and Ferrin, T.E. (2004). UCSF Chimera--a visualization system for exploratory research and analysis. J Comput Chem 25, 1605-1612.

Rank K.C., Chen C.J., Cope J., Porche K., Hoenger A., Gilbert S.P., Rayment I. (2012). Kar3Vik1, a member of the kinesin-14 superfamily, shows a novel kinesin microtubule binding pattern. J. Cell Biol. in press

Rice, S., Lin, A.W., Safer, D., Hart, C.L., Naber, N., Carragher, B.O., Cain, S.M., Pechatnikova, E., Wilson-Kubalek, E.M., Whittaker, M., et al. (1999). A structural change in the kinesin motor protein that drives motility. Nature 402, 778-784.

Rose, M.D. (1996). Nuclear fusion in the yeast Saccharomyces cerevisiae. Annu Rev Cell Dev Biol 12, 663-695.

Sablin, E.P., Case, R.B., Dai, S.C., Hart, C.L., Ruby, A., Vale, R.D., and Fletterick, R.J. (1998). Direction determination in the minus-end-directed kinesin motor ncd. Nature 395, 813-816.

Sablin, E.P., Kull, F.J., Cooke, R., Vale, R.D., and Fletterick, R.J. (1996). Crystal structure of the motor domain of the kinesin-related motor ncd. Nature 380, 555-559.

Sandberg, M., Hammerschmidt, W., and Sugden, B. (1997). Characterization of LMP-1's association with TRAF1, TRAF2, and TRAF3. J Virol 71, 4649-4656.

Sandberg, M.L., Kaykas, A., and Sugden, B. (2000). Latent membrane protein 1 of Epstein-Barr virus inhibits as well as stimulates gene expression. J Virol 74, 9755-9761.

Saunders, W.S., and Hoyt, M.A. (1992). Kinesin-related proteins required for structural integrity of the mitotic spindle. Cell 70, 451-458.

Schroeter, J.P., and Bretaudiere, J.P. (1996). SUPRIM: easily modified image processing software. J Struct Biol 116, 131-137.

Sharp, D.J., Yu, K.R., Sisson, J.C., Sullivan, W., and Scholey, J.M. (1999). Antagonistic microtubule-sliding motors position mitotic centrosomes in Drosophila early embryos. Nat Cell Biol 1, 51-54.

Sindelar, C.V., and Downing, K.H. (2010). An atomic-level mechanism for activation of the kinesin molecular motors. Proc Natl Acad Sci U S A 107, 4111-4116.

Sixbey, J.W., Davis, D.S., Young, L.S., Hutt-Fletcher, L., Tedder, T.F., and Rickinson, A.B. (1987). Human epithelial cell expression of an Epstein-Barr virus receptor. J Gen Virol 68 (Pt 3), 805-811.

Sosa, H., Dias, D.P., Hoenger, A., Whittaker, M., Wilson-Kubalek, E., Sablin, E., Fletterick, R.J., Vale, R.D., and Milligan, R.A. (1997). A model for the microtubule-Ncd motor protein complex obtained by cryo-electron microscopy and image analysis. Cell 90, 217-224.

Sproul, L.R., Anderson, D.J., Mackey, A.T., Saunders, W.S., and Gilbert, S.P. (2005). Cik1 targets the minus-end kinesin depolymerase kar3 to microtubule plus ends. Curr Biol 15, 1420-1427.

Starrett, D.J., and Falke, J.J. (2005). Adaptation mechanism of the aspartate receptor: electrostatics of the adaptation subdomain play a key role in modulating kinase activity. Biochemistry 44, 1550-1560.

Stearns, T. (1990). The yeast microtubule cytoskeleton: genetic approaches to structure and function. Cell Motil Cytoskeleton 15, 1-6.

Stokin, G.B., and Goldstein, L.S. (2006). Linking molecular motors to Alzheimer's disease. J Physiol Paris 99, 193-200.

Swain, K.E., and Falke, J.J. (2007). Structure of the conserved HAMP domain in an intact, membrane-bound chemoreceptor: a disulfide mapping study. Biochemistry 46, 13684-13695.

Swain, K.E., Gonzalez, M.A., and Falke, J.J. (2009). Engineered socket study of signaling through a four-helix bundle: evidence for a yin-yang mechanism in the kinase control module of the aspartate receptor. Biochemistry 48, 9266-9277.

Vale, R.D. (2003). The molecular motor toolbox for intracellular transport. Cell 112, 467-480.

Vale, R.D., and Fletterick, R.J. (1997). The design plan of kinesin motors. Annu Rev Cell Dev Biol 13, 745-777.

Vale, R.D., and Milligan, R.A. (2000). The way things move: looking under the hood of molecular motor proteins. Science 288, 88-95.

Vale, R.D., Reese, T.S., and Sheetz, M.P. (1985). Identification of a novel force-generating protein, kinesin, involved in microtubule-based motility. Cell 42, 39-50.

Walker, R.A., Salmon, E.D., and Endow, S.A. (1990). The Drosophila claret segregation protein is a minus-end directed motor molecule. Nature 347, 780-782.

Walshaw, J., and Woolfson, D.N. (2001). Socket: a program for identifying and analysing coiled-coil motifs within protein structures. J Mol Biol 307, 1427-1450.

Wang, C., Ai, M., Ren, W., Xiao, H., Li, X., Tang, F., Gu, H., Yi, W., Weng, X., Deng, X., et al. (2003). Epstein-Barr virus encoded latent membrane protein 1 induces TRAF1 expression to promote anti-apoptosis activity via NF-kappaB signaling pathway in nasopharyngeal carcinoma. Chin Med J (Engl) 116, 1022-1028.

Wendt, T.G., Volkmann, N., Skiniotis, G., Goldie, K.N., Muller, J., Mandelkow, E., and Hoenger, A. (2002). Microscopic evidence for a minus-end-directed power stroke in the kinesin motor ncd. EMBO J 21, 5969-5978.

Whittaker, M., Carragher, B.O., and Milligan, R.A. (1995). PHOELIX: a package for semi-automated helical reconstruction. Ultramicroscopy 58, 245-259.

Wilson, A., George, A.J., King, C.A., and Stevenson, F.K. (1990). Recognition of a B cell lymphoma by anti-idiotypic T cells. J Immunol 145, 3937-3943.

Winston, S.E., Mehan, R., and Falke, J.J. (2005). Evidence that the adaptation region of the aspartate receptor is a dynamic four-helix bundle: cysteine and disulfide scanning studies. Biochemistry 44, 12655-12666.

Yang, Z., and Goldstein, L.S. (1998). Characterization of the KIF3C neural kinesin-like motor from mouse. Mol Biol Cell 9, 249-261.

Yun, M., Bronner, C.E., Park, C.G., Cha, S.S., Park, H.W., and Endow, S.A. (2003). Rotation of the stalk/neck and one head in a new crystal structure of the kinesin motor protein, Ncd. EMBO J 22, 5382-5389.